


1-1-2012

π -Conjugated Heteroles Containing Group 13 Elements

Sossina Gezahegn
Ryerson University

Follow this and additional works at: <http://digitalcommons.ryerson.ca/dissertations>

 Part of the [Analytical Chemistry Commons](#), [Inorganic Chemistry Commons](#), and the [Polymer Chemistry Commons](#)

Recommended Citation

Gezahegn, Sossina, " π -Conjugated Heteroles Containing Group 13 Elements" (2012). *Theses and dissertations*. Paper 717.

This Thesis is brought to you for free and open access by Digital Commons @ Ryerson. It has been accepted for inclusion in Theses and dissertations by an authorized administrator of Digital Commons @ Ryerson. For more information, please contact bcameron@ryerson.ca.

π -CONJUGATED HETEROLES CONTAINING GROUP 13 ELEMENTS

by

Sossina Gezahegn

BSc, Applied Chemistry and Biology, Ryerson University, 2008

A thesis

presented to Ryerson University

in partial fulfillment of the

requirements for the degree of

Master of Science

in the program of

Molecular Science

Toronto, Ontario, Canada, 2012

© (Sossina Gezahegn) 2012

Author's Declaration

I hereby declare that I am the sole author of this thesis.

I authorize Ryerson University to lend this thesis to other institutions or individuals for the purpose of scholarly research.

Name: _____ Signature: _____

I further authorize Ryerson University to reproduce this thesis by photocopying or by other means, in total or in part, at the request of other institutions or individuals for the purpose of scholarly research.

Name: _____ Signature: _____

π -CONJUGATED HETEROLES CONTAINING GROUP 13 ELEMENTS

Sossina Gezahegn

Master of Science, Molecular Science, Ryerson University 2012

Abstract:

This research targeted the synthesis of group 13 neutral heteroles *via* transmetallation of the tin atom in stannole moieties. The synthesis of Heteroles of **15a** (1-chloro-2,3,4,5-tetraphenylborole), **15b** (1-chloro-2,3,4,5-tetraphenylaluminole) and **15c** (1-chloro-2,3,4,5-tetraphenylgallole) were attempted. The potential formation of Lewis base adducts were explored through the addition of a coordinating solvent of THF, Et₃N, and Et₂O and characterized with NMR (¹H, ¹³C and ¹¹B where applicable). It was attempted to synthesize Polymer **17a** from the di-brominated borole monomer **16a** *via* a Pd-catalyzed polycondensation reaction. THF was subsequently added to the polymer in an attempt to produce the polymer adduct **17a**·THF. This was performed to produce a stable enough material for GPC analysis. The polymer was also characterized with NMR.

Theoretical calculations were undertaken at the B3LYP/6-31G* level of DFT to help identify the effect of HOMO-LUMO energy gap of the above heteroles and their adducts. DFT calculations reveal that monomers and oligomer energy gaps can be tuned by substituents attached to the heterole, the type of Lewis adduct formed and the degree of catenation. These monomers and oligomers could potentially be novel building blocks for the synthesis of small energy gap π -conjugated systems.

Acknowledgements

I would like to acknowledge my supervisor Dr. Andrew McWilliams for giving me an opportunity to work in this thesis. Many thanks to my committee members, Drs. Stefan Wylie and Robert Gossage, as well as Dr. Russ Viirre for their stimulating discussions and suggestions.

Special thanks to Dr. Daniel Foucher for his valuable discussions, guidance and support.

I would like also to extend my thanks to Maria Landau for her useful and kind instructions. Many thanks to all students from synthetic group, especially Aman Khan for his friendship. I also would like to thank Sylvia O’Sullivan and Shawn McFadden for their great technical support.

Most importantly, I would like to thank my family especially my mom Emodish and Kebede for their endless love and support.

Without you all, this work would not have been done. Finally, I would like to thank Ryerson University for the financial support.

TABLE OF CONTENTS

SYMBOLS AND ABBREVIATIONS	xi
INTRODUCTION	1
1.1 π -Conjugated Systems	1
1.1.1 Energy Gap of π -Conjugated Systems.....	3
1.2 Stannoles and Other Group 14 Heteroles	7
1.3 Boron and Boroles	9
1.3.1 Boron	9
1.3.2 Boroles	10
1.4 Aluminole, Gallole and Indacyclopentadiene.....	12
1.5 Molecular Modeling	14
1.6 Aim of This Work.....	17
MATERIALS AND METHODS.....	20
Materials	20
Equipment and characterization	20
Experimental.....	21
2.1 Synthesis of 1,4-Dilithio-1,2,3,4-tetraphenylbutadiene [2]	21
2.2 Synthesis of 1,1-Dimethyl-2,3,4,5-tetraphenylstannacyclopentadiene [10].....	22
2.3 Synthesis of 1-Chloro-2,3,4,5-tetraphenylboracyclopentadiene [15a].....	23
2.4 Synthesis of 1-Chloro-2,3,4,5-tetraphenylaluminacyclopentadiene [15b].....	25
2.5 Synthesis of 1-Chloro-2,3,4,5-tetraphenylgallacyclopentadiene [15c]	26
2.6 Synthesis of Diethyl Dipropargylmalonate (DEDPM) [21]	28

2.7	Synthesis of 4,4-Bis(hydroxymethyl)-1,6-heptadiyne [22]	29
2.8	Synthesis of 4,4-Bis(hexyloxymethyl)-1,6-heptadiyne [23]	30
2.9	Synthesis of 4,4-Bis(hexyloxymethyl)-1,7-bis-p-bromophenyl-1,6-heptadiyne [24]	31
2.10	Attempted Synthesis of $C_{35}H_{48}Br_2SnO_2$, [26]	32
2.11	Synthesis of polymer 17a ·THF	33
RESULTS AND DISCUSSION		35
3.1.	Synthesis of 1-chloro-2,3,4,5-tetraphenyl monomer precursors	35
3.1.1	Synthesis of 1,4-dilithio-1,2,3,4-tetraphenylbutadiene, [2]	35
3.1.2	Synthesis of 1,1-dimethyl-2,3,4,5-tetraphenyl-stannacyclopentadiene, [10]	36
3.2.	Attempted synthesis of 1-chloro-2,3,4,5-tetraphenyl heteroles	38
3.2.1	Analysis of 15a and attempted synthesis of related adducts	39
3.2.2	Analysis of 15b and 15c attempted synthesis of related adducts	40
3.3.	Synthesis of monomer 16 precursors	42
3.3.1	Diethyl dipropargyl malonate, [21]	42
3.3.2	Synthesis of 4,4-bis(hydroxymethyl)-1,6-heptadiyne, [22]	44
3.3.3	Synthesis of 4,4-bis(hexyloxymethyl)-1,6-heptadiyne, [23]	46
3.3.4	Synthesis of 4,4-bis(hexyloxymethyl)-1,7-bis-p-bromophenyl-1,6-heptadiyne, [24]	48
3.3.5	Attempted synthesis of $C_{35}H_{48}Br_2SnO_2$, [26]	49
3.4.	Attempted synthesis of polymer 17a ·THF	52
3.5.	Molecular Modelling of Group 13 Heteroles	54
3.5.1	Methyl, <i>n</i> -Butyl and Phenyl Substituents Effects on 15a	56
3.6.	Theoretical Analysis of Oligomeric Heteroles	63

CONCLUSIONS AND RECOMMENDATIONS	67
4.1 Conclusions.....	67
4.2 Future recommendations	68
APPENDIX.....	69
List of NMR and IR spectra.....	69
REFERENCES	97

LIST OF TABLES

Table 1. 1 All-electron Gaussian basis sets in Spartan.....	16
Table 3. 1 NMR (CDCl ₃) results of results of 1-chloro-2,3,4,5-tetraphenyl heteroles and adducts.	42
Table 3. 2 Theoretical energy gaps E_g of 15a , 15a' and 15a'' borole heteroles calculated at the B3LYP/6-31G* level of DFT.	56
Table 3. 3 Theoretical energy gaps E_g of 1-chloro-2,3,4,5-tetraphenyl heteroles (15a-c) and 2, 5-diphenyl heteroles (16'a-c) with Lewis-base adducts calculated at the B3LYP/6-31G* level of DFT.....	59
Table 3. 4 Theoretical energy gaps of 1-chloro-2,3,4,5-tetraphenylborole for various repeating units calculated at the B3LYP/6-31G* level of DFT.	64

LIST OF FIGURES

Figure 1.1 Organic π -conjugated polymers where E = O, S, NR	2
Figure 1.2 Schematic diagram of LUMO (L) and HOMO (H) demonstrating the effect of increasing π -conjugation from A ($2\pi e^-$), B ($4\pi e^-$), C ($6\pi e^-$), D ($8\pi e^-$) and E ($2n\pi e^-$) system.	5
Figure 1.3 The energy gap comparison of an insulator, semiconductor and conductor.	6
Figure 1.4 Structural factors that affect the HOMO-LUMO gap of linear π -conjugated systems.....	7
Figure 1.5 Boron: trigonal planar geometry (6), Lewis acidity and adduct formation (7) and $P_{\pi}-\pi^*$ conjugation (8). (Nu = Nucleophile).....	10
Figure 1.6 Pentaarylboroles and adducts.	11
Figure.1.7. Heteroles 15a-c and 16a-c	18
Figure 3.1 ^1H NMR spectra of Diethyl dipropargyl malonate 21	43
Figure 3.2 ^1H NMR spectra of 4,4- <i>bis</i> (hexyloxymethyl)-1,6-heptadiyne 22	45
Figure 3.3 ^1H NMR spectra of 4,4- <i>bis</i> (hexyloxymethyl)-1,6-heptadiyne 23	47
Figure 3.4 Heteroles 15 , 16 and 16'	55
Figure 3.5 Heteroles 15a , 15a' and 15a''	56
Figure 3.6 Frontier orbitals of 1-chloro-2,3,4,5-tetra 15a (Ph), 15a' (<i>n</i> -Bu) and 15a''	57
Figure 3.7 Ultraviolet spectrum of 15a (top) and 15a ·Et ₃ N (bottom).	62
Figure 3.8 Ultraviolet spectrum of 16a (top) and 16a' ·Et ₃ N (bottom).....	63
Figure 3.9 Frontier orbitals of 1-chloro-2,3,4,5-tetraphenylborole molecules 15a for up to 3 repeat units.	65

LIST OF SCHEMES

Scheme 1. 1 Synthesis of stannole and related ring systems.	8
Scheme 1. 2 Synthesis of 1-bromo-2,3,4,5-tetraphenylborole <i>via</i> stannole intermediate.	12
Scheme 1. 3 Synthesis of chloro-aluminacyclopentadiene from 1,4-dilithio-1,3-dienes and AlCl ₃	13
Scheme 1. 4 Metallacycle transfer from zirconium.	13
Scheme 1. 5 Utilizing a bulky aryl gallium dichloride strategy to obviate dimerization.	14
Scheme 1. 6 Polymerization of 17a	18
Scheme 3. 1. Synthesis of 1,4-dilithio-1,2,3,4-tetraphenylbutadiene, 2	35
Scheme 3. 2 1, 1-dimethyl-2,3,4,5-tetraphenylstannacyclopentadiene, 10	37
Scheme 3. 3 1-chloro-2,3,4,5-tetraphenyl heteroles, 15(a-c)	39
Scheme 3. 4 Diethyl dipropargyl malonate, 22	42
Scheme 3. 5 4,4-bis(hydroxymethyl)-1,5-heptadiyne, 22	44
Scheme 3. 6 4,4-bis(hexyloxymethyl)-1,6-heptadiyne, 23	46
Scheme 3. 7 4,4-bis(hexyloxymethyl)-1,7-bis-p-bromophenyl-1,6-heptadiyne, 24	48
Scheme 3. 8 Synthesis of C ₃₅ H ₄₈ Br ₂ SnO ₂ , 26	51
Scheme 3. 9 Synthesis of polymer 17a ·THF	53

SYMBOLS AND ABBREVIATIONS

Å	Angstrom
a.k.a.	also known as
AlCl ₃	aluminum trichloride
Ar	aryl
BBr ₃	boron tribromide
BCl ₃	boron trichloride
Bipy	bipyridine
Bu	Butyl
C ₆ D ₆	deuterated benzene
CDCl ₃	deuterated chloroform
Da	Daltons
DMF	dimethylformamide
E _{BLA}	energy of bond length alteration
E _g	energy gap
E _{Int}	energy of intermolecular interactions
E _{Res}	energy of resonance
E _{sub}	energy of substituent
Et ₂ O	diethylether
Et ₃ N	triethylamine
E _θ	energy of dihedral angle
GaCl ₃	gallium trichloride
GPC	Gel permeation chromatography
HOMO	Highest Occupied Molecular Orbital

LiCl	lithium chloride
LUMO	Lowest Unoccupied Molecular Orbital
Me	methyl
Me ₂ SnCl ₂	dimethyltin dichloride
<i>M_w</i>	weight average molecular weight
NH ₃	ammonia
Nu	nucleophile
Ph	phenyl
PhCN	benzonitrile
Py	pyridine
THF	tetrahydrofuran
UV	ultraviolet
λ	Lambda
π	Pi
σ	sigma

CHAPTER 1

INTRODUCTION

This thesis has two main focuses:

- To develop a new synthetic route to conjugated Group 13 heteroles *via* replacement of the tin atom in a stannole moiety.
- To explore the effects of Lewis-base adduct formation on the electronic properties of monomers and polymers containing group 13 heteroles using molecular modelling.

1.1 π -Conjugated Systems

Conjugation can occur in any molecule with three or more adjacent atoms with overlapping p-orbitals.¹ Lewis representations of conjugated systems possess alternating single (indicating sigma bonding only) and multiple bonds (where π -bonding is present). In heavier atoms, d-orbitals can also potentially be involved in conjugation. Delocalization of electrons occurs when π -electrons mobilize across all the appropriately aligned p-orbitals from adjacent atoms. The π -electrons are associated with a group of atoms rather than being localized in either a molecular orbital shared between only two atoms or in an atomic orbital (associated with a single atom). This phenomenon increases stability by it lowering the ground state energy of the molecule.² Due to their unusual optoelectronic properties, a variety of π -conjugated materials have found applications in multidisciplinary fields such as medicinal chemistry,³ material science⁴ and crop protection science.³ The optical and electronic properties (such as electrical conductivity and nonlinear optics) of π -conjugated materials are influenced by the strength of conjugation.^{2,5} π -Conjugated polymers and monomers can be employed as photovoltaic cells,⁵ light emitting diodes,^{4,5} and polymeric sensors.⁶

The foundation for π -conjugated systems applications was born out of the discovery of metallic conductivity in a carbon-based polymer achieved through the doping of polyacetylene. Jointly, Alan G. Macdiarmid, Hideki Shirakawa and Alan J. Heeger observed a billion fold increase in electrical conductivity of a *trans*-syn-polyacetylene **1a** (a linear organic π -conjugated system) when it was oxidized with iodine vapor.⁷ In this procedure, molecules of I_2 stripped electrons from the polyacetylene, becoming I_3^- (negatively charged anions) while making the polyacetylene positively charged (radical cations a.k.a. polarons). Polarons can then delocalize down the polyacetylene chain allowing for conductivity.⁷ Until this discovery, many organic polymers with all carbon backbones were categorized as insulators. This seminal work was awarded the Nobel Prize in Chemistry in 2000.⁸

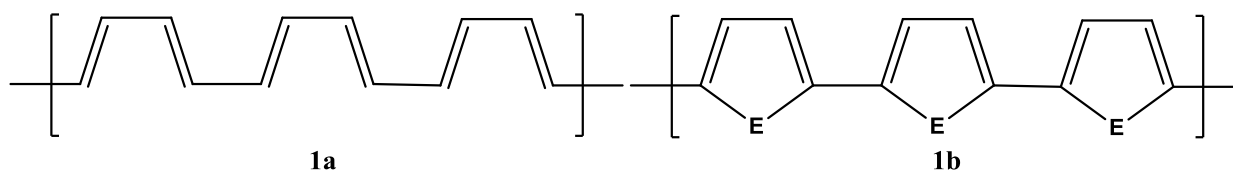


Figure 1.1 Organic π -conjugated polymers where E = O, S, NR⁸

After the discovery of the conductivity of doped polyacetylene, studies focused on the incorporation of heteroatoms into π -conjugated systems with the intention of producing new linear-conjugated frameworks with enhanced conductivity and processibility.⁸ For example, compound **1b** can be simply regarded as modified *trans*-syn-polyacetylene where a heteroatom **E** has been incorporated as a bridging atom (Figure 1.1).⁸ The nature of **E**

directly dictates the electrical and optical properties of materials of the form **1b** and allows fine-tuning of the compound energy level difference.⁸ The advantages of these types of polymers (**1b**) over the strictly carbon-containing **1a** include the potential for substituent alteration *via* electrophilic substitution reactions at the heteroatom center and the potential for increased stability due to its aromatic character.

In order to identify the aromaticity in cyclic molecules, it is useful to consider Huckel's rule. The rule states that the number of π -electrons in aromatic molecules (cyclic planar) must satisfy the formula $4n + 2$, (where n is zero or positive integer). Thus aromatic compounds have two, or six, or ten, etc π -electrons. In contrast, cyclic planar molecules that satisfy formula of $4n$ π -electrons of four, eight, twelve, etc. and are described as anti-aromatic.⁹ The energy in the π -electrons of anti-aromatic compounds are higher than that found with aromatic compounds.¹⁰ A lone pair of electrons from the heteroatom in pyrrole (**E** = NR), furan (**E** = O) and thiophene (**E** = S) reside in the p-orbital interacting in the π -system and thus creating an aromatic system, while the other lone pair (from O and S) in sp^2 orbital is not part of delocalized system.

1.1.1 Energy Gap of π -Conjugated Systems

The discrete molecular orbitals in any extended conjugated system can be divided into stabilized bonding orbitals and destabilized antibonding orbitals, resulting in two continuous bands (energy levels) called valence and conduction bands. The valence band is occupied with electrons while the conduction band remains empty. The energy difference between valence and conduction bands in conducting materials (including conductive

polymers) is analogous to the HOMO (Highest Occupied Molecular Orbital)-LUMO (Lowest Unoccupied Molecular Orbitals) gap of small molecules, generally referred to as the energy gap (E_g).⁸ The HOMO-LUMO gap is a very important parameter in defining the optical and electronic properties of materials. When a molecule absorbs energy, the electron gets promoted from an occupied molecular orbital to a vacant molecular orbital at a higher energy. The most probable electronic transition is from HOMO to LUMO, however other transitions can occur, including $\sigma \rightarrow \sigma^*$, $\sigma \rightarrow \pi^*$, $n \rightarrow \sigma^*$, $n \rightarrow \pi^*$ and additional $\pi \rightarrow \pi^*$ transitions.⁸ The energy difference between the HOMO and LUMO decreases as conjugation is extended due to relative energies of the increasing number of conjugated π -orbitals (Figure 1.2). Experimentally, the energy gap can be determined using a UV-VIS spectrometer by identifying the lowest energy absorption edge (λ_{onset}) in the spectrum of the material.⁸

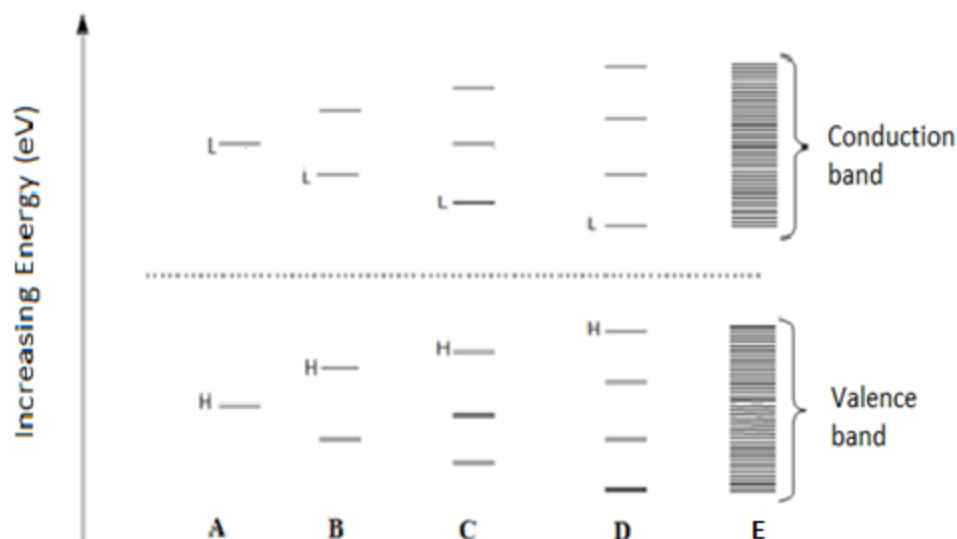


Figure 1.2 Schematic diagram of LUMO (L) and HOMO (H) demonstrating the effect of increasing π -conjugation from A ($2\pi e^-$), B ($4\pi e^-$), C ($6\pi e^-$), D ($8\pi e^-$) and E ($2n\pi e^-$) system.

The conjugated molecular orbitals of linear polyenes, $\{\text{CH}\}_n$, such as polyacetylene **1a**, are delocalized throughout the structure and theoretically, the HOMO-LUMO gap of this molecule could approach zero. However, studies on the effective conjugation length show that there is an upper limit (saturation of monomer units at which conjugation occurs) for the addition of double bonds to linear polymers where no additional effect is observed.⁸

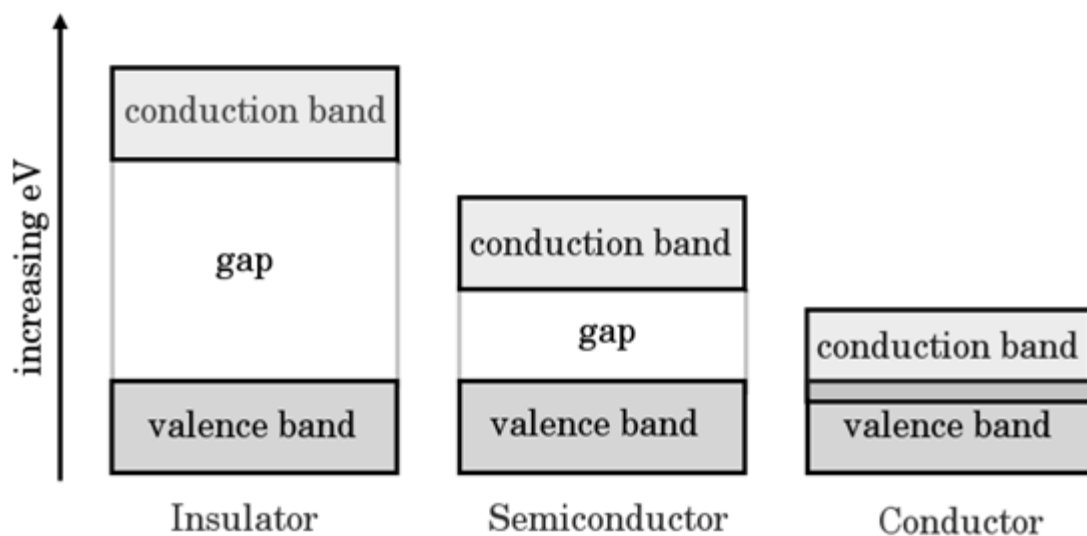


Figure 1.3 The energy gap comparison of an insulator, semiconductor and conductor.

The conductivity of a π -conjugated system is directly dependent on the energy gap; the smaller the energy gap, the greater the conductivity (Figure 1.3).⁸ Insulators, such as diamond have an energy gap of 5.5 eV, while a semiconductor material such as silicon has 1.1 eV¹¹ while the energy gap of any metal will be ≈ 0 eV due to the overlap of the conduction and the valence bands.

Conjugation needs to extend over the length of the entire molecule in order to obtain the narrowest possible energy gap. Many studies have been carried out to identify suitable conjugated systems (possessing a small energy gap) that could act as alternatives to metals.^{8,12} For example, Roncali has reported on the considerations that affect the value of the HOMO-LUMO gap for linear π -conjugated systems that incorporate aromatic moieties, such as polythiophene (Figure 1.4).¹² The energy gap (E_g) of these linear π -conjugated systems can be influenced by the sum of five structural contributors: $E_g = E_{BLA}$

+ E_{Res} + E_{Sub} + E_{θ} + E_{Int} where BLA represents the bond length alteration; Res , resonance; Sub , the effect of substituent; θ , for dihedral angle; and Int , intermolecular interactions.¹²

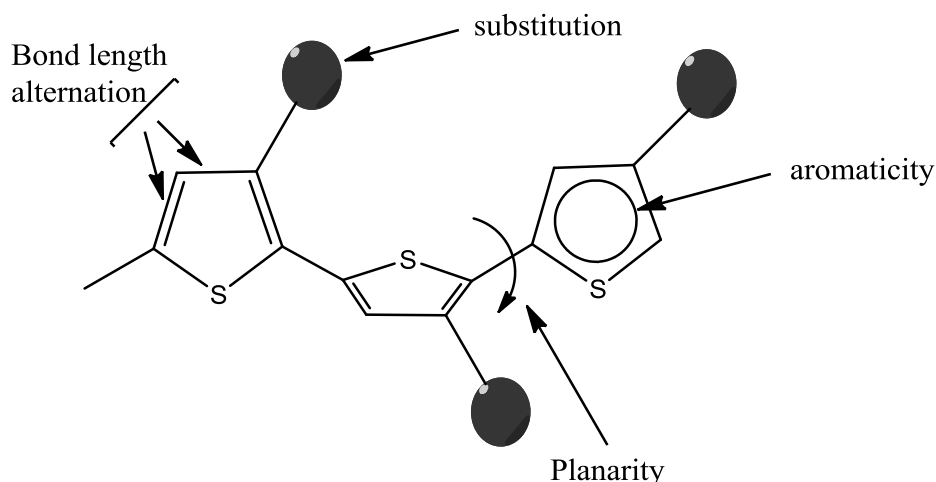


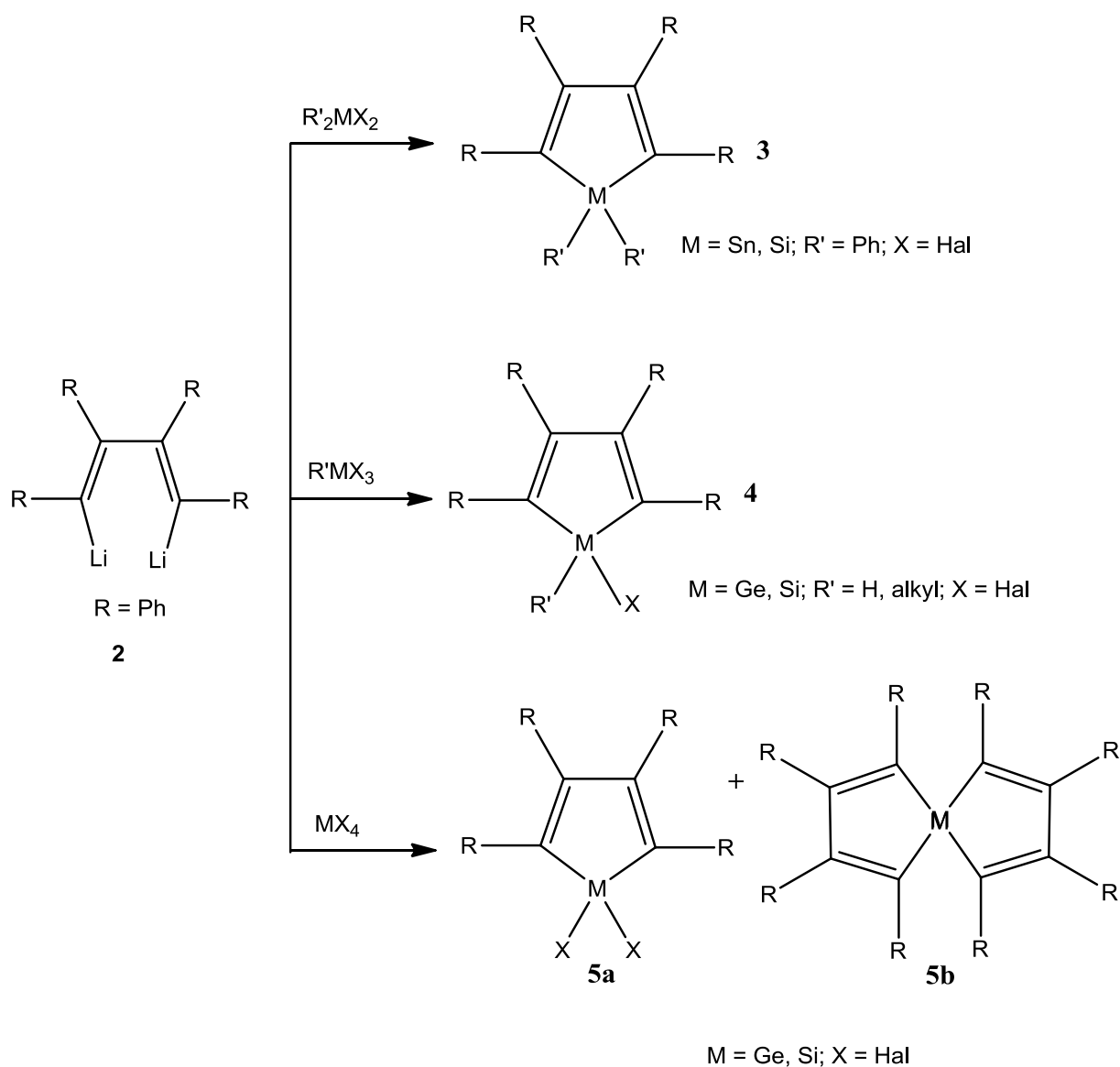
Figure 1.4 Structural factors that affect the HOMO-LUMO gap of linear π -conjugated systems.¹²

E_{Res} confines the delocalization of π -electrons within the aromatic ring while the E_{θ} between the consecutive units limit the π -electrons along the conjugated backbone. The E_{Sub} directly modulates the energy levels based on the electron withdrawing or donating substituents. When individual molecules or polymer chains are assembled into a material, the E_{Int} can affect the magnitude of the molecules of the energy gap because each polymer chain experiences weak intermolecular interaction.¹² Therefore, the five energy gap influencers of E_{BLA} , E_{Res} , E_{Sub} , E_{θ} , and E_{Int} are essential parameters to synthetic approaches for conjugated polymer synthesis.¹²

1.2 Stannoles and Other Group 14 Heteroles

There are several known routes to five-membered heterocycles that incorporate heavier group 14 elements such as tin. The first successful synthesis and isolation of a

stannole and its silole analogue was carried out by Braye and Hubel back in 1950's where 1,1,2,3,4,5-hexaphenyl-1H-metalloles were prepared through the reaction of 1,4-dilithiotetraphenylbutadiene with Ph_2MCl_2 ($\text{M} = \text{Si}, \text{Sn}, \text{Ge}, \text{Pb}$)^{8,13} (Scheme 1.1, 3).



Scheme 1. 1 Synthesis of stannole and related ring systems.⁸

This route has been extended by Jutzi and Mitzel where 1-haloheteroles (Scheme 1.1, 4) are synthesized in a similar fashion from the dilithio precursor and trihalo-silanes and -germanes.⁸ Reactions of GeCl_4 or SiCl_4 with **2** leads to a mixture of products including the low yielding spirocyclic compounds **5b**, and the desired heterole **5a** (Scheme 1.1). Fagan and Nugent have also reported on the conversion of zirconacyclopentadienes into stannoles.¹³

Previous studies suggest that the majority of these routes are applicable only to heavily substituted heteroles because less sterically encumbered species are more likely to undergo Diels Alder dimerization.⁸ In order to suppress this process, the incorporation of alkyl groups at the 3- and 4- positions of the metalloles is recommended. The nature of various substituents at 3- and 4-positions can also affect the characteristics of the metalloles besides the metal atom on the conjugated system.⁸

1.3 Boron and Boroles

1.3.1 Boron

Boron has three important features or properties that make it a good candidate for incorporation into π -conjugated materials: (i) the formation of trivalent boron compounds with trigonal planar geometry, (ii) Lewis acidity resulting from empty p-orbital that can act as an electron acceptor site, and (iii) the ability to participate in extensive $\text{P}_\pi\text{-}\pi^*$ conjugation due to its empty p-orbital.¹⁴

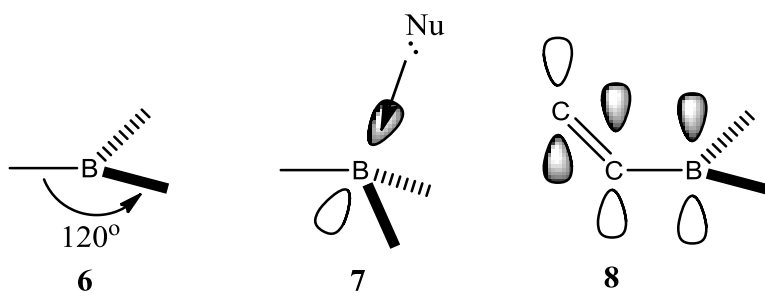


Figure 1.5 Boron: trigonal planar geometry (6), Lewis acidity and adduct formation (7) and $P_{\pi}-\pi^*$ conjugation (8). (Nu = Nucleophile).¹⁴

Boron can participate in $P-\pi$ conjugation with its vacant p-orbital¹⁴ overlapping with the π molecular orbitals of a neighbouring carbon when incorporated in conjugated frameworks. The inclusion of boron in a conjugation results in unique absorption and emission spectra, a lower reduction potential that provides a suitable material for n-doping (doped by reduction) and good electron-transporting properties.¹⁵

1.3.2 Boroles

Boroles are anti-aromatic species which incorporate boron into a five membered ring that is isoelectronic to the cyclopentadienyl cation.¹⁶ Boroles are capable of accepting two electrons into the empty p-orbital of boron.¹⁷ For example, when complexed with bases such as amines, boroles become more stable due to the breakup the anti-aromatic system.

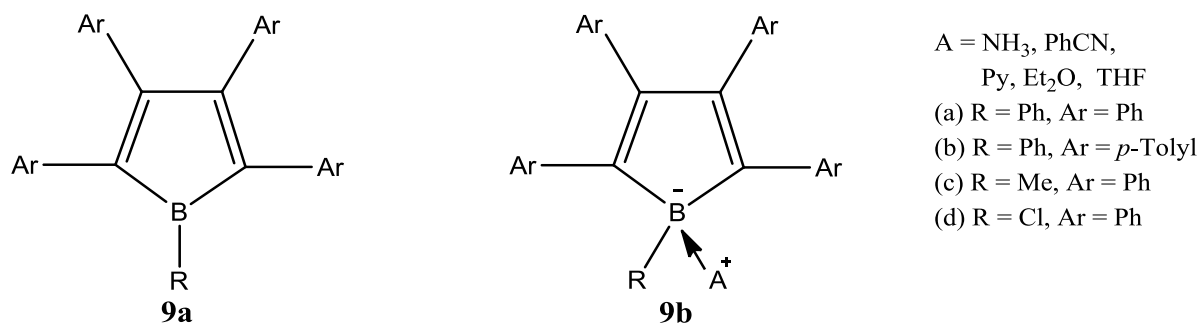
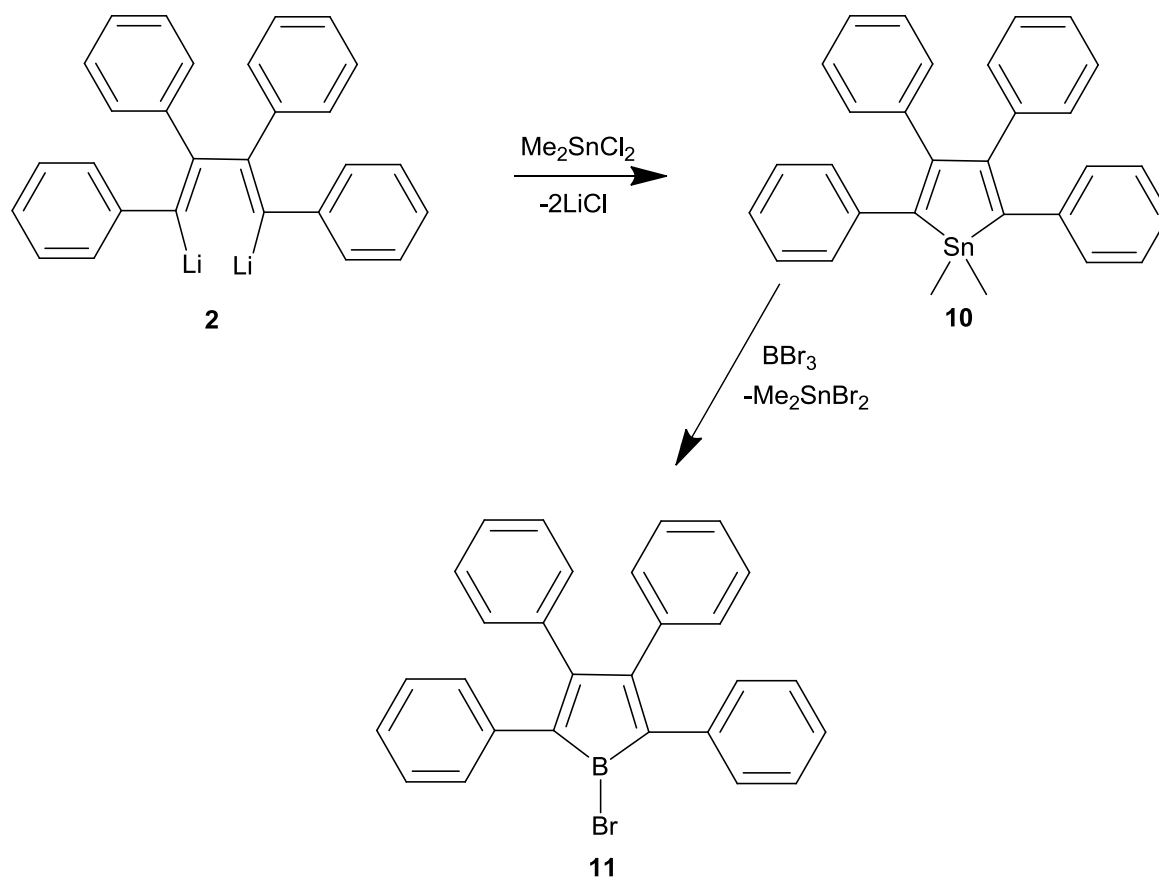


Figure 1.6 Pentaarylbaboroles and adducts.¹⁷

Synthetic routes to boroles are rather limited due to their highly reactive nature. The first monomeric borole **9a** was isolated in 1961.¹⁷ This simple borole was stabilized with different Lewis-base ligands (**9b**) including NH₃, PhCN, Py, Et₂O, and THF to form stable adducts.

Further studies of boroles continued and in 1986, Eisch and coworkers synthesized 1-chloro-2,3,4,5-tetraphenylborole (*via* metal-tin metathesis reactions) using lithiated dienes by first forming stannole intermediates, **10**, thus providing an important general route to a variety of boroles.¹⁸ This work was a modification of previous report by Eisch in 1969.¹⁸ Recently, Braunschweig¹⁶ and coworkers synthesized and isolated the free 1-bromo-2,3,4,5-tetraphenylborole and its adduct form with THF using the methodology used by Eisch and coworkers.¹⁸

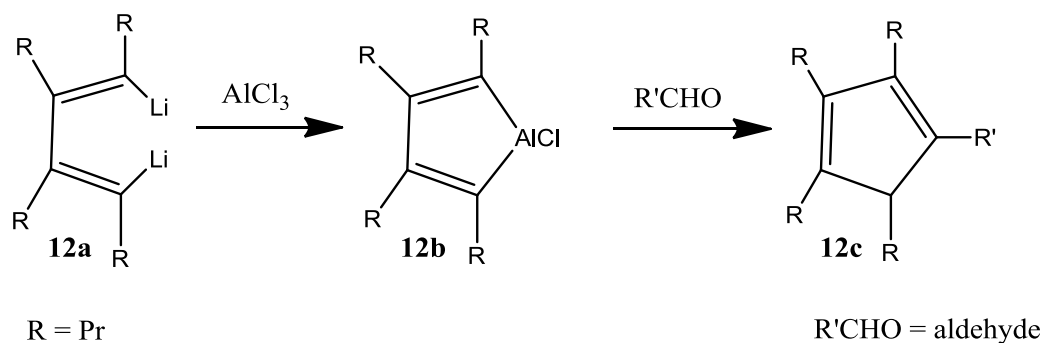


Scheme 1. 2 Synthesis of 1-bromo-2,3,4,5-tetraphenylborole *via* stannole intermediate.¹⁶

1.4 Aluminole, Gallole and Indacyclopentadiene

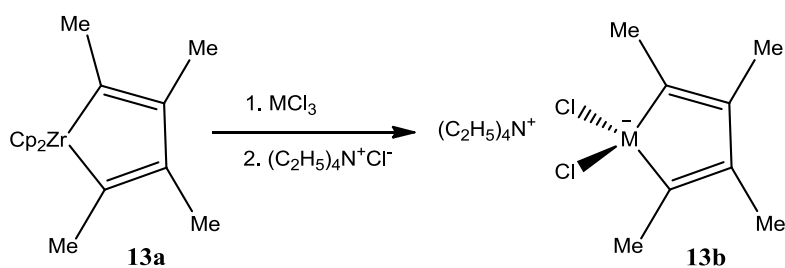
Aluminoles, galloles and indacyclopentadiene are borole analogs where the boron atom has formally been replaced by aluminum, gallium and indium, respectively. Only one aluminole, pentaphenylaluminacyclopentadiene, has ever been isolated.¹⁹ This compound was synthesized from the reaction of 1,4-dilithio-1,2,3,4-tetraphenylbutadiene with Cl_2AlPh as an Et_2O adduct and was analyzed by X-ray crystallography. In 2003, Xi and coworkers were able to synthesize chloro-aluminacyclopentadiene **12b** from 1,4-dilithio-1,3-dienes **12a** and AlCl_3 . However, **12a** was not isolated, but rather used as an

intermediate which was further reacted with aldehydes yielding a variety of substituted cyclopentadienes **12c**.²⁰



Scheme 1.3 Synthesis of chloro-aluminacyclopentadiene from 1,4-dilithio-1,3-dienes and AlCl_3 .²⁰

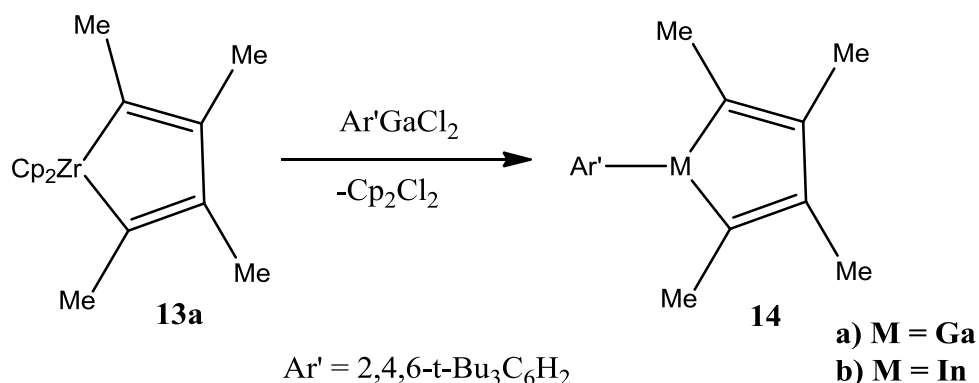
Other classes of Group 13 heteroles that have received less attention than boroles are galloles and indacyclopentadiene. Fagan and Nugent have developed a general synthetic route that utilizes metallacycle transfer of a carbon fragment from zirconacyclopentadiene and were able to synthesize and isolate the gallole salt **13b** (Scheme 1.4).²¹



Scheme 1.4 Metallacycle transfer from zirconium.²¹

Cowley and coworkers were able to synthesize organogalla- **14a** and indacyclopentadienes **14b** from the zirconium metallacycle **13a**. In order to avoid self-dimerization of **14a** and **14b**, Cowley and coworkers attached a bulky supermesityl (2,4,6-tri-*tert*-butylphenyl) substituent at the heterole atom which sterically protects the empty p-orbital of the heteroatoms (Scheme 1.5).²⁰

The structure of **14a** was verified using x-ray crystallography analysis which revealed two independent planar molecules packed within the symmetric unit.²⁰



Scheme 1.5 Utilizing a bulky aryl gallium dichloride strategy to obviate dimerization.²⁰

1.5 Molecular Modeling

Molecular modeling has become an important tool for synthetic chemists. It provides a pictorial interpretation of molecular orbital electron distributions and their electrostatic potentials.²² For example, potential energy surfaces can be analyzed using the coordination between energy and structure obtained from a modeling program. This could potentially unveil critical thermodynamic and kinetic information as well as molecular

equilibrium and transition state geometry.²² It is often possible to create visual presentations of a molecule's likely conformation even without crystallographic analysis, synthesis or isolation.

Creation of modeling software can be challenging due to the exactness of the Schrodinger equation (a mathematical equation resulting from the application of quantum mechanics to chemistry). The Schrodinger equation can only be solved for a one electron system such as hydrogen. As a result, the modeling of more complex molecular structures and resultant properties cannot be fully solved. Therefore, approximations are made to provide a more practical method. Severe approximations can, however, potentially lead to methods that do not provide accurate information. The more accurate a method is the more computationally expensive it will be.²² However, since there is no ideal method for all applications, a balance between cost and accuracy must be found.

In 1950's, a Hartree-Fock approximation was applied to help solve a multiple electron systems model. After much trial and error, Hartree-Fock models (except for transition metals involved) were shown to provide useful kinds of thermochemical comparisons, yet poorly accounted for explicit bond making and breaking. Improvements to the Hartree-Fock model have now been established using the Møller-Plesset, density functional and semi-empirical models. The Møller-Plesset model is an excellent model to analyze equilibrium geometries, conformations and the reaction thermochemistry for bond breaking and making. Density functional models and semi-empirical models do a nearly

similar task to Møller-Plesset model, except that the latter also includes transition-metals, however these are not satisfactory for conformational and thermochemical calculations.²²

Models such as Hartree-Fock, Density Functional and Møller-Plesset use Gaussian type functions. Gaussian basis sets are used widely and documented thoroughly.²² The simplest atomic orbital representations are called a minimal basis set and contain functions that only require accommodation of the total electron count for the atom, at the same time maintaining its overall spherical symmetry. For example, hydrogen and helium have a single (1s) function while atoms from lithium to neon have five functions (1s, 2s, 2p_x, 2p_y, and 2p_z).²²

Table 1. 1 All-electron Gaussian basis sets in Spartan.²²

Basis set	Available elements
6-31G*, 6-31G**	H-Kr
6-31+G*, 6-31+G**	
6-31++G*, 6-31++G**	
6-311G*, 6-311G**	H-Ar
6-311+G*, 6-311+G**	
6-311++G*, 6-311G**	
cc-pVDZ	H-Ar, Ga-Kr
cc-pVTZ	
cc-pVQZ	

The basis sets shown in Table 1.1 can be supplemented with polarization to make them suitable for correlated models such as the Density Functional and Moller-Plesset models and give lower energy for representative molecule. For example, the simplest polarization basis sets are 6-31G* and 6-311G* which are constructed from the 6-31G and 6-311G basis sets respectively, by adding a set of d-type polarization functions. The basis sets that are designated by “+” as in 6-311+G** or 6-311++G** could be used to calculate anions to accommodate the extra electrons that may be loosely associated with atoms. Basis sets such as cc-pVDZ, cc-pVTZ and cc-pVQZ, (correlation consistent-polarized Valence Double, Triple Quadruple, and Zeta) respectively are formulated to calculate the lowest possible ground state atom energies. These basis sets do better in capturing the correlation energy for free atoms than basis set with “*”.²² In general, it is important to compare both the models and basis sets for a given calculation since no method will be perfect for all applications.

1.6 Aim of This Work

This thesis targets the synthesis of π -conjugated group 13 heteroles **15** (**a** = 1-chloro-2,3,4,5-tetraphenylborole, **b** = 1-chloro-2,3,4,5-tetraphenylaluminol, and **c** = 1-chloro-2,3,4,5-tetraphenylgallole), monomer **16a** and the attempted synthesis of polymer **17a** *via* replacement of the tin atom in a stannole moiety. Compounds of **15** form an adduct through the vacant p-orbital of the metal center by accepting a lone pair from Lewis-bases of Et₃N, THF and Et₂O. As well, the synthesis of polymer **17a** and its THF adduct will be investigated.

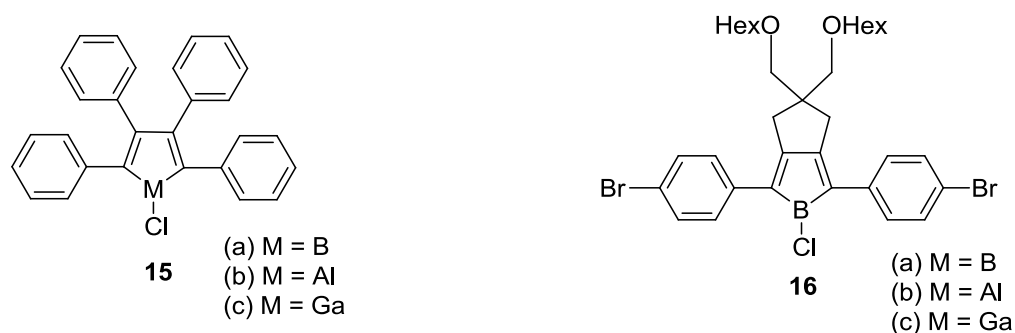
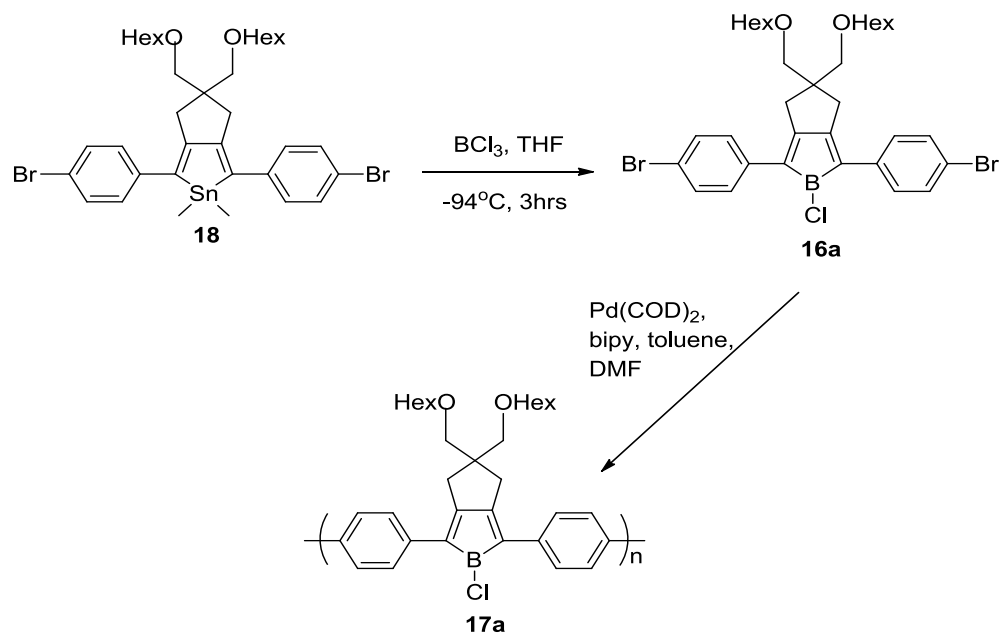


Figure.1.7. Heteroles **15a-c** and **16a-c**.

The synthetic pathway to polymer **17a** (Scheme 1.6) was analogous to the preparation of poly (2,5-diphenylgermoles) *via* zirconocene coupling of 4,4-*bis*(hexyloxymethyl)-1,7-bis-*p*-halophenyl-1,6-heptadiynes reported by Tilley and coworkers.²³ Tilley's approach to monomer synthesis was a modification of Fagan and Nugent metallacycle transfer from zirconium to germanium.²¹



Scheme 1. 6 Polymerization of **17a**.

Theoretical studies were also performed for heteroles and oligometric heteroles using Spartan 10 software at the B3LYP/6-31 G* level in order to evaluate the general feasibility of a synthetic approach and alteration of the heteroatom. Influence of the heteroatom on the energy gap as well, the influence of Lewis-base adduct formation on the energy gap were analyzed. The energy gaps were evaluated with DFT on the basis of calculated HOMO and LUMO levels. DFT also was used to analyze the molecules electron density to see which orbital is responsible as reaction center.

CHAPTER 2

MATERIALS AND METHODS

Materials

All reagents and chemicals were obtained from Aldrich. Me_2SnCl_2 was purchased from Gelest Inc. Organometallic reagents were stored and handled under an N_2 atmosphere in a glovebox or using Schlenk techniques. Dry hexane, THF, and Et_2O were obtained from solvent system that delivered solvents under N_2 . Et_3N and DMSO were taken from sure seal bottles under N_2 . MeOH was used without further purification.

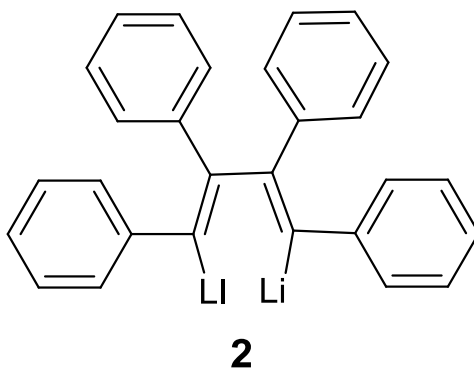
Equipment and Characterization

^1H NMR (400 MHz), ^{13}C $\{^1\text{H}\}$ NMR (100.6 MHz), ^{119}Sn NMR (149 MHz) and ^{11}B $\{^1\text{H}\}$ NMR (160.46 MHz) were recorded on Bruker Avance 400 MHz spectrometer. ^1H spectra were referenced to the deuterated solvents peaks, ^{13}C spectra were referenced internally to the deuterated solvent resonances that are referenced to SiMe_4 ($\delta = 0$ ppm), ^{119}Sn spectra were referenced to SnMe_4 ($\delta = 0$ ppm) and ^{11}B NMR were referenced to $\text{BF}_3\cdot\text{OEt}_2$. Infrared spectra were recorded on Perkin Elmer Spectrum One. Molecular weight of polymer was determined by Gel Permeation Chromatography (GPC) using Viscotek Triple Model 302 Detector with a Refractive Index Detector (RI), a right angle (90°) laser light scattering detector ($\lambda_0 = 670$ nm) and a low angle

(7°) laser light scattering detector, and a four capillary differential viscometer (VISC). Theoretical calculations were done by Spartan 10 software at the B3LYP/6-31G* level of Density Functional Theory.

Experimental

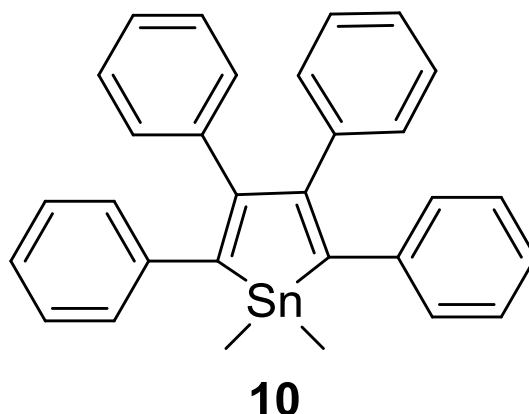
2.1 Synthesis of 1,4-Dilithio-1,2,3,4-tetraphenylbutadiene [2]



In a typical reaction, diphenylacetylene (5.0 g, 28.0 mmol) was dissolved in 37 mL of Et₂O in 250-mL Schlenk flask. A lithium wire (0.2 g, 34.0 mmol) was added to the solution under argon gas. The lithium wire was washed with hexane to remove the mineral oil in which it was conserved. After 30 min of vigorous stirring, the colorless reaction mixture changed to scarlet color. At this point the unreacted lithium wire was picked out while stirring continued for 2 hrs. The mixture was added *in situ* for the preparation of **10** (see section 2.2).²⁴

For **2**: ^1H NMR (400 MHz, CDCl_3) δ_{H} 6.52-7.52 (m, C_6H_5) ppm. ^{13}C $\{^1\text{H}\}$ NMR (100 MHz, CDCl_3) δ_{C} 125.61, 126.06, 126.13, 126.42, 126.84, 126.90, 127.50, 130.02, 131.23, 131.50 (Ar) ppm.

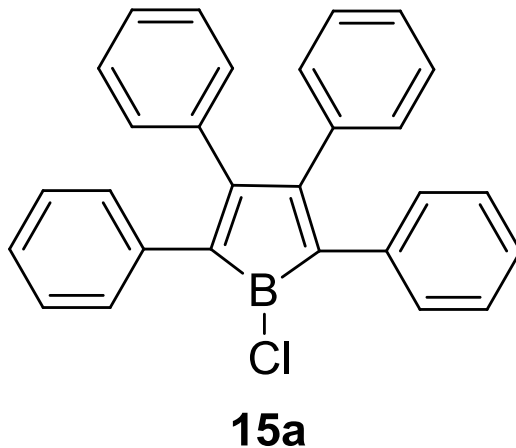
2.2 Synthesis of 1,1-Dimethyl-2,3,4,5-tetraphenylstannacyclopentadiene [10]



In a 100-mL round bottom flask Me_2SnCl_2 (7.5 g, 34.0 mmol) was dissolved in 40 mL of THF under nitrogen. The mixture was then slowly added to a *in situ* solution of **2** (≈ 28.0 mmol) in Et_2O . Upon addition, the scarlet color of dilithio mixture turned into transparent amber color. The solvent was removed *in vacuo*.²⁴ The residue was washed (3 x 10 mL) with EtOH to remove residual tin halides and LiCl. The crude product was purified by recrystallization from CH_2Cl_2 in air.²⁵ This was in good agreement with the published literature.²⁴

For **10**: Yield 61%. m.p. 186-188°C. ^1H NMR (400 MHz, CDCl_3) δ_{H} 0.73 (s, 6H, CH_3), 6.94-7.29 (m, 20H, C_6H_6) ppm. ^{13}C $\{^1\text{H}\}$ NMR (100 MHz, CDCl_3) δ_{C} -7.72 ($\text{Sn}-\text{CH}_3$), 125.03, 125.62, 127.23, 127.81, 128.26, 130.30, 140.81, 143.07, (C_6H_6), 144.96 ($\text{C}-\text{Sn}$), 153.62 ($\text{C}=\text{C}-\text{Sn}$) ppm. ^{119}Sn NMR (149 MHz, CDCl_3) δ_{Sn} 52.81 ppm.

2.3 Synthesis of 1-Chloro-2,3,4,5-tetraphenylboracyclopentadiene [**15a**]



To 100-mL Schlenk flask, pure crystals of stannole **10** (1.0 g, 2.1 mmol) was dissolved in 25 mL of hexane. To this, (0.5 mL, 0.6 g, 5.1 mmol) of BCl_3 (liquid in hexane) was added under N_2 atmosphere at 0 °C and the mixture immediately changed to a dark red color. After 3 hrs, the reaction was stopped and the solvent removed *in vacuo*. The residue was further washed with cold hexane and again the solvent removed under reduced pressure.

In a typical reaction, the entire product of **15a** was dissolved in 3 mL of cold hexane (0 °C). Coordinating solvents such as Et_3N and Et_2O (1 ml each) were added dropwise to 1 ml solution of **15a** over 1 min in separate flasks. Immediate color changes were observed from dark red to yellowish (in the case of Et_2O), or a clear solution with a small amount of white precipitate (upon addition of Et_3N) then the solvent was removed under reduced pressure. In the ^1H NMR spectra, the integrations for the number of protons of the ligands were not consistent with the structures. In the case of **15a**· Et_2O , the multiplicity of the chemical shifts were not consistent either. In both ^1H

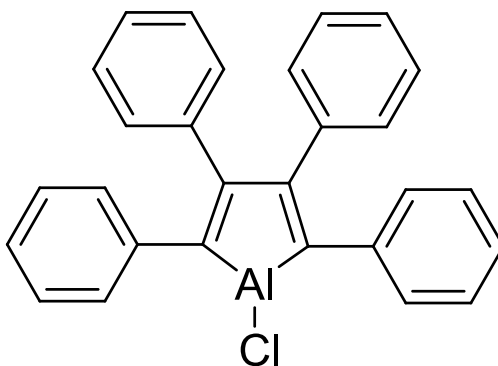
and ^{13}C NMR spectra, other impurities were observed besides the expected ligand signals.

For 15a: Yield; 63% (crude), ^{11}B { ^1H } NMR (160.46 MHz, CDCl_3) δ_{B} 26.15 (b, B- CH_2) ppm. ^1H NMR (400 MHz, CDCl_3) δ_{H} 7.19-7.39 (m, C_6H_5) ppm. ^{13}C { ^1H } NMR (100 MHz, CDCl_3) δ_{C} 120.42, 122.34, 123.82, 125.01, 126.50, 127.78, 130.66, 132.59, 134.83, 165.89 (C_6H_5) ppm.

15a· Et_3N : off white colour: ^{11}B { ^1H } NMR (160.46 MHz, CDCl_3) δ_{B} 34.95 (b, B- NEt_3) ppm. ^1H NMR (400 MHz, CDCl_3) δ_{H} 1.72 (t, $-\text{CH}_3$), 2.40 (q, N- CH_2), 7.09-7.21 (C_6H_5) ppm. ^{13}C { ^1H } NMR (100 MHz, CDCl_3) δ_{C} 9.80 (CH_3), 50.35 (CH_2) 116.89, 119.46, 121.38, 123.944, 126.18, 127.95, 130.02, 131.95, 133.55, 163.33 (C_6H_5) ppm.

15a· Et_2O light yellow colour: ^{11}B { ^1H } NMR (160.46 MHz, CDCl_3) δ_{B} 32.07 (b, B- OEt_2) ppm. ^1H NMR (400 MHz, CDCl_3) δ_{H} 1.40 (m, $-\text{CH}_3$), 3.76 (m, O- CH_2), 7.36-7.65 (C_6H_5) ppm. ^{13}C { ^1H } NMR (100 MHz, CDCl_3) δ_{C} 14.73 (CH_3), 66.09 (CH_2), 116.89, 118.81, 120.74, 122.98, 124.58, 126.50, 128.74, 130.34, 133.55, 164.61 (C_6H_5) ppm.

2.4 Synthesis of 1-Chloro-2,3,4,5-tetraphenylaluminacyclopentadiene [15b]



15b

To 100-mL Schlenk flask, pure stannole crystal **19** (1.0 g, 2.1 mmol) was dissolved in 25 mL of hexane. (0.6 g, 5.1 mmol) AlCl_3 solid was added under N_2 at 0 °C and the mixture changed into dark red color. After 3 hrs, the reaction stopped and the solvent was removed *in vacuo*. The residue was further washed with cold hexane and again the solvent was removed under reduced pressure.

In a typical reaction, the entire product of **15b** was dissolved in 3 mL of cold hexane (0 °C). Coordinating solvents such as THF and Et_2O (1 ml each) were added dropwise to the solution of **15b** over 1 minute in separate flasks. Immediate color changes were observed from dark red to yellowish (in both cases of THF and Et_2O), then the solvent was removed under reduced pressure. In the ^1H NMR spectra, the integrations for the number of protons of the ligands were not consistent with the structures. In both ^1H and ^{13}C NMR spectra, other impurities were observed besides the expected ligand signals.

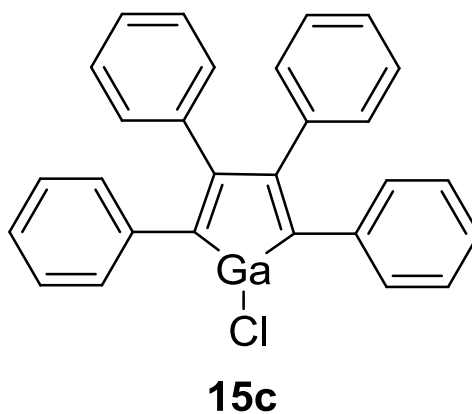
For 15b: Yield; 68 % (crude), ^1H NMR (400 MHz, CDCl_3) δ_{H} 7.48-7.65 (m, C_6H_5) ppm.

^{13}C $\{^1\text{H}\}$ NMR (100 MHz, CDCl_3) δ_{C} 123.01, 124.85, 132.69, 135.63, 137.60, 140.54, 143.15, 146.42, 148.71, 164.72 (C_6H_5) ppm.

15b•THF light yellow colour: ^1H NMR (400 MHz, CDCl_3) δ_{H} 1.80 (m, CH_2), 3.72 (m, O- CH_2), 7.09-7.22 (m, C_6H_5) ppm. ^{13}C $\{^1\text{H}\}$ NMR (100 MHz, CDCl_3) δ_{C} 23.56 (CH_2), 66.18 (CH_2O), 114.06, 116.02, 117.66, 120.60, 123.21, 125.05, 127.95, 128.77, 137.40, 162.24 (C_6H_5) ppm.

15b• Et_2O light yellow colour: ^1H NMR (400 MHz, CDCl_3) δ_{H} 1.23 (t, $-\text{CH}_3$), 4.23 (q, O- CH_2), 6.96-7.12 (m, C_6H_5) ppm. ^{13}C $\{^1\text{H}\}$ NMR (100 MHz, CDCl_3) δ_{C} 13.72 (CH_3), 55.21 (CH_2), 123.54, 125.56, 128.50, 129.29, 133.02, 135.63, 138.27, 138.27, 142.50, 145.11, 163.74 (C_6H_5) ppm.

2.5 Synthesis of 1-Chloro-2,3,4,5-tetraphenylgallacyclopentadiene [15c]



To 100-mL Schlenk flask, pure stannole crystal **19** (1.0 g, 2.1 mmol) was dissolved in 25 mL of hexane. (0.9 g, 5.1 mmol) GaCl_3 solid was added under nitrogen atmosphere and at 0°C the mixture changed into dark red colour. After 3 hrs, the reaction stopped and the

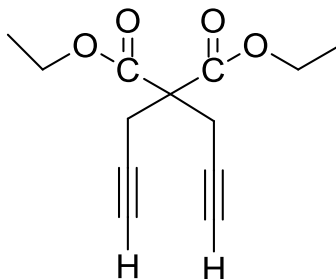
solvent was removed *in vacuo*. The residue was further washed with cold hexane and again the solvent was removed in reduced pressure.

In a typical reaction, **15c** was dissolved in 3 mL of cold hexane (0 °C). Coordinating solvent THF was added dropwise to the solution of **15c** over 1 minute. Immediate color changes were observed from dark red to yellowish upon addition of THF, and then the solvent was removed under reduced pressure. In the ^1H NMR spectra, the integrations for the number of protons of the ligands were not consistent with the structures. In both ^1H and ^{13}C NMR spectra, other impurities were observed besides the expected ligand signals.

For **15c**: Yield; 72 % (crude), ^1H NMR (400 MHz, CDCl_3) δ_{H} 7.41-7.53 (m, C_6H_5) ppm. ^{13}C $\{^1\text{H}\}$ NMR (100 MHz, CDCl_3) δ_{C} 122.19, 123.07, 124.16, 125.04, 126.14, 127.24, 128.33, 130.75, 136.89, 160.58 (C_6H_5) ppm.

For **15c**·THF slight yellow colour: ^1H NMR (400 MHz, CDCl_3) δ_{H} 1.85 (m, CH_2), 3.74 (m, O- CH_2), 7.15-7.29 (m, C_6H_5) ppm. ^{13}C $\{^1\text{H}\}$ NMR (100 MHz, CDCl_3) δ_{C} 24.21 (CH_2), 67.25 (CH_2O), 117.85, 120.10, 122.34, 124.26, 126.18, 127.78, 129.06, 130.66, 135.47, 157.89 (C_6H_5) ppm.

2.6 Synthesis of Diethyl Dipropargylmalonate (DEDPM) [21]

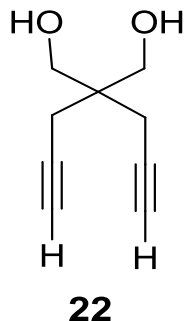


21

Diethyl malonate (2.0 g, 12.5 mmol) was added to sodium ethoxide (from sodium, 0.6 g, 27.5 mmol and absolute ethanol 10 mL) in 250-mL round bottom flask. After 5 mins, propargyl bromide (3.3g, 27.5 mmol) was slowly added to the stirred suspension and heated for 12 hrs at 60°C. The alcohol was removed under reduced pressure and the residue was diluted with 10 mL water. The mixture was transferred into separatory funnel where it was shaken with 3 x 5 mL hexane. The hexane layer was kept and upon evaporation of the solvent with vacuum, diethyl dipropargylmalonate (2.4 g, 10.5 mmol) was obtained in needle form.²⁶

For 21: Yield; 83 %. mp 45-47 °C. ¹H NMR (400 MHz, CDCl₃) δ_H 1.26 (t, ³J = 7.1 Hz, 6H, -CH₃), 2.03 (t, ⁴J = 2.6 Hz, 2H, ≡C-H), 2.99 (d, ⁴J = 2.6, 4H, CH₂-C≡), 4.24 (q, ³J = 7.1 Hz, 4H, CH₂-O) ppm. ¹³C { ¹H } NMR (100 MHz, CDCl₃) δ_C 13.98 (-CH₃), 22.48 (CH₂C≡), 56.24 (-C-), 62.05 (-OCH₂-), 71.04 (≡C-H), 78.43 (-C≡), 168.58 (C=O) ppm. IR (neat, KBr, cm⁻¹) 3300 (≡C-H), 1700 (C=O).

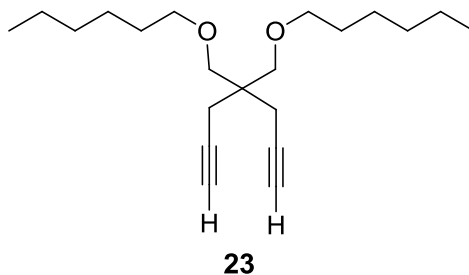
2.7 Synthesis of 4,4-Bis(hydroxymethyl)-1,6-heptadiyne [22]



Diethyl dipropargylmalonate (2.0 g, 8.4 mmol) **21** was dissolved in 4.8 mL of Et₂O in 100mL Schlenk flask. The flask was charged with nitrogen and placed in ice bath. The solution was added dropwise over a period of 1 hour to a suspension of lithium aluminum hydride (LiAlH₄) (0.5 g, 12.4 mmol) in 18 mL of Et₂O that was placed in ice bath as well under nitrogen atmosphere. The reaction was stirred for 6 hrs. Water was added dropwise to the grey suspension until it turned white and evolution of H₂ was ceased. Et₂O was removed under reduced pressure and the residue was diluted with 30 mL of water. The solution was then placed in 500 mL separatory funnel and extracted with (3 x 15 mL) of Et₂O. The organic layer was dried over magnesium sulfate (MgSO₄). After filtering off the MgSO₄, the Et₂O was removed *in vacuo* to give a white solid and it was recrystallized from Et₂O at room temperature.²⁷

For 22: Yield; 69 %. ¹H NMR (400 MHz, CDCl₃) δ 2.05 (t, ⁴J = 2.7 Hz, 2H, ≡C-H), 2.13 (brs, 2H, O-H), 2.38 (d, ⁴J = 2.7 Hz, 4H, CH₂-C_{quat}), 3.75 (s, 4H, CH₂-O) ppm. ¹³C {¹H} NMR (100 MHz, CDCl₃) δ_C 21.71 (CH₂C≡), 42.03 (C_{quat}), 66.57 (OCH₂), 71.19 (≡CH), 80.20 (-C≡). IR (neat, KBr, cm⁻¹) 3400-3300 (O-H), 1100 (C-O) ppm.

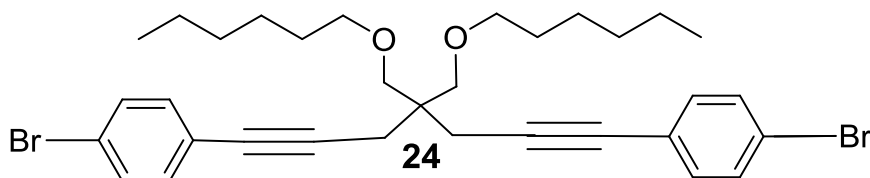
2.8 Synthesis of 4,4-Bis(hexyloxymethyl)-1,6-heptadiyne [23]



A 100-mL Erlenmeyer flask was charged with 4,4-*bis*(hydroxymethyl)-1,6-heptadiyne **22** (2.0 g, 13.1 mmol), 1-bromohexane (4.9 g, 30.0 mmol), KOH (3.0 g, 53.3 mmol), and DMSO (41.6 mL). The reaction mixture was stirred for 10 hrs at room temperature. The reaction mixture was then poured into a 500 mL separatory funnel along with 100 mL of water and extracted with Et₂O (3 x 125 mL). The solvent was removed by rotoevaporation. Then the residue was subjected to column chromatography on silica gel (20% EtOAc in hexanes) and colorless, oily product was obtained.²³

For 23: Yield; 80 %, ¹H NMR (400 MHz, CDCl₃) δ_H 0.89 (t, 6H, -CH₃), 1.26-1.37 (m, 12H, -CH₂-), 1.51-1.58 (apparent quintet, 4H, -CH₂-CH₂), 1.97 (t, ⁴J = 2.6 Hz, 2H, ≡C-H), 2.36 (d, ⁴J = 2.6 Hz, 4H, ≡C-CH₂), 3.38 (s, 4H, O-CH₂-C_{quat}), 3.41 (t, 4H, O-CH₂) ppm. ¹³C {¹H} NMR (100 MHz, CDCl₃) δ_C 14.05 (-CH₃), 21.87, 22.64, 25.80, 29.53, 31.66 (-CH₂-), 71.16 (C_{quat}), 70.26, 71.253 (O-CH₂), 71.98 (-C≡CH), 80.30 (CH≡C-) ppm. IR (neat, NaCl, cm⁻¹) 3311, 2955, 2930, 2860, 2798 (sp³ C-H str), 2119 (C≡C), 1465, 142 (CH₂ bends), 1377, 1115 (C-O str), 636.

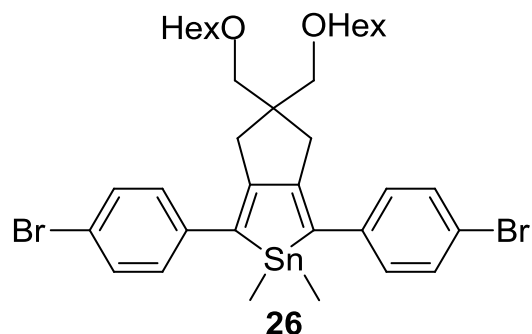
2.9 Synthesis of 4,4-Bis(hexyloxymethyl)-1,7-bis-*p*-bromophenyl-1,6-heptadiyne [24]



A 100-mL Schlenk flask was charged with 4,4-*bis*(hexyloxymethyl)-1,6-heptadiyne **23** (1.3 g, 6.6 mmol), 1-bromo-4-iodobenzene (3.6 g, 13.3 mmol), Pd(PPh₃)₄ (0.14 g, 0.12 mmol), and CuI (0.05 g, 0.26 mmol) was dissolved in 33 mL of THF under nitrogen atmosphere. After addition of 13 mL diisopropylamine, the reaction was stirred for 2 days. The white precipitate was filtered and the filtrate was washed with 5 mL of 10% NH₄OH, 5 mL of water, and 5 mL of brine. The filtrate was then dried over MgSO₄. After removing the solvent *in vacuo*, the brownish oily residue was subjected to column chromatography on silica gel. First the residue was eluted with hexane followed by mixture of (hexane/ethylacetate = 2:1) to obtain a colorless oil as 76% crude yield.²³

Isolation did not fully work since impurities were shown in both ¹H and ¹³C NMR spectra after column chromatography. No characterization data of ¹H is available. Crude ¹³C NMR is available in appendix.

2.10 Attempted Synthesis of $C_{35}H_{48}Br_2SnO_2$, [26]

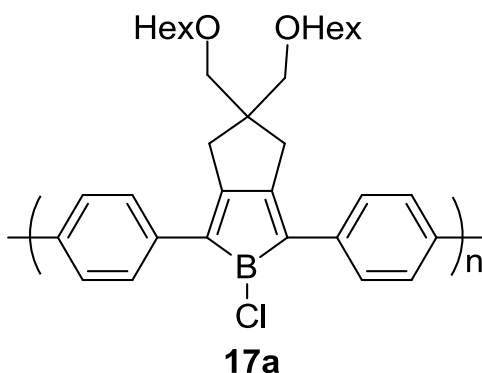


Method I: In a 100-mL Schlenk flask dimethyl tindichloride (2.0 g, 8.6 mmol) was dissolved in 10 mL THF. The solution was cooled to -98°C in MeOH and liquid N_2 bath. In a 250-mL Schlenk flask, $n\text{-BuLi}$ (5.7 mL, 1.0 M, 14 mmol) was added to cool (-98°C) solution of **24** (4,4-bis(hexyloxymethyl)-1,7-bis-*p*-bromophenyl-1,6-heptadiyne (3.0 g, 6.6 mmol in 7 mL dry THF) drop wise over a period of 5 mins under N_2 . After the solution was stirred at -98°C for 15 mins, the tin solution was dropwise added to it. The light yellow mixture was slowly warmed up to room temperature while it was stirred for 5 hrs and left *in situ*. ^{119}Sn NMR (149 MHz, CDCl_3) $\delta_{\text{Sn}} = 117.60$ ppm.

Method II: In a 100-mL Schlenk flask Cp_2ZrCl_2 (2.0 g, 7.3 mmol) was dissolved in 10 mL THF. The solution was cooled to -98°C in MeOH and liquid N_2 bath. In a 250-mL Schlenk flask, $n\text{-BuLi}$ (5.7 mL, 14.0 mmol) was added to to cool (-98°C) solution of **24** (4,4-bis(hexyloxymethyl)-1,7-bis-*p*-bromophenyl-1,6-heptadiyne) (3.0g, 6.6 mmol) in 6.6 mL dry THF drop wise over 5 min under nitrogen. After the solution was stirred at -98°C for 15 mins, the Cp_2ZrCl_2 solution was added slowly over 5 min period. The reaction slowly warmed up to room temperature while it was stirred for 4 hrs. Then Me_2SnCl_2 (2.0

g, 8.6 mmol) and CuI (0.16 g, 0.86 mmol) were added at 0°C. The light yellow mixture was further stirred for 3 hrs at room temperature and left *in situ*. ^{119}Sn NMR (149 MHz, CDCl_3) $\delta_{\text{Sn}} = 117.44$ ppm.

2.11 Synthesis of Polymer 17a·THF



In a 100-mL Schlenk flask, approximately 1.0 g stannacycle product **26** was dissolved in 30 mL hexane and BCl_3 (liquid in hexane) (1 mL, 1.0 g, 8.5 mmol) was added to it at -98°C in methanol and liquid N_2 bath under N_2 . The mixture turned a scarlet color upon addition. The reaction was stirred for 3 hrs. In separate 50-mL Schlenk flask, toluene (5 mL), DMF (10 mL), $\text{Pd}(\text{COD})_2$ (0.1 g, 0.5 mmol) and 2,2'-bipyridine (0.1 g, 0.5 mmol) were added under nitrogen atmosphere. The deep blue solution was covered with aluminum foil from light while it was heated at 60°C for 20 min. Then the blue solution was added to the 100-mL flask (monomer) at once with gas tight syringe and stirred for additional 3 hours while the color was changed to brownish. THF was added to the 100-mL flask and the polymeric material was stirred for 30 min. The polymer was pumped *in vacuo* to obtain a thicker consistency then dropwise precipitated into a 100-mL of rapidly stirred methanol. The precipitated polymer was dried in air then analyzed with NMR and

GPC. From ^{11}B NMR analysis in C_6D_6 , a single resonance was obtained at $\delta_{\text{B}} = 32.20$ ppm and was similar to monomer **16a** in CDCl_3 signal of $\delta_{\text{B}} = 30.96$ ppm. ^1H NMR analysis provided very broad signals between $\delta_{\text{H}} = 0.48\text{-}3.34$ ppm possibly substituents, solvents and impurities signals overlap and $\delta_{\text{H}} = 6.73\text{-}7.63$ ppm for phenyl regions. ^{13}C NMR analysis provided resonance signals at $\delta_{\text{C}} = 10.83\text{-}45.13$ ppm again could be from substituents, solvents and impurities and $\delta_{\text{C}} = 124.78\text{-}162.05$ ppm for phenyl regions. From GPC analysis, **17a**.THF gave $M_w = 55,000$ Da with PDI = 1.6.

CHAPTER 3

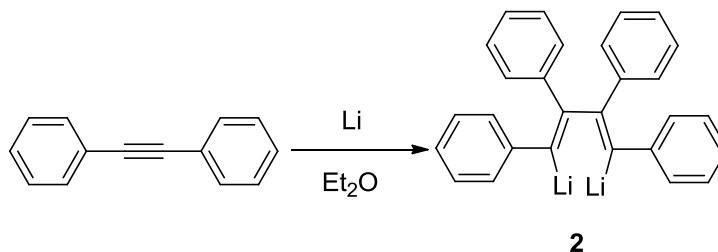
RESULTS AND DISCUSSION

3.1. Synthesis of 1-chloro-2,3,4,5-tetraphenyl monomer precursors

3.1.1 Synthesis of 1,4-dilithio-1,2,3,4-tetraphenylbutadiene, [2]

1,4-Dilithio-1,2,3,4-tetraphenylbutadiene, **2**, was synthesized *via* a modified approach based upon the work of Tracy and coworkers.²⁴ In the literature route, reaction mixtures were allowed to stir for 4 hrs before removal of excess lithium and then subsequently stirred for further 2 hrs. However, it was noted these longer reaction times could result in the formation of 2,3,4-triphenyl-1-naphthyl lithium as a byproduct. In order to prevent this side reaction, overall reaction time was reduced.

A solution of diphenylacetylene in Et₂O was added to a flask containing Li wire under argon (Scheme 3.1). Within 20-30 mins of stirring the clear transparent diphenylacetylene solution in Et₂O turned to an opaque dark red colour upon reaction with Li wire, indicating the formation of the dilithio dimer **2**.²⁴



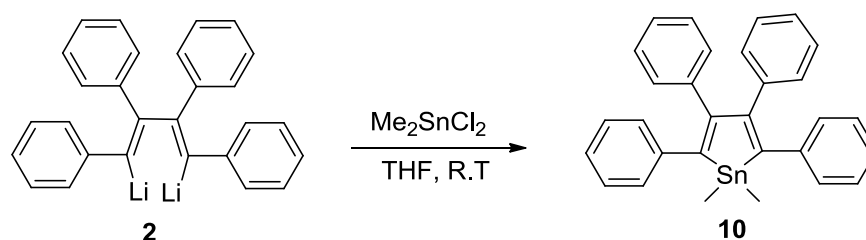
Scheme 3. 1. Synthesis of 1,4-dilithio-1,2,3,4-tetraphenylbutadiene, **2**.²⁵

In the literature preparation of **2**, the reaction mixture was allowed to stir for 4 hrs. In this research, after 2 hrs an aliquot of the reaction mixture was removed for ^1H NMR (CDCl_3) analysis, showing chemical shift data similar to literature values.²⁴ At this point, the excess Li (m) was removed to prevent the potential formation of 2,3,4-triphenyl-1-naphthyl lithium (a potential ring closure product observed after longer reaction times).²⁴ The other modification to the literature preparation was that subsequent to the removal of the unreacted Li (m), no further stirring of the mixture (1-2 hrs) was undertaken. Compound **2** was not isolated (because exhibited to show decomposition upon isolation),²⁵ and was used *in situ* for the proceeding step. ^1H NMR (CDCl_3) revealed resonance signals of **2** at $\delta_{\text{H}} = 6.30\text{-}7.50$ ppm as compared to diphenylacetylene (down shifted signals of diphenylacetylene due to triple bonds at $\delta_{\text{H}} = 7.22\text{-}7.41$ and 7.51 ppm respectively) phenyl regions. From the ^{13}C NMR (CDCl_3) analysis of **2**, 10 peaks were observed in the aromatic region with chemical shifts at $\delta_{\text{C}} = 125.61, 126.06, 126.13, 126.42, 126.84, 126.90, 127.50, 130.02, 131.23,$ and 131.50 ppm that are also consistent to the formation of **2** because there are two Ph environments. Even with the reduced reaction time, full consumption of the diphenyl acetylene starting materials was confirmed by the absence of acetylene carbon signals expected at $\delta_{\text{C}} = 89.43$ ppm.²⁴

3.1.2 Synthesis of 1,1-dimethyl-2,3,4,5-tetraphenylstannacyclopentadiene, [10]

1,1-Dimethyl-2,3,4,5-tetraphenylstannacyclopentadiene **10** was prepared through the *in situ* reaction of **2** from the previous step, following the procedure outlined by Tracy.²⁴ A solution of Me_2SnCl_2 in THF was added to a solution of **2** in THF at room

temperature in a 2:1 molar ratio (Scheme 3.2). The stoichiometric ratio must be carefully controlled because, as Tracy and coworkers noted²⁴ an excess of the dilithium reagent **2** is known to cause the formation of the spirostannole *bis*-(1,2,3,4-tetraphenyl-1,3-butadiene-1,4-ylidene). Similarly, an excess of Me_2SnCl_2 would result in the cleavage of the stannole ring from ethanolysis of Me_2SnCl_2 that generates HCl .²⁸



Scheme 3. 2 1, 1-dimethyl-2,3,4,5-tetraphenylstannacyclopentadiene, **10**.²⁵

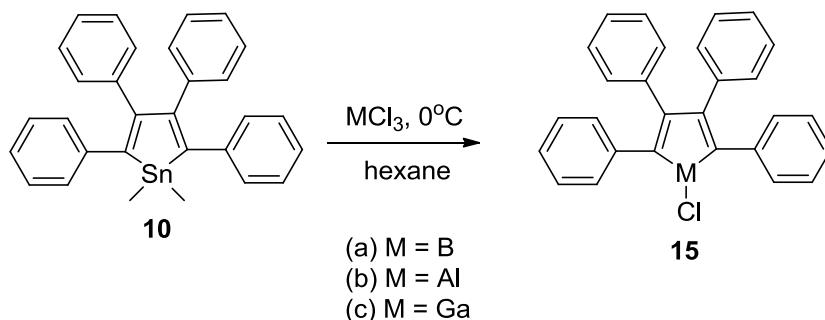
Upon addition of Me_2SnCl_2 , the red dilithio solution changed color to orange-amber, indicative of the formation of a stannole. The solvent and excess starting material were removed *in vacuo* and the resulting ^{119}Sn NMR (CDCl_3) analysis showed a singlet resonance signal for **10** at $\delta_{\text{Sn}} = 52.81$ ppm which is significantly upfield from the Me_2SnCl_2 ($\delta_{\text{Sn}} = \approx 144$). The observed ^{119}Sn shift does not appear to be consistent with values previously reported by Zuckerman for **10** ($\delta_{\text{Sn}} = -52.0$ ppm).²⁹ This difference could be simply a typographical error or the solvent, CH_2Cl_2 played a role to change the signal compared to the solvent the experimental sample ran in, CDCl_3 . In the ^1H NMR (CDCl_3), a singlet signal for the methyl proton at $\delta_{\text{H}} = 0.73$ (characteristic change versus starting material, **2**) and broad multiplet signal at 6.94-7.29 ppm for the overlapping aromatic protons with the expected relative integration of 6 and 20 (3:10) respectively was observed. In the ^{13}C NMR (CDCl_3), 11 resonance signals at $\delta_{\text{C}} = -7.72$

(Sn-CH₃), 125.03, 125.62, 127.23, 127.81, 128.26, 130.31, 140.81, 143.07, (C₆H₅), 144.96 (C-Sn), and 153.62 (C=C-Sn) ppm were obtained. ¹H and ¹³C NMR results were in agreement with previously reported literature values and structure of **10**. Compound **10** proved to be air-stable after recrystallization and was isolated as a yellow powder with an overall yield of 61% and 187°C melting point (both consistent with literature values).^{26 25}

3.2. Attempted Synthesis of 1-chloro-2,3,4,5-tetraphenyl Heteroles

The synthesis of **15a** (1-chloro-2,3,4,5-tetraphenylboracyclopentadiene), **15b** (1-chloro-2,3,4,5-tetraphenylaluminacyclopentadiene) and **15c** (1-chloro-2,3,4,5-tetraphenylgallacyclopentadiene) were all attempted through the addition of the corresponding MCl₃ (M = B, Al, Ga) to **10** solution in a 1.5:1 ratio in hexane at 0 °C under N₂ (Scheme 3.3). In all cases, an immediate colour change into dark red reaction mixtures was observed upon addition of MCl₃. The reactions were left to stir for 3 hrs while slowly warming to room temperature. After the removal of the solvent and any excess volatile materials *in vacuo*, the remaining residue was washed with cold hexane. The hexanes was removed *in vacuo* prior to performing NMR (¹H, ¹³C and ¹¹B where applicable) analysis for all compounds (Table 3.1).

3.2.1 Analysis of **15a** and Attempted Synthesis of Related Adducts



Scheme 3.3 1-chloro-2,3,4,5-tetraphenyl heteroles, **15(a-c)**.

For **15a**, ^{11}B NMR analysis showed a resonance signal at $\delta_{\text{B}} = 26.15$ ppm while ^1H NMR analysis revealed overlapping multiplet resonance signals in the aromatic region (see Table 3.1) consistent with the formation of the target borole. Further analysis by ^{13}C NMR revealed 10 resonance signals were observed at $\delta_{\text{C}} = 120.42, 122.34, 123.82, 125.01, 126.50, 127.78, 130.66, 132.59, 134.83,$ and 165.89 ppm and is consistent with the number of expected carbon environments in **15a**.

Attempts to isolate x-ray quality crystals of **15a** were unsuccessful therefore the potential synthesis of Lewis acid-base adducts **15a** was explored through the addition of coordinating solvents in an attempt to stabilize the system. In a typical reaction, **15a** was dissolved in 3 mL of cold hexane (0°C). Coordinating solvents such as Et_3N and Et_2O were added dropwise to the solution of **15a** over 1 minute. Immediate color changes were observed from dark red to yellow (in the case of Et_2O), or a clear solution with a small amount of white precipitate (upon addition of Et_3N). After removal of the solvent, NMR analysis of the resulting materials was by ^{11}B NMR show the adduct formation resulted in

downfield shift of the resonance signal versus **15a** (Table 3.1) suggesting coordination at boron. Curiously, for the ^1H NMR, the resonance signals for the aromatic protons observed in the Et_3N adduct of **15a** had shifted slightly upfield while for the ether adduct were shifted slightly downfield. In contrast, the ^{13}C NMR analysis showed that in both cases the aromatic resonance signals shifted upfield. These differences could potentially be due to the differences in base strength for the coordinating species.

Subsequent to the attempted preparation of **15a** and the corresponding adducts, it was discovered that Braunschweig³⁰ had reported on the synthesis of borole *via* the same approach. In this work, **15a** was isolated as deep blue crystals from toluene in a 87% yield. Unfortunately, ^{11}B NMR analysis reported for isolated **15a** showed a singlet resonance signal at $\delta = 66.4$ ppm was significantly upfield from the experimental value. In this work Braunschweig also prepared coordination adducts of **15a** with bases such as 4-Me- $\text{C}_5\text{H}_4\text{N}$ (Pry') in which the boron resonance signal was shifted significantly upfield to $\delta = 5.6$ ppm. One significant difference in the experimental procedure of Braunschweig was that the byproduct, Me_2SnCl_2 , was sublimed out of the crude product at 50 °C. Therefore, the differences observed in the NMR data compared to these literature values might be attributed to the presence of Me_2SnCl_2 which may be coordinating to boron in some fashion.

3.2.2 Analysis of 15b and 15c Attempted Synthesis of Related Adducts

Simultaneous to the preparation of **15a**, the same procedures were followed substituting for AlCl_3 and GaCl_3 in attempts to isolate the corresponding aluminole **15b**

and gallole **15c**. In both cases, the analysis of the crude products by ^1H NMR revealed the resonance signals for aromatic protons had shifted slightly downfield compared to the corresponding protons in **10**, suggesting a transmetallation had taken place. As with the borole counterpart, attempts to recrystallize **15b** and **15c** from a variety of solvents were unsuccessful.

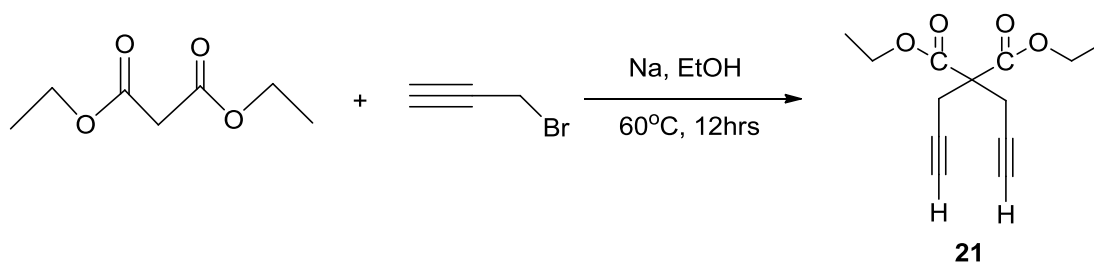
As with **15a**, coordinating solvents (Et_2O and THF) were added to the crude products in an attempt to isolate coordinated adducts of **15b** and **15c**. In all cases, ^1H NMR analysis showed slight upfield shifts for aromatic protons versus the crude products. This suggested that there may be coordination of the ethers to the metal centers. Table 3.1 summarizes the ^1H and ^{13}C NMR signals observed for the crude products containing **15b**, **15c**, and their corresponding adducts. However, as was the case with **15a**, failure to remove the Me_2SnCl_2 byproduct through sublimation may be interfering with attempts to isolate any of the compounds.

Table 3.1 NMR (CDCl₃) results of results of 1-chloro-2,3,4,5-tetraphenyl heteroles and adducts.

	Ligand	¹¹ B NMR (ppm)	¹ H NMR (ppm)	¹³ C NMR (ppm)
15a	none	26.15	7.19-7.39	120.42-165.89 (Ar)
	Et ₃ N	34.95	7.09-7.21	9.80 (CH ₃), 50.35 (CH ₂), 116.89-163.33 (Ar)
	Et ₂ O	32.07	7.26-7.56	14.73 (CH ₃), 66.09 (CH ₂), 116.89-164.61 (Ar)
15b	none	N/A	7.48-7.65	123.01-164.72 (Ar)
	THF	N/A	7.09-7.22	23.56 (CH ₂), 66.18 (CH ₂ O), 114.06-162.24 (Ar)
	Et ₂ O	N/A	6.96-7.12	13.72 (CH ₃), 55.21 (CH ₂), 123.54-163.74 (Ar)
15c	none	N/A	7.41-7.53	122.19-160.58 (Ar)
	THF	N/A	7.15-7.29	24.21 (CH ₂), 67.25 (CH ₂ O), 117.85-157.89 (Ar)

3.3. Synthesis of Monomer 16 Precursors

3.3.1 Diethyl Dipropargyl Malonate, [21]



Scheme 3.4 Diethyl dipropargyl malonate, **22**.²⁶

Compound **21** was prepared according to procedures described by Gal²⁶ by reaction of a 1:2.2:2.2 ratio of diethyl malonate: sodium ethoxide: propargyl bromide in ethanol (Scheme 3.4).

The reaction was stirred for 12 hrs at 60°C to ensure completion. After removal of EtOH under reduced pressure, the neutral fraction was separated and dissolved in hexane where colourless needle crystals of **21** formed.

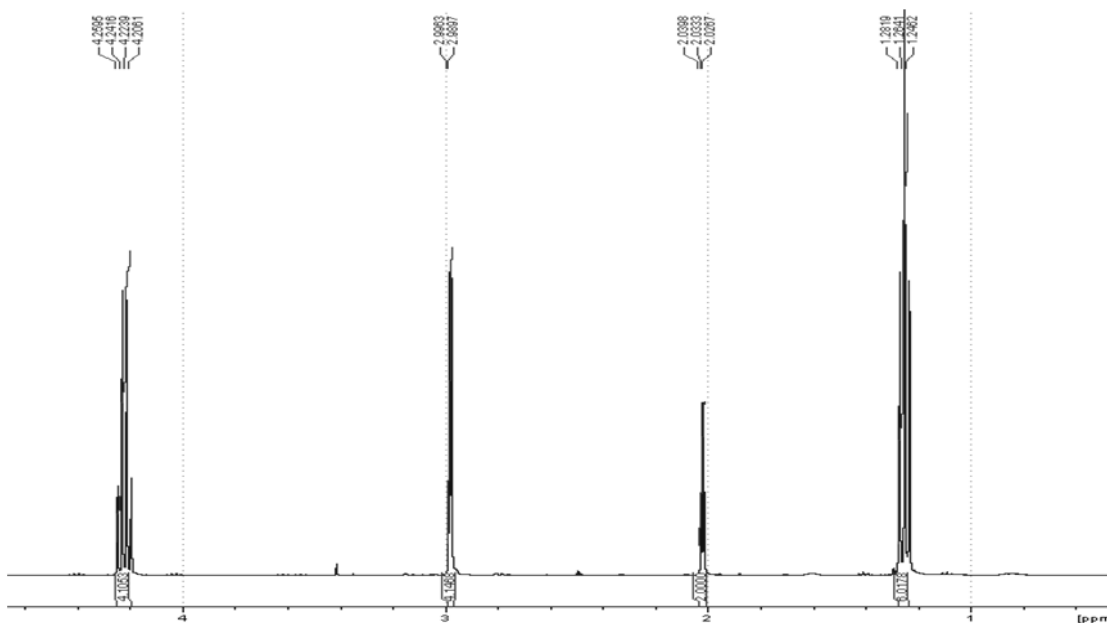


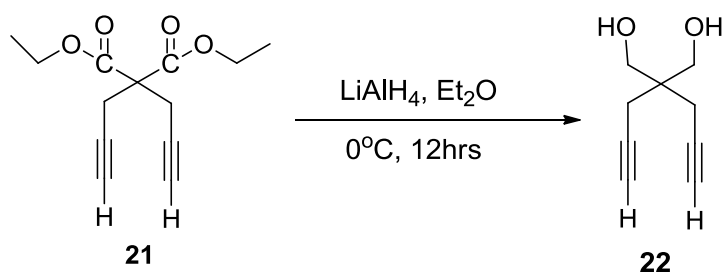
Figure 3.1 ^1H NMR spectra of Diethyl dipropargyl malonate **21**.

From the ^1H NMR analysis, four resonance signals were obtained: a triplet ($-\text{CH}_3$, $^3J = 7.1$ Hz) at $\delta_{\text{H}} = 1.26$ ppm, a triplet ($\equiv\text{C}-\text{H}$, $^4J = 2.6$ Hz) at $\delta_{\text{H}} = 2.03$ ppm, a doublet ($\text{CH}_2-\text{C}\equiv$, $^4J = 2.6$ Hz) at $\delta_{\text{H}} = 2.99$ ppm and a quartet (CH_2-O , $^3J = 7.1$ Hz) at $\delta_{\text{H}} = 4.24$ ppm. The coupling constant $^3J = 7.1$ Hz and the integration values of 6 and 4 respectively corresponds to the methyl and methylene protons of ester on the structure of **21**. Similarly, the coupling constant $^4J = 2.6$ Hz corresponds to the methylene ($\text{CH}_2-\text{C}\equiv$) and methine

($\equiv\text{C-H}$) protons coupling with integration of 4 and 2 respectively. Most importantly, there is no longer any significant signal observed for either the malonate methylene groups ($\text{O}=\text{C}-\text{CH}_2-\text{C}=\text{O}$ at $\delta_{\text{H}} = 3.36$ ppm) or propargyl bromide (CH_2-Br at $\delta_{\text{H}} = 3.30$ ppm) starting materials suggesting that the reaction had gone to completion. From the ^{13}C NMR analysis six resonance signals were obtained: at $\delta_{\text{C}} = 13.98$ ppm ($-\text{CH}_3$), 22.48 ppm ($\text{CH}_2-\text{C}\equiv$), 56.24 ppm (C_{quat}), 62.05 ppm ($-\text{O}-\text{CH}_2-$), 71.04 ppm ($\equiv\text{C-H}$), 78.43 ppm ($-\text{C}\equiv$), 168.58 ppm ($\text{C}=\text{O}$) respectively. Both ^1H and ^{13}C NMR results were consistent with the reported literature values for **21**. The overall yield of 83% was a slight improvement compared to the literature value (79%). The melting point of 45-47°C was consistent with the literature (46°C).²⁶

3.3.2 Synthesis of 4,4-bis(hydroxymethyl)-1,6-heptadiyne, [22]

4,4-Bis(hydroxymethyl)-1,6-heptadiyne, **22**, was synthesized according to Jin and coworkers²⁷ by reducing 1:5 ratio of diethyl dipropargyl malonate **21** with LiAlH_4 in Et_2O solution (Scheme 3.5).



Scheme 3.5 4,4-bis(hydroxymethyl)-1,5-heptadiyne, **22**.²⁷

During initial attempt to replicate Jin's work at ambient temperature the desired product **22** was not obtained. Therefore, the reaction was repeated with the solution of **21** in Et₂O first being cooled to 0 °C followed by subsequent addition of a cooled suspension (0 °C) of LiAlH₄ drop wise over a period of 1 hr.

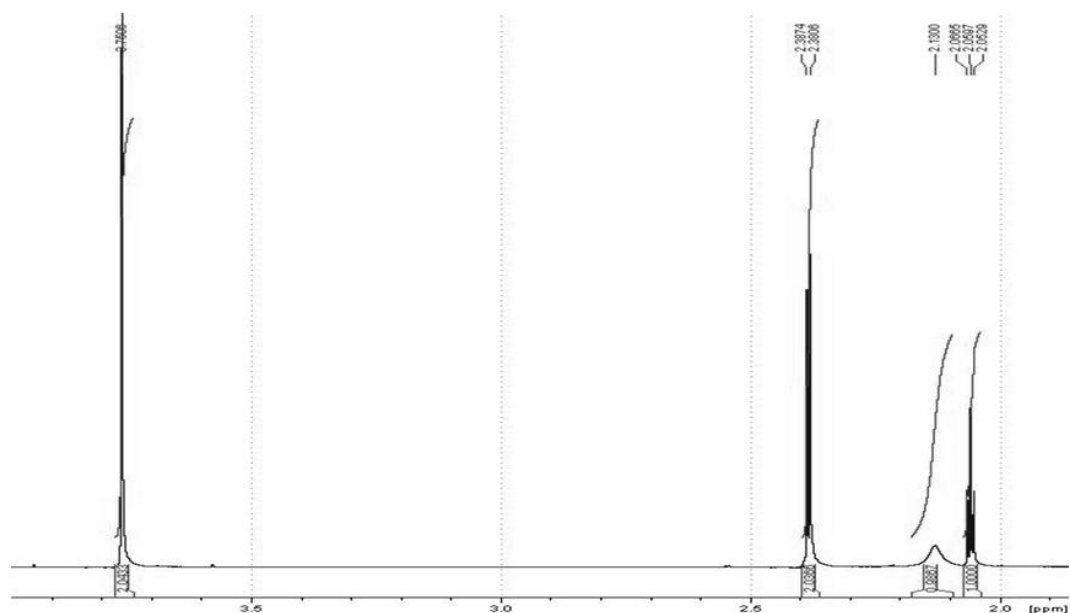


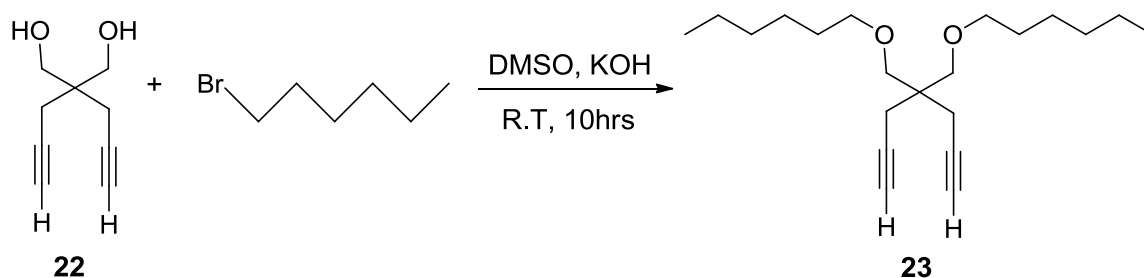
Figure 3.2 ¹H NMR spectra of 4,4-*bis*(hexyloxymethyl)-1,6-heptadiyne **22**.

A white solid was removed and recrystallized from Et₂O at room temperature. ¹H NMR analysis of **22** showed four resonance signals were obtained: a triplet at $\delta_H = 2.05$ ppm ($\equiv\text{C-H}$, $^4J = 2.7$ Hz), a broad peak at $\delta_H = 2.13$ ppm (O-H), a doublet at $\delta_H = 2.38$ ppm ($\text{CH}_2\text{-C}_{\text{quat}}$, $^4J = 2.7$ Hz), and a singlet at $\delta_H = 3.75$ ppm ($\text{CH}_2\text{-O}$). Methylene ($\text{CH}_2\text{-C}_{\text{quat}}$) and methine ($\equiv\text{C-H}$) protons integrate for 4 and 2 protons respectively and the coupling constant $^4J = 2.7$ Hz further indicates that these protons are coupled. The characteristic

broad peak of O-H and singlet peak for methylene (CH₂-O) further support the structure of **22** with integration values of 2 and 4 respectively that corresponds to the number of protons. From ¹³C NMR analysis, five resonance signals were obtained: at δ_C = δ 21.71 (CH₂C≡), 42.03 (C_{quat}), 66.57 (OCH₂), 71.19 (≡CH), 80.20 (-C≡) ppm respectively. Both NMR analyses were in good agreement with literature values²⁶ and confirmed the formation of **22**.

3.3.3 Synthesis of 4,4-bis(hexyloxymethyl)-1,6-heptadiyne, [23]

4,4-*Bis*(hexyloxymethyl)-1,6-heptadiyne, **23**, was synthesized by adding 1-bromohexane, and potassium hydroxide to **22** in DMSO following procedures outlined by Tilley and coworkers²³ (Scheme 3.6) with slight modification noted below.



Scheme 3. 6 4,4-*bis*(hexyloxymethyl)-1,6-heptadiyne, **23**.²³

The recommended eluant of 10/90 ethylacetate/hexane mixture did not provide a clean product as outlined in literature. Various ratios (%ethylacetate/%hexane i.e. 5/95, 10/80, 15/85 and 20/80) were tried and 20% ethylacetate to 80% hexane gave the desired

colorless oily product with 80% yield. Therefore, increasing the solvent polarity by higher % of ethyl acetate aids in separating **23** from the mixture.

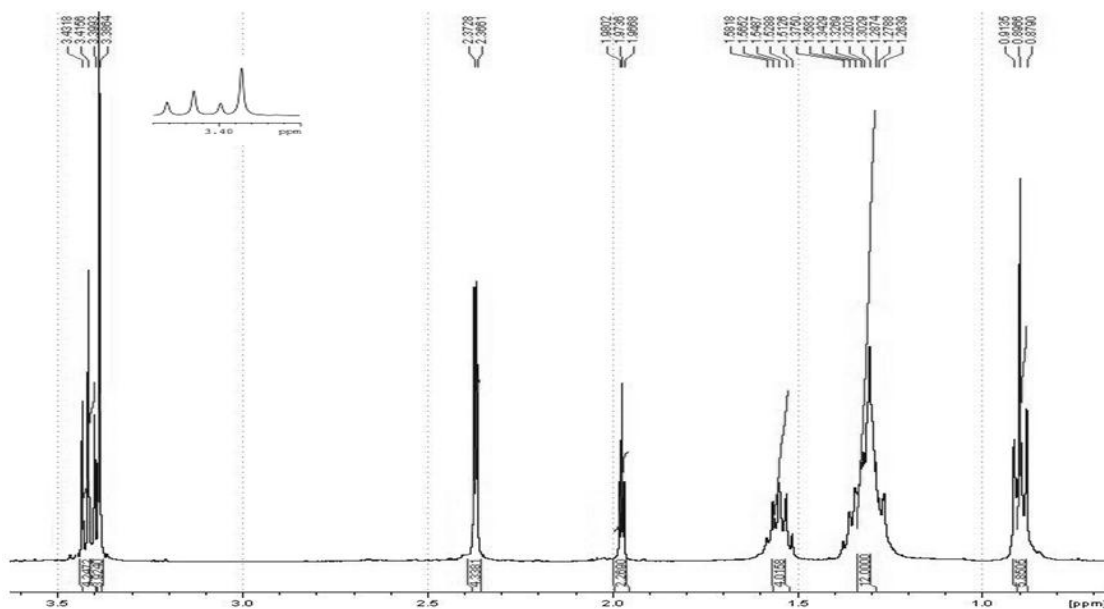


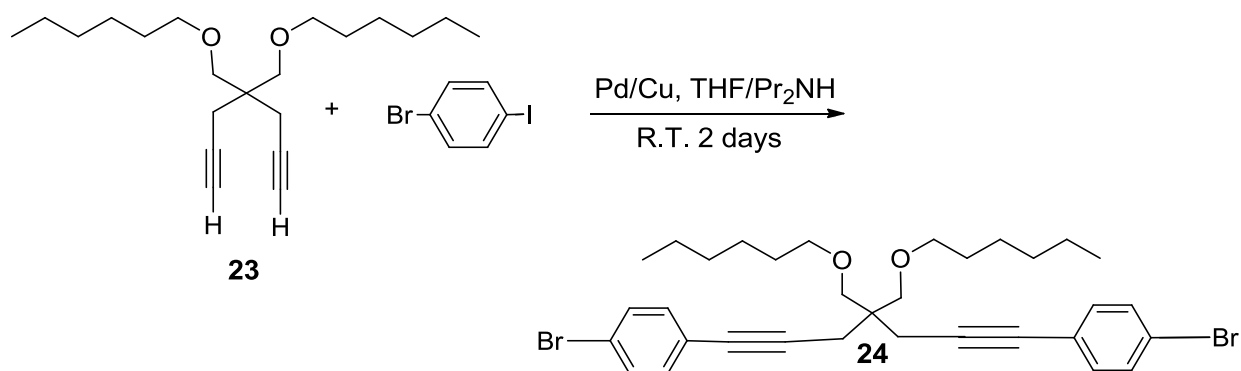
Figure 3.3 ^1H NMR spectra of 4,4-*bis*(hexyloxymethyl)-1,6-heptadiyne **23**.

From ^1H NMR analysis, 7 resonance signals were obtained: a triplet ($-\text{CH}_3$) at $\delta_{\text{H}} = 0.89$ ppm, a multiplet ($-\text{CH}_2-$) at $\delta_{\text{H}} = 1.26$ - 1.37 ppm, an apparent quintet ($-\text{CH}_2-$) at $\delta_{\text{H}} = 1.51$ - 1.58 ppm, a triplet ($\equiv\text{C}-\text{H}$, $^4J = 2.6$ Hz) at $\delta_{\text{H}} = 1.97$ ppm, a doublet ($\equiv\text{C}-\text{CH}_2$, $^4J = 2.6$ Hz) at $\delta_{\text{H}} = 2.36$ ppm, a singlet ($\text{O}-\text{CH}_2-\text{C}_{\text{quat}}$) at $\delta_{\text{H}} = 3.38$ ppm and a triplet ($\text{O}-\text{CH}_2$) at $\delta_{\text{H}} = 3.41$ ppm. Looking at the structure of **23**, 9 signals are expected yet only 7 were observed due to an overlap of three CH_2 signals that appeared as a multiplet at $\delta_{\text{H}} = 1.26$ - 1.37 ppm and integrated for 12 protons. The total number of 36 hydrogen was also consistent with the sum of all integrations and 4J coupling of 2.6 Hz was observed between methylene ($\equiv\text{C}-\text{CH}_2$) and methine ($\equiv\text{C}-\text{H}$). The absence of O-H broad signal ($\delta_{\text{H}} = 2.13$

ppm) from **22** suggested that the starting materials have been completely consumed. For ^{13}C NMR analysis, eleven resonance signals were obtained at $\delta_{\text{C}} = 14.05$ ($-\text{CH}_3$), 21.87, 22.64, 25.80, 29.53, 31.66 ($-\text{CH}_2-$), 71.16 (C_{quat}), 70.26, 71.25 ($\text{O}-\text{CH}_2$), 71.98 ($-\text{C}\equiv\text{CH}$), and 80.30 ($\text{CH}\equiv\text{C}-$) ppm respectively. Both NMR analyses were in good agreement with literature values²³ and the formation of **23**.

3.3.4 Synthesis of 4,4-bis(hexyloxymethyl)-1,7-bis-*p*-bromophenyl-1,6-heptadiyne, [24]

4,4-Bis(hexyloxymethyl)-1,7-bis-*p*-bromophenyl-1,6-heptadiyne, **24**, was synthesized according to Tilley and coworkers²³ (Scheme 3.7). Product **23**, 1-bromo-4-iodobenzene, $\text{Pd}(\text{PPh}_3)_4$ and CuI were dissolved in THF under nitrogen atmosphere. Diisopropylamine was then added to promote a Sonogashira reaction³¹ requires a basic medium to neutralize the byproducts. The mixture was stirred for 2 days.



Scheme 3. 7 4,4-bis(hexyloxymethyl)-1,7-bis-*p*-bromophenyl-1,6-heptadiyne, **24**.²⁴

A solid white byproduct was removed by filtration. The filtrate was diluted with hexane, washed with 10% NH_4OH , water and brine respectively. The filtrate was then dried over MgSO_4 . After removing the solvent *in vacuo*, the brownish oily residue was subjected to column chromatography on silica gel, eluting first with hexane as described by Tilley.²³ The hexane/ethylacetate = 10:1 mixture did prove unsuccessful and a hexane/ethylacetate = 2:1 ratio for mobile phase allowed for isolation of the colorless oily product in 76% crude yield (slightly lower than the literature yield).

Even after column chromatography, analysis of the crude sample by ^1H and ^{13}C NMR showed that there were significant amount of impurities remaining in the sample. However, many of the observed resonance signals were in close agreement with literature values.²³ Although attempts to purify and isolate **24** have thus far been unsuccessful, fresh samples of **24** were prepared and used *in situ* for subsequent steps without additional purification rather than column chromatography.

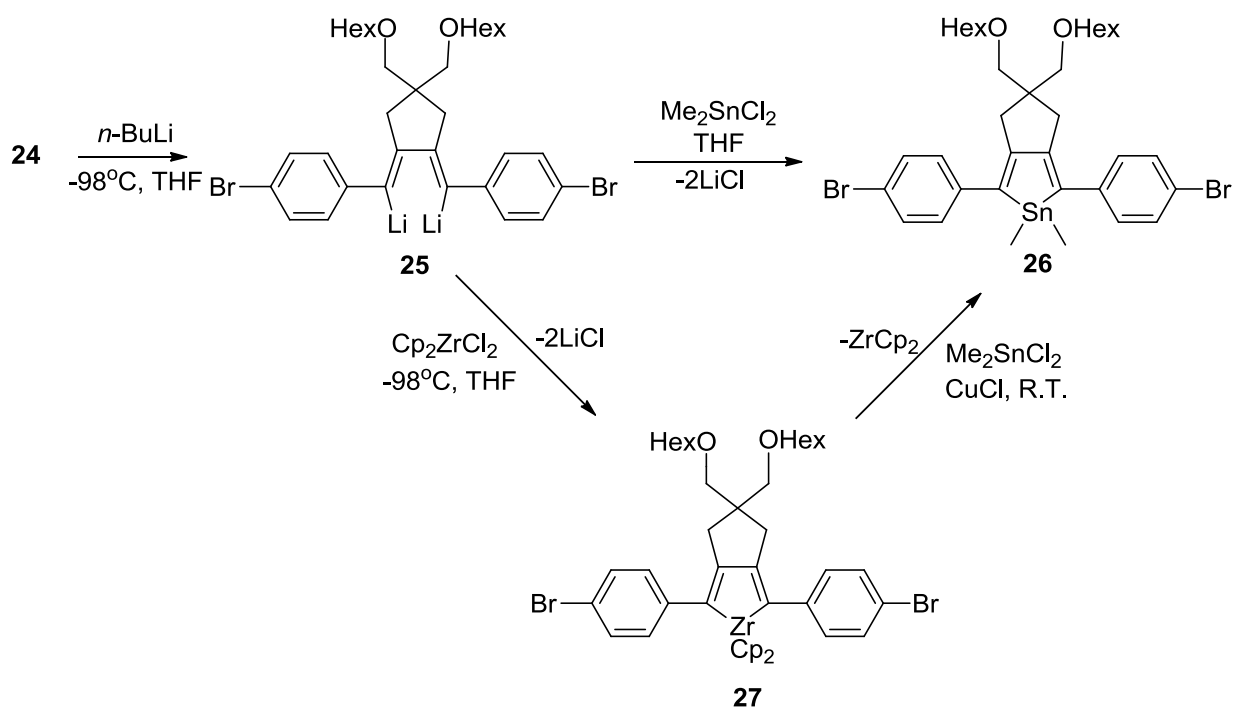
3.3.5 Attempted Synthesis of $\text{C}_{35}\text{H}_{48}\text{Br}_2\text{SnO}_2$, [26]

Two potential routes for the preparation of **26** (Scheme 3.8), both of which involved the use of **24** that had been prepared *in situ*, were investigated as part of an attempt to incorporate conjugated boroles into the main chain of a polymer. Unlike the tetraphenylstannole **10**, compound **26** has the potential to form polymers through a polycondensation reaction.

In the first method, Me_2SnCl_2 was first dissolved in THF and cooled to -98°C using liquid N_2 and MeOH slurry. A solution of *n*-BuLi in (1M in THF) was then added

dropwise to an *in situ* prepared solution of **24** in cooled THF (-98°C) over a period of 5 minutes under N₂ forming compound **25**. The mixture was stirred for 15 mins at low temperature followed by the dropwise addition of a solution of Me₂SnCl₂ over 5 mins. The resulting light yellow mixture was slowly warmed up to room temperature and stirred for 5 hrs.

In the alternate method, a solution of **25** was prepared using the same route as described above and a cooled solution of Cp₂ZrCl₂ in THF was added dropwise to the mixture over 5 mins forming compound **27**. After the reaction mixture was stirred for 15 mins at -98 °C, the solution was slowly warmed to room temperature and stirred for a total of 4 hrs. At this time, a solution of Me₂SnCl₂ with 10% CuCl³² was added to the reaction mixture at room temperature and the resulting light yellow solution was stirred for an additional 3 hrs.



Scheme 3. 8 Synthesis of $\text{C}_{35}\text{H}_{48}\text{Br}_2\text{SnO}_2$, **26**.

^{119}Sn NMR analysis of both routes showed singlet resonance signals at $\delta_{\text{Sn}} = 117.60$ and 117.44 ppm, respectively. These resonance signals were significantly upfield from the resonance signals expected for Me_2SnCl_2 ($\delta_{\text{Sn}} = 144$ ppm) and suggest the possible formation of **26** in solution. The ^{119}Sn NMR signal for **26** appeared significantly downfield from the stannole **10** discussed in section 3.1.2. The aromatic rings for **26** may lie in the same plane as the stannole moiety allowing for the greater conjugation of the system compared with **10** where the bulk of the four phenyl substituents prevent each other from aligning with the plane of the stannole which could account for the difference in the observed positions of the resonance signals in the two compounds.

Further characterization of **26** using ^1H and ^{13}C NMR, mass spectrometry and elemental analysis is required for this compound. Attempt to purify and isolate **26** from the crude reaction mixture have thus far been unsuccessful.

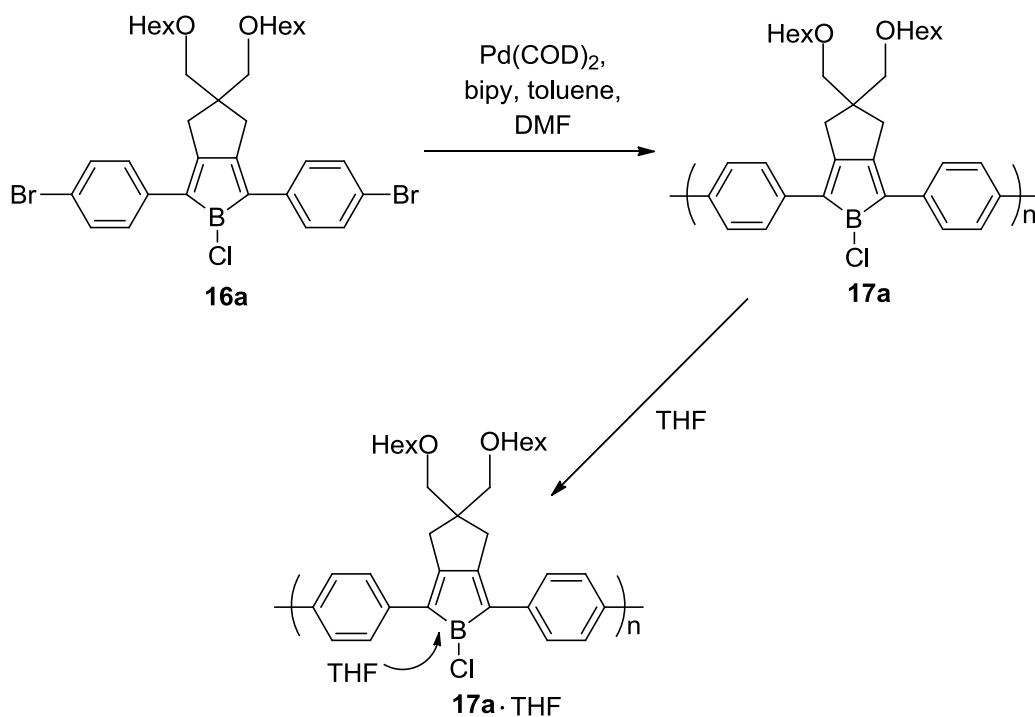
3.4. Attempted Synthesis of Polymer **17a**·THF

Bonifacio has previously demonstrated that dibrominated diaryl boroles can remain intact during polycondensation polymerization³³ under the same conditions utilized by Tilley for Ni(0) mediated coupling in the synthesis of poly(2,5-diphenylgermole).²³

BCl_3 in hexane was added dropwise over 1 min to a solution of **26** that had been prepared *in situ* (at $-98\text{ }^\circ\text{C}$ under N_2). The resulting solution turned a scarlet red color and the resulting reaction mixture was stirred for a further 3 hrs after warming to room temperature. An aliquot was removed and analyzed using ^{11}B NMR, which showed a broad resonance signal at $\delta_{\text{B}} = 30.96\text{ ppm}$ indicating the BCl_3 had been consumed.

In a separate flask, toluene, DMF, $\text{Pd}(\text{COD})_2$ and bipyridine were added under nitrogen and covered with Al foil to protect the sample from light and heated at 60°C for 20 mins. This mixture was then transferred to the scarlet solution dropwise in the hope of polymerizing any **16a** that had been formed *in situ*. The resulting reaction mixture was stirred for an additional 3 hrs, during which time the colour of the solution changed to light brown. In the hope of producing a material stable enough for GPC analysis in air, THF was subsequently added to the reaction mixture in an attempt to produce the polymer adduct **17a**·THF. The resulting solution stirred for 30 mins and the solvent removed *in vacuo*

yielding a thick polymer-like material. The polymer was then purified by precipitation in MeOH and the precipitated polymers were dried in air.



Scheme 3. 9 Synthesis of polymer **17a**·THF.

Analysis of the dried polymer using ^{11}B NMR revealed a singlet resonance signal at $\delta_{\text{B}} = 32.20$ ppm similar to what obtained before polymerization indicating that the heterole structure was similar to the monomer that had been prepared *in situ*. GPC analysis of polymer revealed a molecular weight of 55,000 Da for the sample with PDI = 1.6. The ^1H NMR analysis of the material showed very broad resonance signals between $\delta_{\text{H}} = 0.48$ -3.34 ppm, whereas the possible substituents, solvents and impurities signals overlapped with each other between $\delta_{\text{H}} = 6.73$ -7.63 ppm in the phenyl region. ^{13}C NMR analysis

provided multiple peaks at $\delta_C = 10.83\text{-}45.13$ ppm which could again be from substituents, solvents and impurities and $\delta_C = 124.78\text{-}162.05$ ppm for phenyl regions.

However, in light of the discovery that Me_2SnCl_2 must be removed from the crude product of any borole, it is unlikely that the target compounds **16a** and **17a** were formed. The entire polymerization process must be repeated after purification of **16a** and any future attempts to form **17a** should not be repeated *in situ*.

3.5. Molecular Modelling of Group 13 Heteroles

Molecular modeling analysis of **15** (1-chloro-2,3,4,5-tetraphenyl heteroles) and **16** or **16'** dibromo heteroles ($M = \text{B, Al, Ga}$) was carried out using Spartan 10 software at the B3LYP/6-31G* level of Density Functional Theory (DFT). These calculations were designed to complement the synthetic studies by acting as a guide for identifying potentially useful target molecules.

Performing efficient calculations required a slight modification of heteroles of type **16**, where hexyloxy (OC_6H_{13}) had been simplified to methoxy (OCH_3) substituents to form **16'** (Figure 3.4, **16'**). This slight simplification of the structure resulted in a significant reduction of calculation time from days and weeks to only hours. A comparative analysis was done on both **16** and **16'** ($M = \text{B, Al, Ga}$) and the calculated energy gap difference ($\Delta E_g = -0.01$ eV (B); -0.08 eV (Al); and $+0.01$ eV (Ga)) showed no significant differences (see Table 3.2) between **16** and **16'**. Therefore, all further calculations for the Lewis base adducts of these heteroles were calculated using OCH_3 substituents (**16'**).

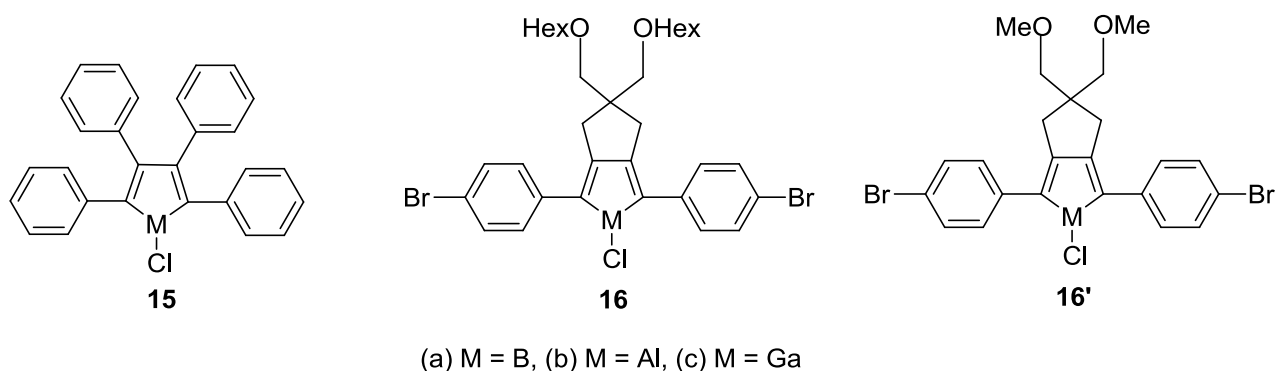


Figure 3.4 Heteroles **15**, **16** and **16'**.

The graphical model representations for **15** and **16'** showed several similarities, including that their heterole unit were all planar (with an endocyclic bond angle of 90-100°). The calculated carbon-carbon bond lengths of the heterole unit show alternating areas of π bonding character (≈ 1.35 Å) and areas where only σ bonding is expected (≈ 1.52 Å) suggesting no delocalization in the heteroles. These bond lengths are more consistent with the bond length observed in coordinated adducts of **15** where antiaromatic character had been broken as reported by Braunschweig.³⁰ In contrast, the planar geometry of the ring and trigonal planar geometry of the group 13 atoms should allow for conjugation with the four carbons, facilitating the delocalization of π -electrons and formation of antiaromatic conjugated rings.

3.5.1 Methyl, *n*-Butyl and Phenyl Substituents Effects on **15a**.

The effect on energy gap values for various alkyl or aryl substituents on **15a** (M = B, R = Me, *n*-Bu, Ph, Figure 3.6) was analyzed by DFT (Table 3.2).

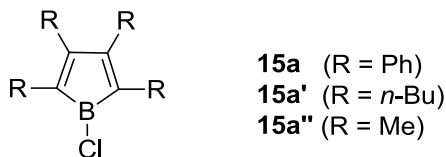


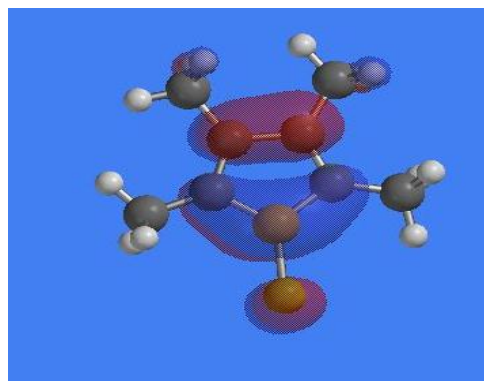
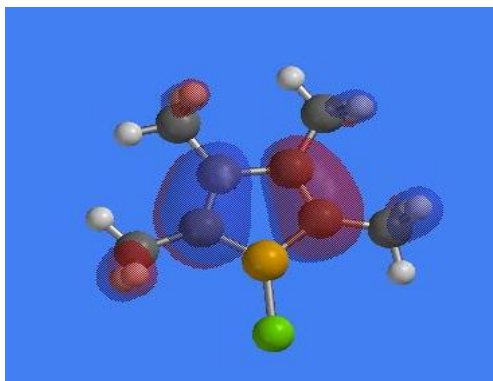
Figure 3.5 Heteroles **15a**, **15a'** and **15a''**

Table 3. 2 Theoretical energy gaps E_g of **15a**, **15a'** and **15a''** borole heteroles calculated at the B3LYP/6-31G* level of DFT.

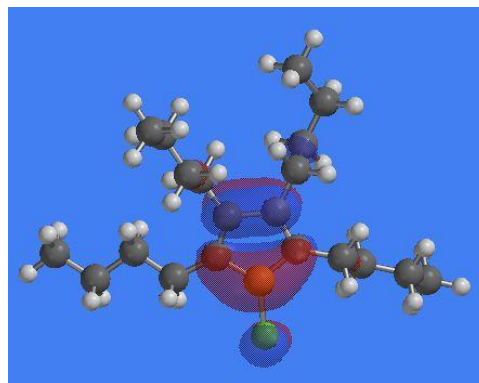
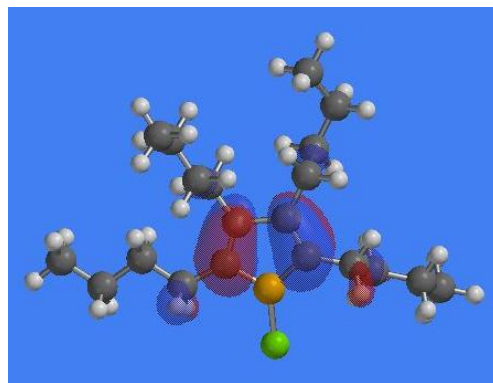
Substituent	HOMO (eV)	LUMO (eV)	E_g (eV)
15a (Ph)	-5.37	-2.78	2.59
15a' (<i>n</i> -Bu)	-5.41	-2.18	3.23
15a'' (Me)	-5.46	-2.26	3.20

The energy gap values for Me and *n*-Bu substituents were very similar (approximately 3.2 eV), yet the Ph substituent was considerably lower at 2.6 eV. This data suggests that electron donating groups (Me, *n*-Bu) have a similar effect on the energy gap. In contrast, an electron withdrawing group, (Ph) reduced the energy gap by lowering the LUMO energy level (Table 3.1).

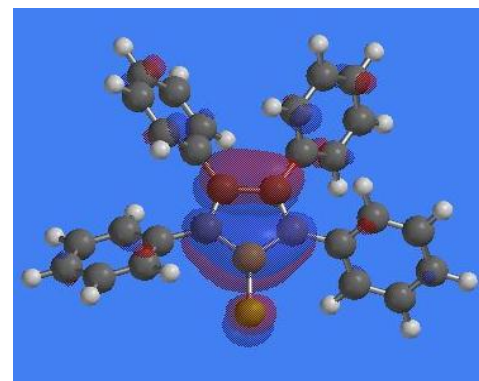
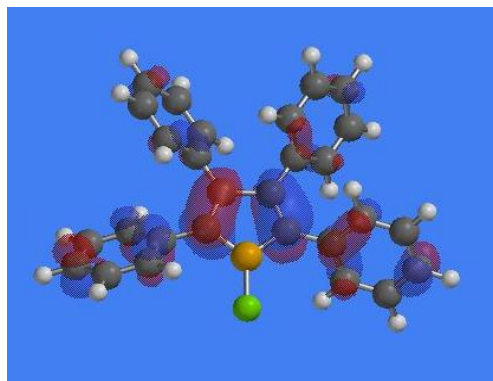
15a''



15a'



15a



HOMO

LUMO

Figure 3.6 Frontier orbitals of 1-chloro-2,3,4,5-tetra **15a** (Ph), **15a'** (*n*-Bu) and **15a''**.

Another contributor to this energy difference is the possibility of conjugation between the π cloud of the heterole and that of the Ph substituents. The structure of **15a** has a larger delocalized framework (Figure 3.6) compared to **15a'** or **15a''**. Modification of substituents that are isolated from the π framework have little effect on the energy gap as has been observed in comparison to **16** to **16'** where the isolated electron donating side groups was changed from OC_6H_{13} to OCH_3 .

As shown in Figure 3.6, the electron density on the LUMO orbitals involve the boron atom, making it a good site for adduct formation. In contrast, the electron density of the HOMO orbitals is largely located on the carbon skeleton with little or no electron density on the boron atom. Also, greater electron density is observed with the Ph substituents compared to Me and *n*-Bu substituents, supporting the idea that Ph substituents participate in a greater delocalized system. Therefore, the chemistry of these systems allows for potential electronic fine-tuning *via* the substituents, where Ph substituent would appear red shifted in UV spectra compared to Me and *n*-Bu substituents. As a result, this tuning could lead to interesting optoelectronic properties.

Table 3. 3 Theoretical energy gaps E_g of 1-chloro-2,3,4,5-tetraphenyl heteroles (**15a-c**) and 2, 5-diphenyl heteroles (**16'a-c**) with Lewis-base adducts calculated at the B3LYP/6-31G* level of DFT.

	Ligand	HOMO (eV)	LUMO (eV)	E_g (eV)
Cyclopentadiene	none	-5.09	-1.33	3.76
15a	none	-5.37	-2.78	2.59
	THF	-4.93	-1.27	3.66
	Et ₃ N	-4.94	-1.41	3.53
	Et ₂ O	-4.96	-1.29	3.67
15b	none	-5.77	-2.53	3.24
	THF	-5.05	-1.46	3.54
	Et ₃ N	-5.00	-1.48	3.52
	Et ₂ O	-5.07	-1.46	3.61
15c	none	-5.49	-2.45	3.04
	THF	-5.03	-1.46	3.60
	Et ₃ N	-5.01	-1.47	3.54
	Et ₂ O	-5.00	-1.44	3.56
16	none	-5.52	-2.86	2.66
16'a	none	-5.54	-2.89	2.65
	THF	-5.00	-1.59	3.41
	Et ₃ N	-5.06	-1.24	3.82
	Et ₂ O	-5.08	-1.52	3.56
16b	none	-5.62	-2.32	3.30
16'b	none	-5.63	-2.41	3.22
	THF	-5.10	-1.42	3.68
	Et ₃ N	-5.19	-1.46	3.73
	Et ₂ O	-5.16	-1.42	3.74
16c	none	-5.53	-2.54	2.99
16'c	none	-5.54	-2.54	3.00
	THF	-5.20	-1.81	3.39
	Et ₃ N	-5.18	-1.61	3.57
	Et ₂ O	-5.23	-1.60	3.93

An intriguing piece of information identified by DFT calculations at the B3LYP/6-31G* level is that both boron-containing heteroles, **15a** and **16'a**, have much narrower energy gaps than those of the corresponding heteroles with Al and Ga (Table 3.3). Theoretically, ascending in a group in the periodic table usually results in a decrease in metal character, resulting in larger energy gap. However, in the case of boron, the borole

energy gap is smaller by (15-20% for example; **15a** = 2.59 eV, **15b** = 3.24 eV, and **15c** = 3.04 eV). This could be due to boron's atomic size that allows for better orbital overlap with the carbon atoms of ring system, which in turn affords a lower energy gap. Aluminole and gallole showed very similar energy gaps even though gallole (Ga is found below Al in the group) was expected to show a smaller energy gap than that of aluminole. This similarity in energy gap difference (about 0.2 eV) was observed for both **15** and **16'** heteroles (Table 3.2). The DFT calculation also revealed that the HOMO energy levels of the heteroles **15a-c** are 0.28-0.40 eV lower compared to cyclopentadiene (Table 3.2). Additionally, their LUMO levels are 1.12-1.45 eV lower in energy than that of Cp. This indicates that the heteroles have better electron affinity than Cp, resulting in a significant lowering of the LUMO energy level.

3.5.2 Effect of Adduct Formation

The energy gap of **15** and **16'** (with the Lewis-base adducts formed with THF, Et₃N and Et₂O) have also been calculated. All adducts provide wider energy gaps compared to their parent compound (Table 3.2). This suggests that the energy gap can also be tuned with adduct formation. The adduct formed between **15** and Et₃N (**15a**·Et₃N) provided the narrowest energy gap compared to THF and Et₂O analogs. Whereas in the case of **16'**, an adduct formed with THF had the narrowest energy gap. In general, the Lewis bases (Et₃N, THF and Et₂O) react *via* their HOMO orbitals and donate electron pairs whereas Lewis acids (borole, aluminole and gallole) react *via* their LUMO orbitals and accept electron pairs. As a result, Et₃N (through the nitrogen atom) and THF (through the oxygen atom)

donate an electron pair into the empty p-orbital of the B, Al and Ga atom to form adducts. Therefore, Et₃N and THF appear to be the better π -donors than Et₂O to stabilize the **15** and **16'** respectively, based on the values of energy gap of the bonding molecular orbitals (Lewis acid/base complex). This is counter intuitive because it is expected that the THF would be more similar to the Et₂O with respect to base strength and donating abilities than to Et₃N.

The effect of adduct formations is also observed in the simulated UV-VIS spectra (Figure 3.7 and 3.8). The parent heteroles are expected to have three major absorption signals each. For **15a**, λ_{max} = 380, 420, and 640 nm while for **16a'** λ_{max} = 350, 400, and 610 nm. The expected absorbances at >600 nm are consistent with the blue colour observed by Braunschweig in the synthesis of **15a**. Coordination of any Lewis base would be expected to disrupt the antiaromatic character of the borole resulting in the alteration of the UV-VIS spectra. Calculations have shown coordination of Et₃N to either **15a** or **16a** resulted in the elimination of the absorbance that is responsible for the expected blue colour of the system. The spectra of **15a**·Et₃N (λ_{max} = 280 and 380 nm) and **16a'**·Et₃N (λ_{max} = 280 and 380 nm) each indicate that the adduct would be expected to be yellow in colour. This is also consistent with the observation of Braunschweig.

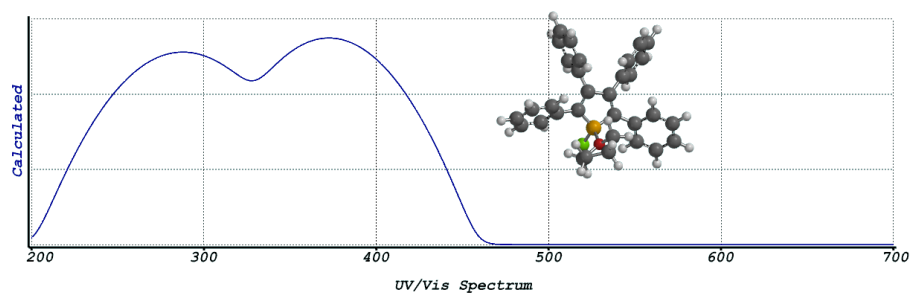
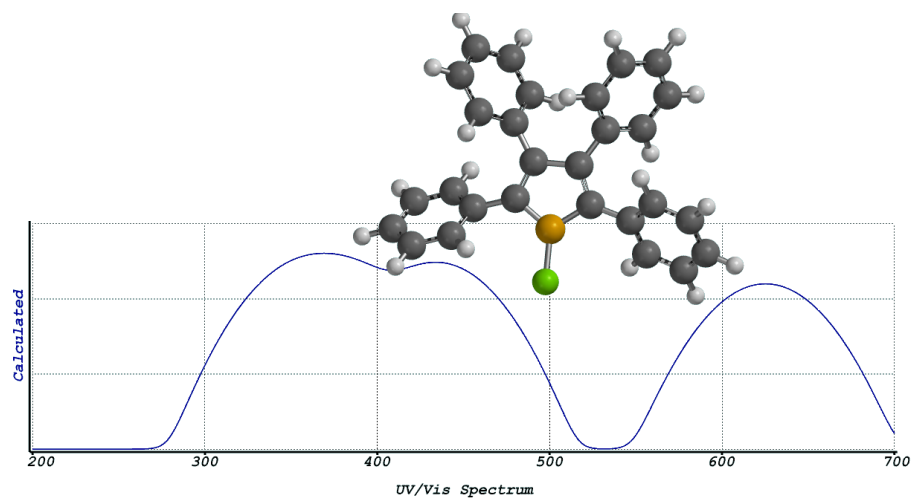


Figure 3.7 Ultraviolet spectrum of **15a** (top) and **15a·Et₃N** (bottom).

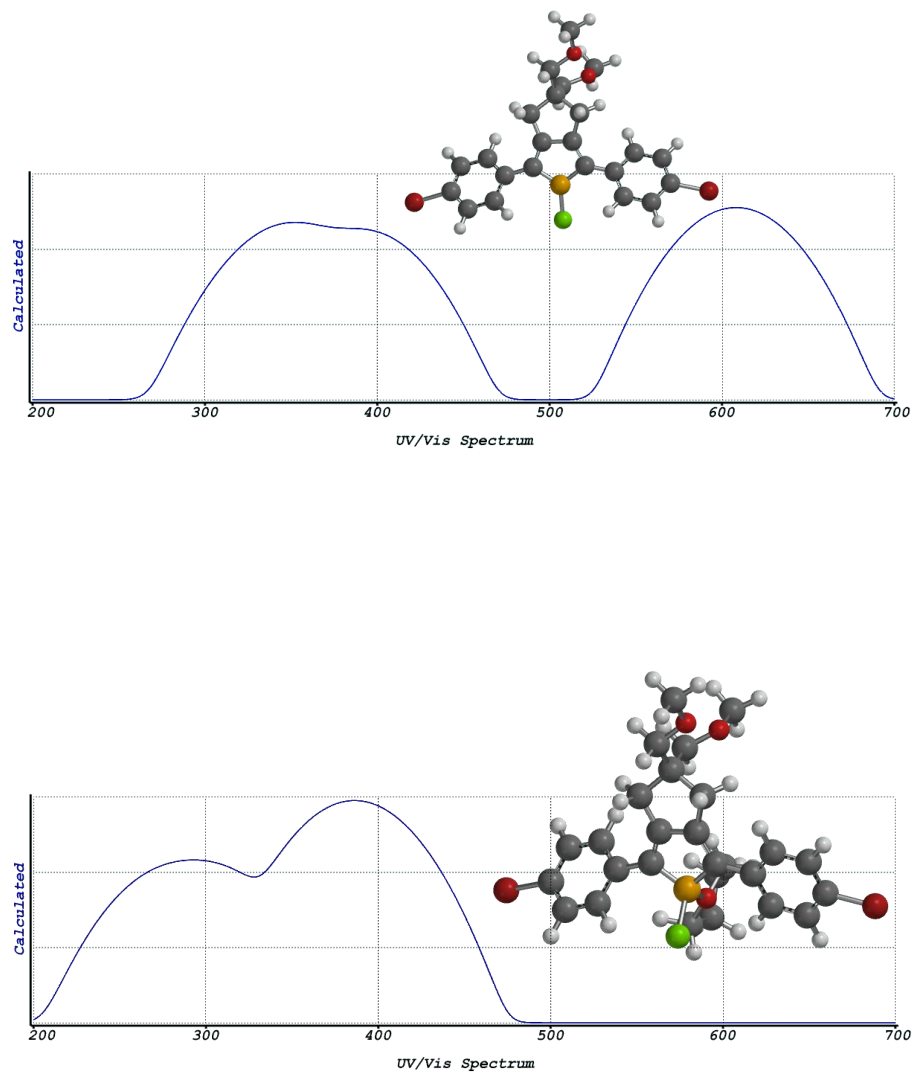


Figure 3.8 Ultraviolet spectrum of **16a** (top) and **16a'·Et₃N** (bottom).

3.6. Theoretical Analysis of Oligomeric Heteroles

In order to study the effect of increasing the number of repeating units on the energy gap, calculations for heteroles with up to six repeating units of **15** were analyzed by DFT. Initially it was found that the calculations would fail frequently due to the increasing

size of the molecules (number of atoms). Therefore, to obtain the data in Table 3.3, the calculation for 6 repeating units was undertaken at one level higher (B3LYP/6-31G** level) to accommodate more atoms. The remainder of the molecules (with 2, 3, or 4 repeating units) were calculated at (B3LYP/6-31G* level). It should be noted that the two basis sets of 6-31G* and 6-31G** have a similar function, except that 6-31G** also gives p-type polarization functions for hydrogen which adds flexibility to the basis set thus molecular orbitals will be asymmetric about the hydrogen nucleus.²³

Up to 3 repeat units of **15a** frontier orbitals are shown in Figure 3.9 where electron density is exhibited over the oligomers.

Table 3. 4 Theoretical energy gaps of 1-chloro-2,3,4,5-tetraphenylborole for various repeating units calculated at the B3LYP/6-31G* level of DFT.

Repeat Units	HOMO (eV)	LUMO (eV)	E _g (eV)
One	-5.37	-2.78	2.59
Two	-5.17	-2.82	2.35
Three	-5.04	-2.84	2.20
Four	-4.97	-2.85	2.12
Six*	-4.92	-2.86	2.06

* calculated at B3LYP/6-31G** level

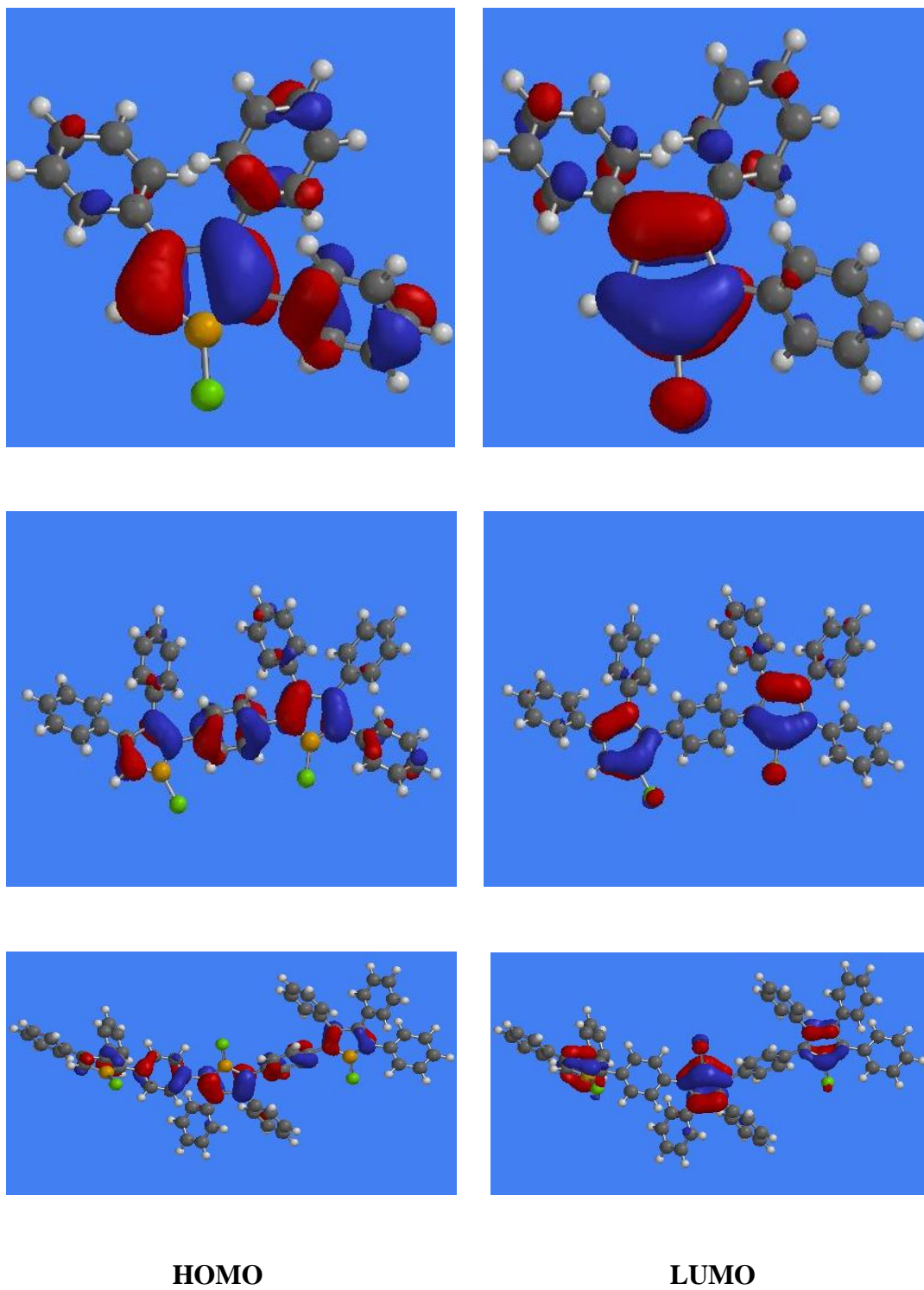


Figure 3.9 Frontier orbitals of 1-chloro-2,3,4,5-tetraphenylborole molecules **15a** for up to 3 repeat units.

It was previously mentioned that the energy gap between HOMO-LUMO decreases in conjugated systems due to the increasing number of π -orbitals (Figure 1.2). The more repeating units, the more π -orbitals are introduced, therefore the narrower the energy gaps are expected within a molecule. This is shown in Table 3.3 where the energy gap decreased from 2.5 eV for one repeating unit to 2.06 eV for six repeating units. A lower energy gap was observed between each repeating unit. By comparison, changes based upon adduct formation were more significant in comparison to the addition of the number of repeat units beyond the second.

CHAPTER 4

CONCLUSIONS AND RECOMMENDATIONS

4.1 Conclusions

Electrical properties governing the group 13 heteroatomic moiety demonstrated interesting results for HOMO-LUMO energy gap. Based on DFT calculations, boroles, possessing a boron atom in its five membered ring provided the lowest calculated energy gap compared to aluminole or gallole. Adduct formations resulted in additional fine-tuning of the monomer energy levels with **15**·Et₃N and **16**·THF adducts possessing the smallest energy gap. Electron donating and withdrawing substituents dramatically impact monomer electronics with more delocalized π -electrons in **15a** and resulted in the smallest energy gap. Also, it was observed in all cases that the π -orbital of LUMO in heteroles involved the main group atom, unlike HOMO orbital that do not hence showed the adduct formation site on the LUMO. DFT also revealed that the B, Al, or Ga in the LUMO orbital participate in the adduct formation. DFT calculation of oligomer units revealed that by increasing the number of repeating units of **15a**, a lower HOMO-LUMO energy gap is found. However, the decreased energy gap between each repeat unit was small (Table 3.4) compared to changes based upon adduct formation (Table 3.1). In general, monomers and oligomeric units possess small energy gaps and thus have the potential to be building blocks for the synthesis of low energy gap π -conjugated systems.

4.2 Future Recommendations

Future work will focus on the synthesis and isolation of monomer precursor **24** where additional precaution on the purifications of starting materials will be taken. Also, the removal of solvents from the product will be done using rotoevaporation rather than just *in vacuo* on Schlenk line to help separation of the product before introducing it to column chromatography. After obtaining pure **24**, isolation of monomer **16a** will also be attempted. Tilley and coworkers²³ have obtained pure monomer in the germole case (analogous to monomer **16a**) by vacuum drying the reaction mixture, then washing with cold pentane and extracting the product into benzene. If this isolation method works for monomer **16a**, the next step will be synthesizing monomer **16a** and **16b**, and subsequently polymer **17a-c**. Synthesis of polymeric system should be attempted *via* a nickel (0) catalyzed condensation polymerization.¹⁸ Two types of polymerization could then be analyzed: polymerization following adducts formation versus polymerization of adducts. Then the energy gaps of the two systems and their molecular weight compared.

Purification and isolation of heteroles **15a-c** is also required and can be accomplished by sublimation of the crude solid product to remove the unreacted stannole and other impurities.¹⁷ Growing crystals will also be attempted to help in identifying the structures of monomers and monomers precursors using x-ray crystallography analysis.

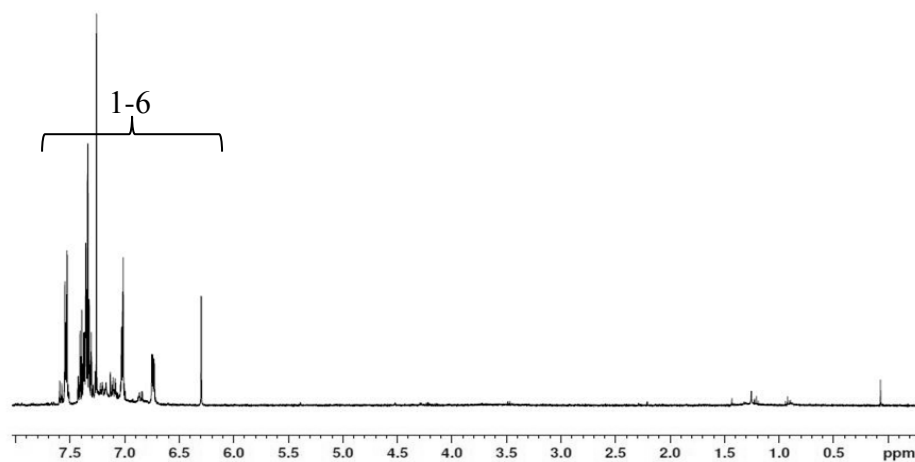
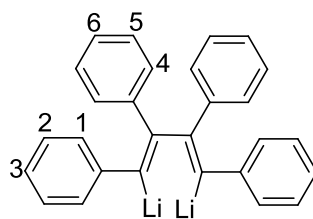
APPENDIX

List of NMR and IR spectra

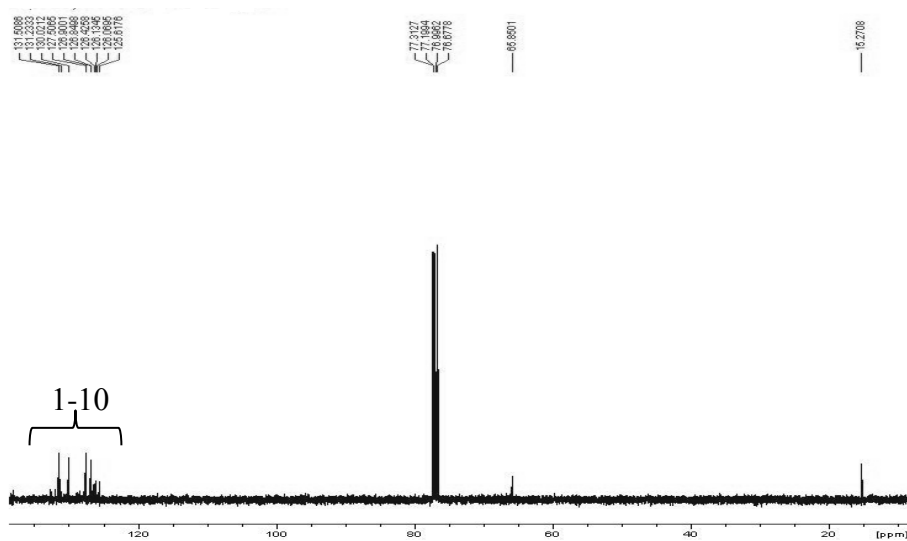
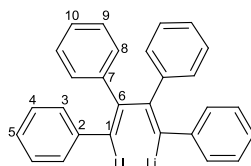
Spectrum 1: ^1H NMR of 1,4-Dilithio-1,2,3,4-tetraphenylbutadiene [2].	72
Spectrum 3: ^1H NMR of 1,1-Dimethyl-2,3,4,5-tetraphenylstannacyclopentadiene [10].	73
Spectrum 4: ^{13}C NMR of 1,1-Dimethyl-2,3,4,5-tetraphenylstannacyclopentadiene [10].	73
Spectrum 5: ^{119}Sn NMR of 1,1-Dimethyl-2,3,4,5-tetraphenylstannacyclopentadiene [10].	74
Spectrum 6: ^{11}B NMR of 1-Chloro-2,3,4,5-tetraphenylboracyclopentadiene [15a].	74
Spectrum 7: Enlarged view of the aromatic region ^1H NMR of 1-Chloro-2,3,4,5-tetraphenylboracyclopentadiene [15a].	75
Spectrum 8: ^1H NMR of 1-Chloro-2,3,4,5-tetraphenylboracyclopentadiene [15a].	75
Spectrum 9: ^{13}C NMR of 1-Chloro-2,3,4,5-tetraphenylboracyclopentadiene [15a].	76
Spectrum 10: ^{11}B NMR of 1-Chloro-2,3,4,5-tetraphenylboracyclopentadiene·Et ₃ N [15a ·Et ₃ N].	76
Spectrum 11: Enlarged view of the aromatic region ^1H NMR of 1-Chloro-2,3,4,5-tetraphenylboracyclopentadiene·Et ₃ N [15a ·Et ₃ N].	77
Spectrum 12: ^1H NMR of 1-Chloro-2,3,4,5-tetraphenylboracyclopentadiene·Et ₃ N [15a ·Et ₃ N].	77
Spectrum 13: ^{13}C NMR of 1-Chloro-2,3,4,5-tetraphenylboracyclopentadiene·Et ₃ N [15a ·Et ₃ N].	78
Spectrum 14: ^{11}B NMR of 1-Chloro-2,3,4,5-tetraphenylboracyclopentadiene·Et ₂ O [15a ·Et ₂ O].	78
Spectrum 15: Enlarged view of the aromatic region ^1H NMR of 1-Chloro-2,3,4,5-tetraphenylboracyclopentadiene·Et ₂ O [15a ·Et ₂ O].	79

Spectrum 16: ^1H NMR of 1-Chloro-2,3,4,5-tetraphenylboracyclopentadiene·Et ₂ O [15a ·Et ₂ O].....	79
Spectrum 17: ^{13}C NMR of 1-Chloro-2,3,4,5-tetraphenylboracyclopentadiene·Et ₂ O [15a ·Et ₂ O].....	80
Spectrum 18: Enlarged view of the aromatic region ^1H NMR of 1-Chloro-2,3,4,5- tetraphenylaluminacyclopentadiene [15b].....	80
Spectrum 19: ^1H NMR of 1-Chloro-2,3,4,5-tetraphenylaluminacyclopentadiene [15b].....	81
Spectrum 20: ^{13}C NMR of 1-Chloro-2,3,4,5-tetraphenylaluminacyclopentadiene [15b]....	81
Spectrum 21: Enlarged view of the aromatic region ^1H NMR of 1-Chloro-2,3,4,5- tetraphenylaluminacyclopentadiene·THF [15b ·THF].....	82
Spectrum 22: ^1H NMR of 1-Chloro-2,3,4,5-tetraphenylaluminacyclopentadiene·THF [15b ·THF].....	82
Spectrum 23: ^{13}C NMR of 1-Chloro-2,3,4,5-tetraphenylaluminacyclopentadiene·THF [15b ·THF].....	83
Spectrum 24: Enlarged view of the aromatic region ^1H NMR of 1-Chloro-2,3,4,5- tetraphenylaluminacyclopentadiene·Et ₂ O [15b ·Et ₂ O].....	83
Spectrum 25: ^1H NMR of 1-Chloro-2,3,4,5-tetraphenylaluminacyclopentadiene·Et ₂ O [15b · Et ₂ O]	84
Spectrum 26: ^{13}C NMR of 1-Chloro-2,3,4,5-tetraphenylaluminacyclopentadiene·Et ₂ O [15b ·Et ₂ O]	84
Spectrum 27: Enlarged view of the aromatic region ^1H NMR of 1-Chloro-2,3,4,5- tetraphenylgallacyclopentadiene [15c]	85
Spectrum 28: ^1H NMR of 1-Chloro-2,3,4,5-tetraphenylgallacyclopentadiene [15c]	85
Spectrum 29: ^{13}C NMR of 1-Chloro-2,3,4,5-tetraphenylgallacyclopentadiene [15c]	86
Spectrum 30: Enlarged view of the aromatic region ^1H NMR of 1-Chloro-2,3,4,5- tetraphenylgallacyclopentadiene·THF [15c ·THF]	86
Spectrum 31: ^1H NMR of 1-Chloro-2,3,4,5-tetraphenylgallacyclopentadiene·THF [15c ·THF]	87

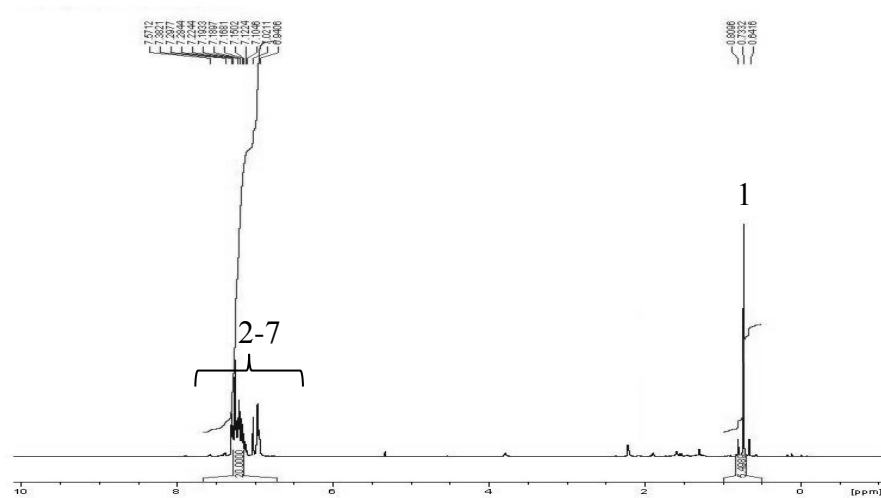
Spectrum 32: ^{13}C NMR of 1-Chloro-2,3,4,5-tetraphenylgallacyclopentadiene·THF [15c ·THF]	87
Spectrum 33: ^1H NMR of Diethyl dipropargyl malonate [21]	88
Spectrum 34: ^{13}C NMR of Diethyl dipropargyl malonate [21]	88
Spectrum 35: IR (neat, KBr, cm^{-1}) of Diethyl dipropargylmalonate [21]	89
Spectrum 36: ^1H NMR of 4,4-bis(hydroxymethyl)-1,6-heptadiyne [22]	89
Spectrum 37: ^{13}C NMR of 4,4-bis(hydroxymethyl)-1,6-heptadiyne [22]	90
Spectrum 38: IR (neat, KBr, cm^{-1}) of 4,4-bis(hydroxymethyl)-1,6-heptadiyne [22]	90
Spectrum 39: ^1H NMR of 4,4-bis(hexyloxymethyl)-1,6-heptadiyne [23].....	91
Spectrum 40: ^{13}C NMR of 4,4-bis(hexyloxymethyl)-1,6-heptadiyne [23].....	91
Spectrum 41: IR (neat, KBr, cm^{-1}) of 4,4-bis(hexyloxymethyl)-1,6-heptadiyne [23].....	92
Spectrum 42: ^1H NMR of 4,4-bis(hexyloxymethyl)-1,7-bis- <i>p</i> -bromophenyl-1,6-heptadiyne [24].....	92
Spectrum 43: ^{119}Sn NMR of 2,5-diphenylstannole [26] <i>via</i> method (I)	93
Spectrum 44: ^{119}Sn NMR of 2,5-diphenylstannole [26] <i>via</i> method (II).....	93
Spectrum 45: ^{11}B NMR of monomer [16a]	94
Spectrum 46: ^1H NMR of monomer [16a]	94
Spectrum 47: ^{13}C NMR of monomer [16a]	95
Spectrum 48: ^{11}B NMR of polymer [17a ·THF]	95
Spectrum 49: ^1H NMR of polymer [17a ·THF]	96
Spectrum 50: ^{13}C NMR of polymer [17a ·THF]	96



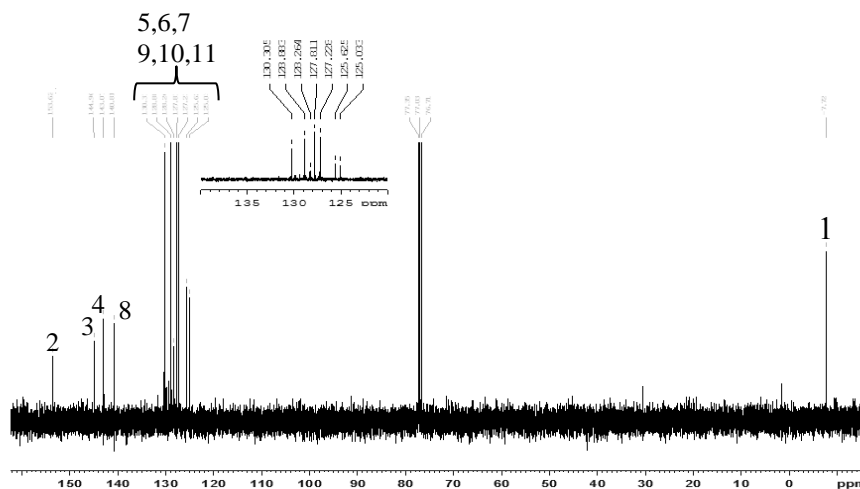
Spectrum 1: ^1H NMR of 1,4-Dilithio-1,2,3,4-tetraphenylbutadiene [2]



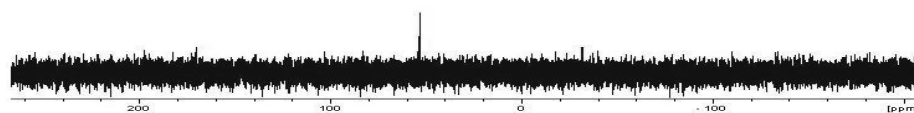
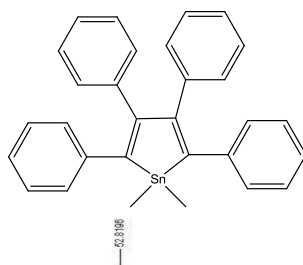
Spectrum 2: ^{13}C NMR of 1,4-Dilithio-1,2,3,4-tetraphenylbutadiene [2]



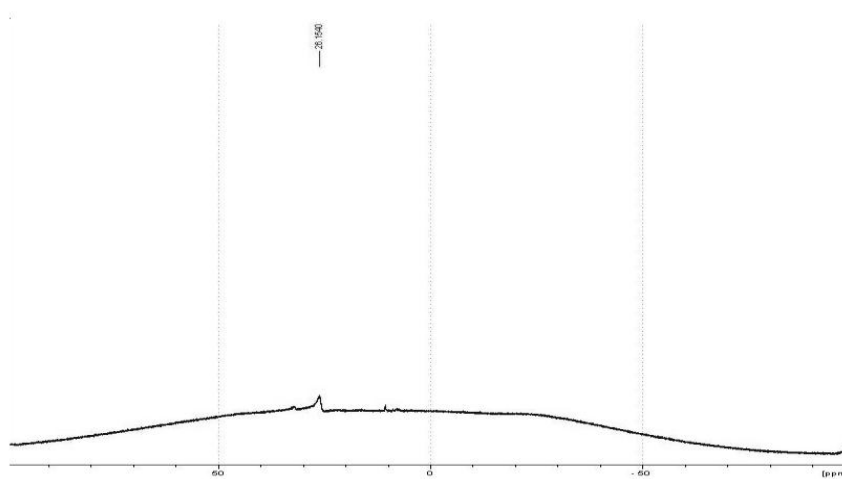
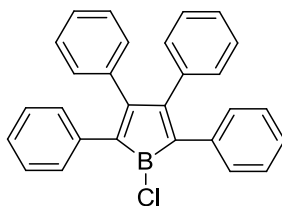
The chemical structure shows a central indole ring system. The indole ring is substituted at the 2-position with a phenyl group (atoms 4, 5, 6, 7) and at the 3-position with a phenyl group (atoms 8, 9, 10, 11). The nitrogen atom of the indole ring is labeled 'Sn' and has a methyl group attached to it (atom 1). The numbering of the atoms is as follows: 1 (methyl carbon), 2 (indole C2), 3 (indole C3), 4 (phenyl C1), 5 (phenyl C2), 6 (phenyl C3), 7 (phenyl C4), 8 (phenyl C1), 9 (phenyl C2), 10 (phenyl C3), 11 (phenyl C4).



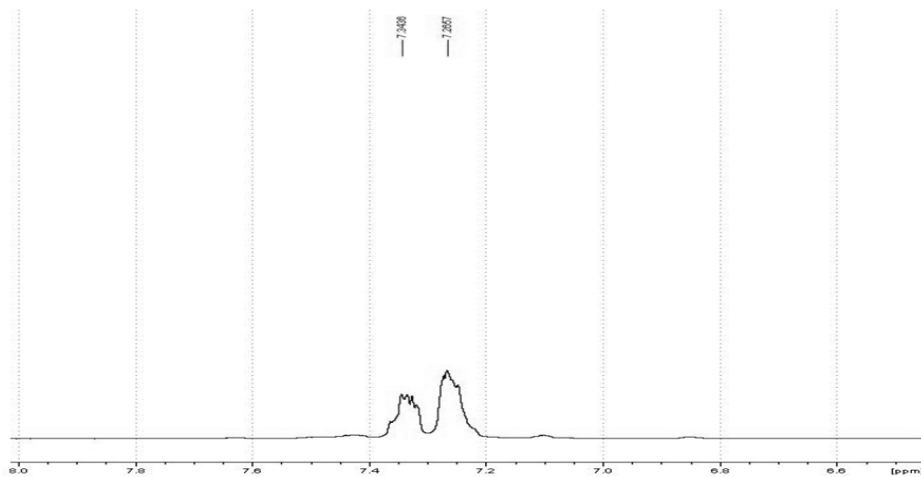
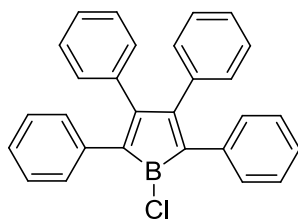
73



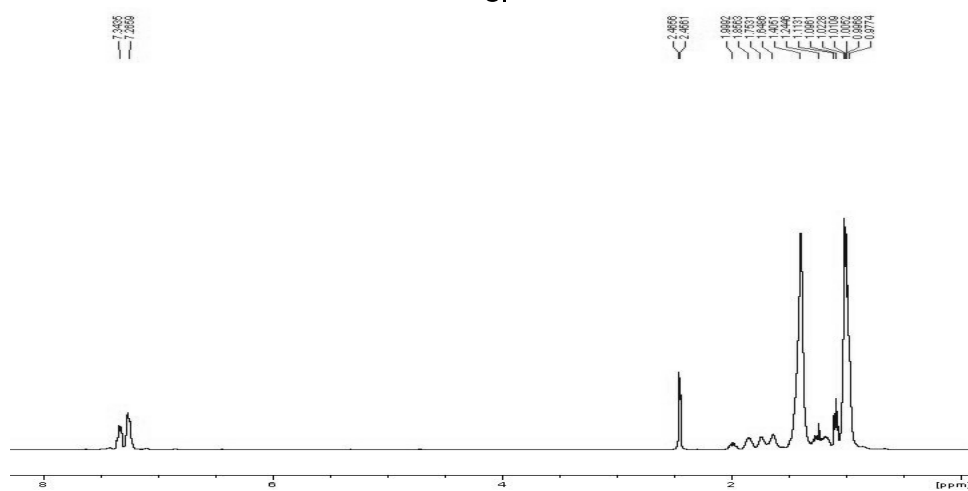
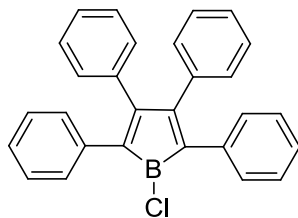
Spectrum 5: ^{119}Sn NMR of 1,1-Dimethyl-2,3,4,5-tetraphenylstannacyclopentadiene [10]



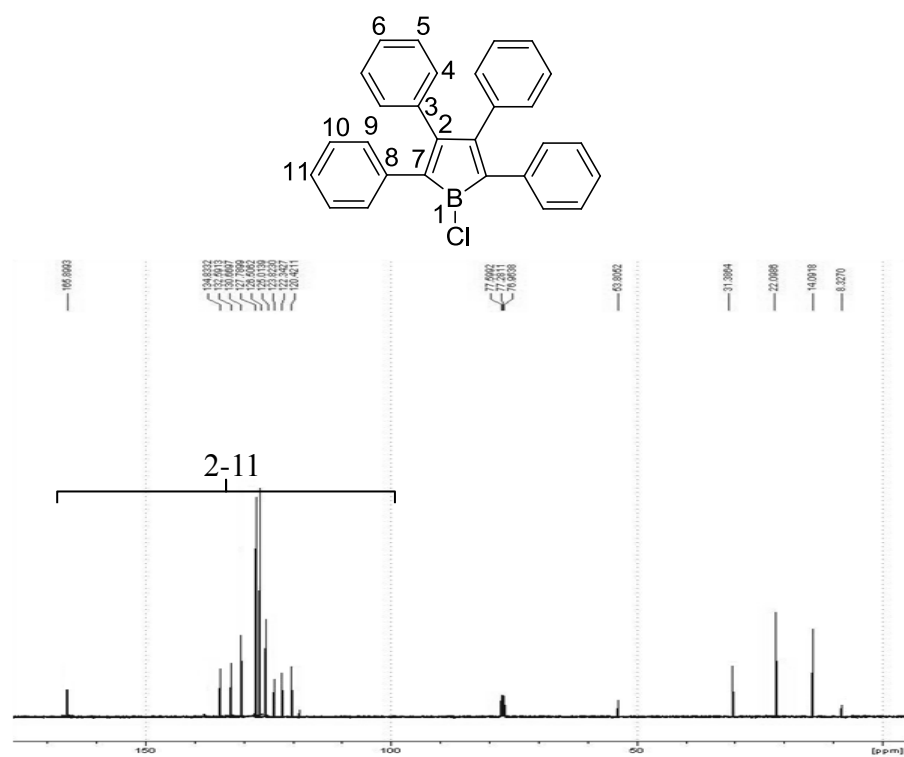
Spectrum 6: ^{11}B NMR of 1-Chloro-2,3,4,5-tetraphenylboracyclopentadiene [15a]



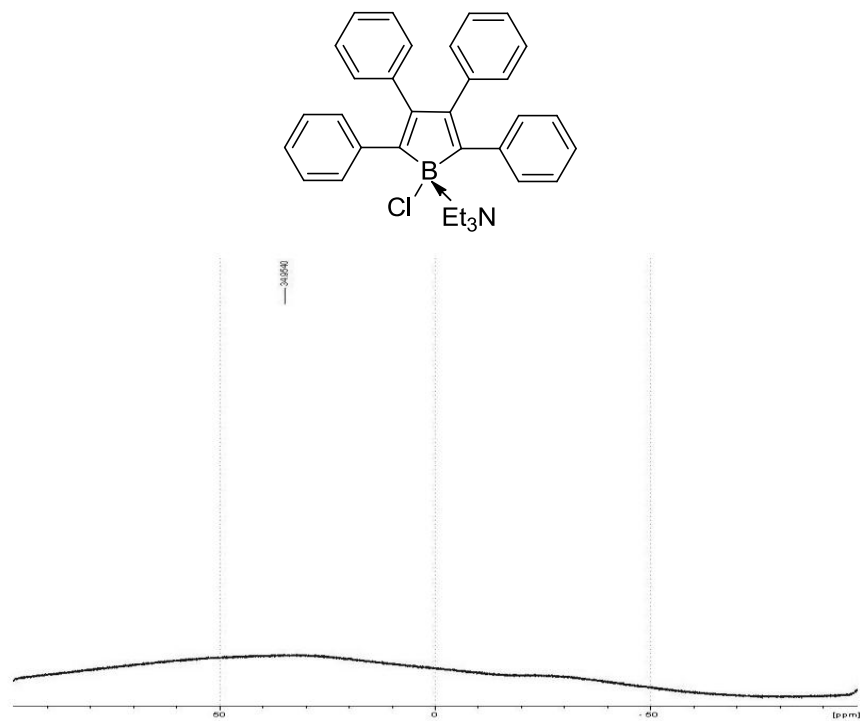
Spectrum 7: Enlarged view of the aromatic region ^1H NMR of 1-Chloro-2,3,4,5-tetraphenylboracyclopentadiene [15a]



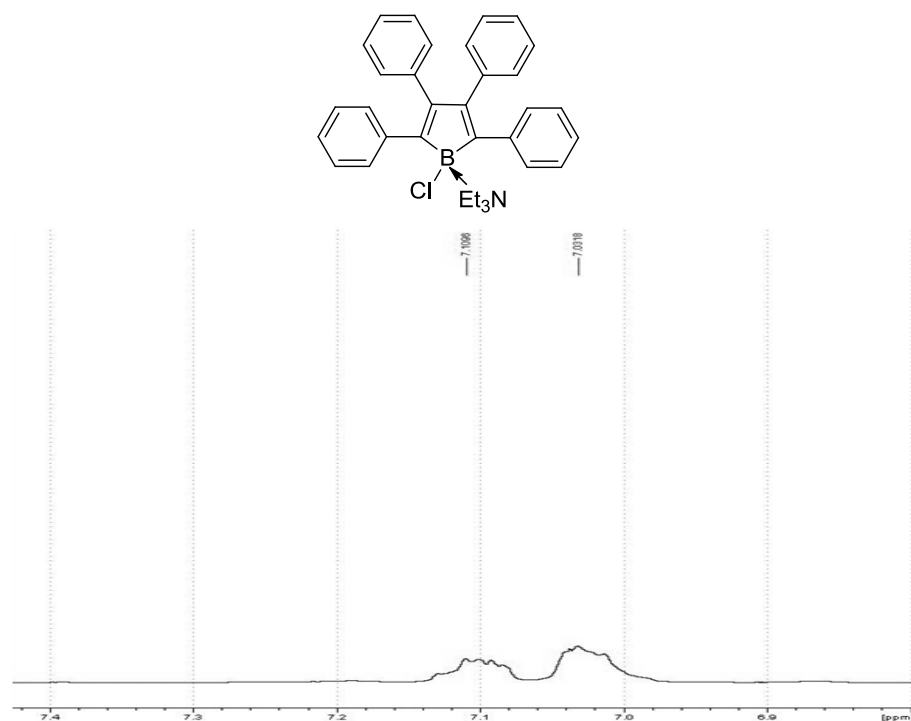
Spectrum 8: ^1H NMR of 1-Chloro-2,3,4,5-tetraphenylboracyclopentadiene [15a]



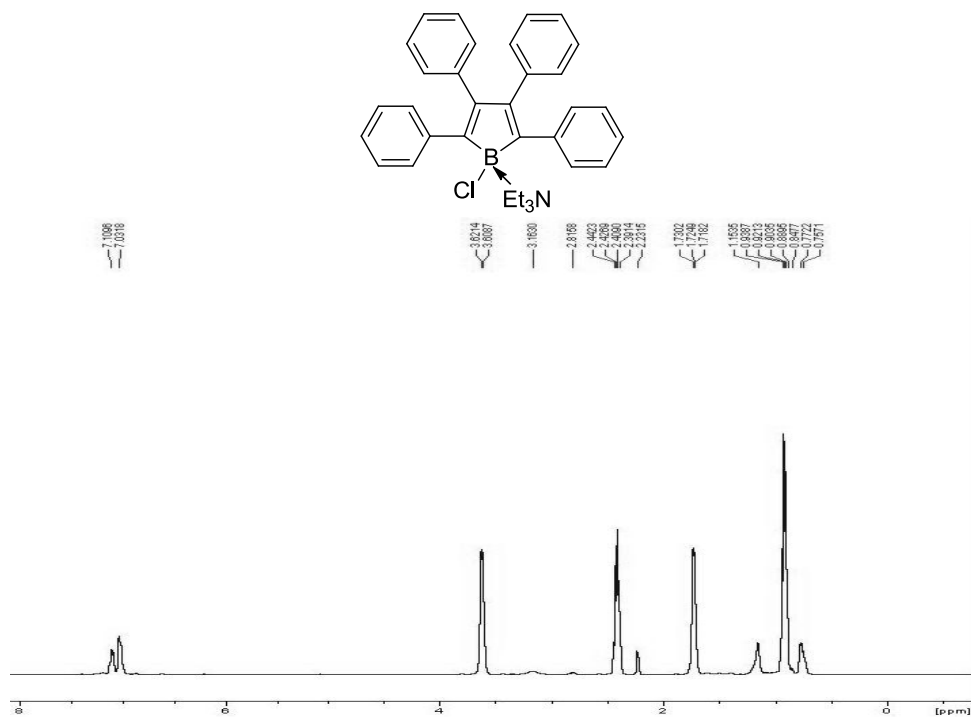
Spectrum 9: ^{13}C NMR of 1-Chloro-2,3,4,5-tetraphenylboracyclopentadiene [15a]



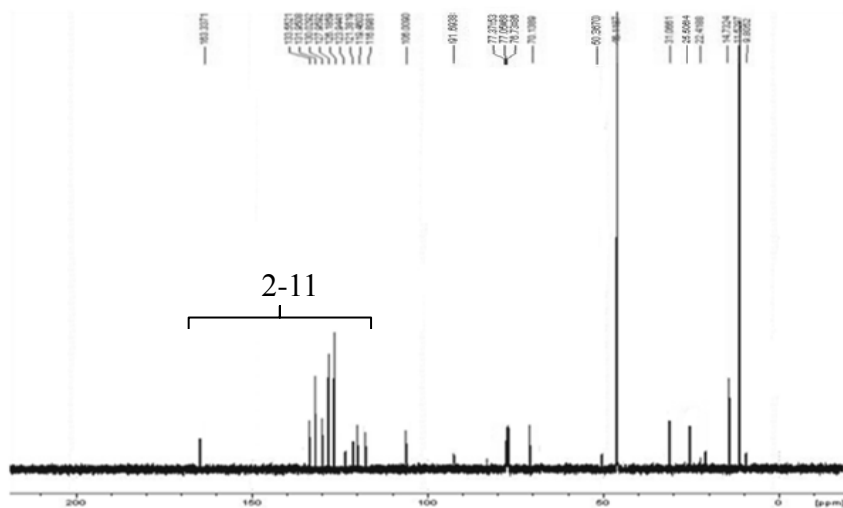
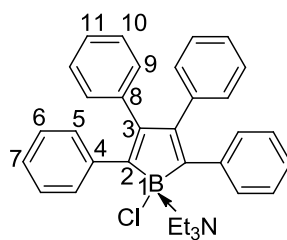
Spectrum 10: ^{11}B NMR of 1-Chloro-2,3,4,5-tetraphenylboracyclopentadiene· Et_3N [15a· Et_3N]



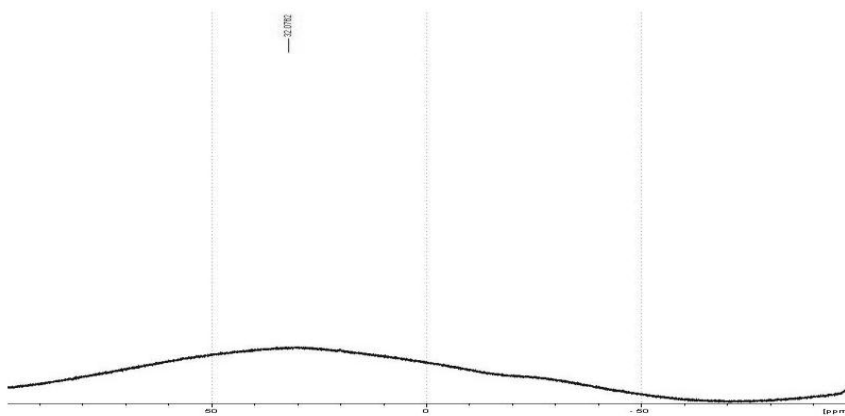
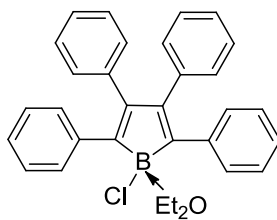
Spectrum 11: Enlarged view of the aromatic region ¹H NMR of 1-Chloro-2,3,4,5-tetraphenylboracyclopentadiene·Et₃N [15a·Et₃N]



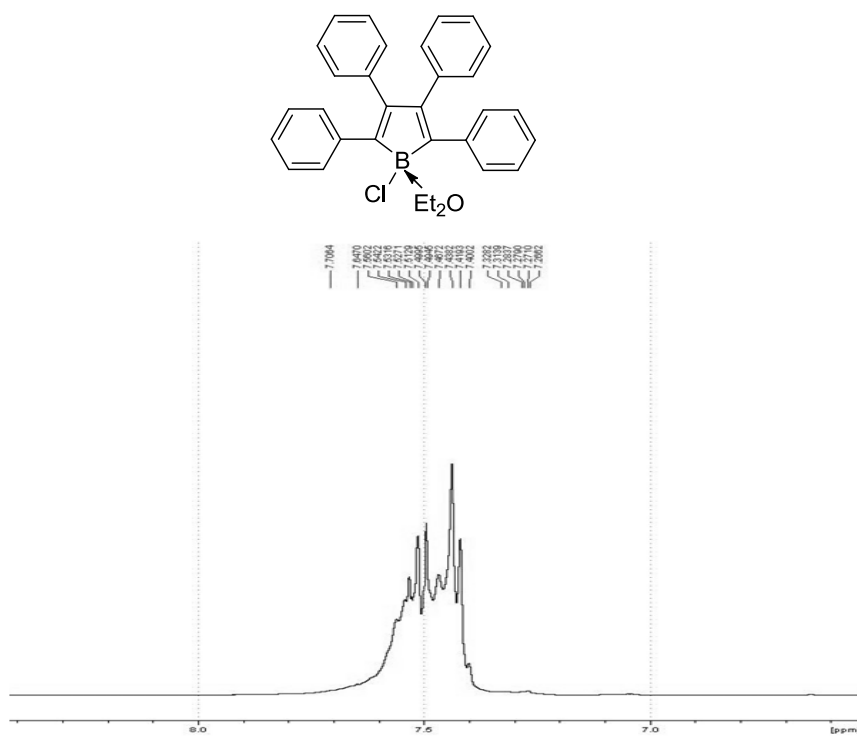
Spectrum 12: ¹H NMR of 1-Chloro-2,3,4,5-tetraphenylboracyclopentadiene·Et₃N [15a·Et₃N]



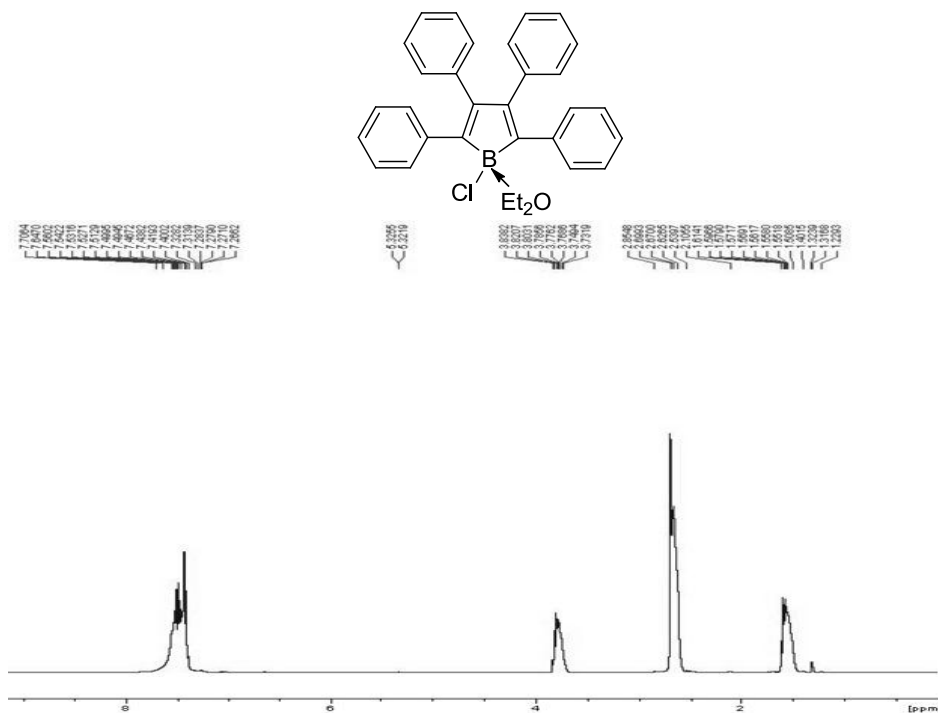
Spectrum 13: ^{13}C NMR of 1-Chloro-2,3,4,5-tetraphenylboracyclopentadiene· Et_3N [15a· Et_3N]



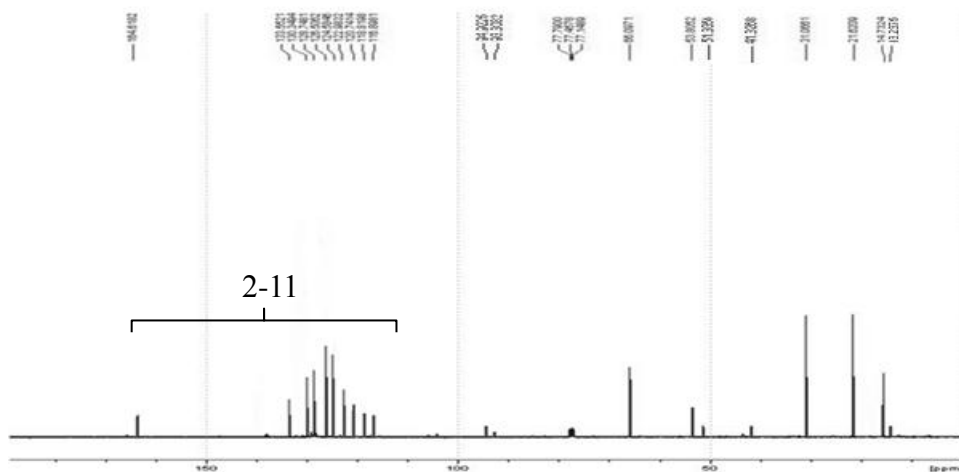
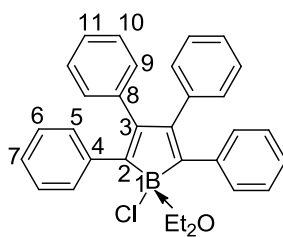
Spectrum 14: ^{11}B NMR of 1-Chloro-2,3,4,5-tetraphenylboracyclopentadiene· Et_2O [15a· Et_2O]



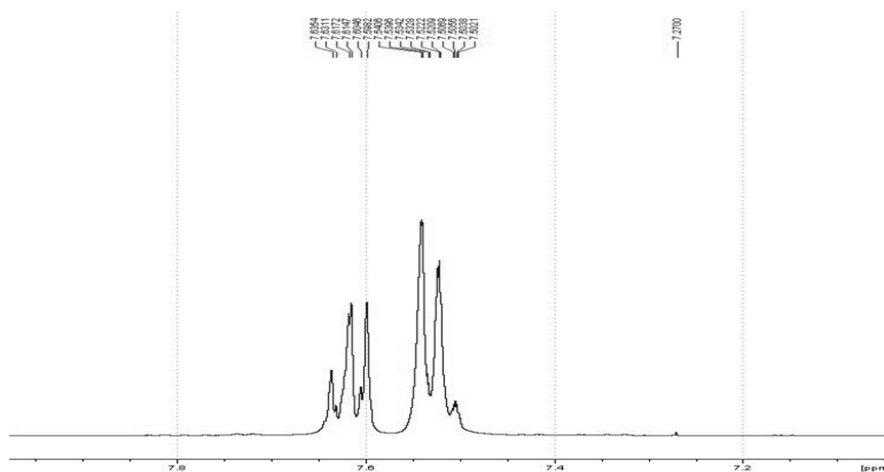
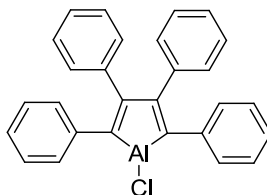
Spectrum 15: Enlarged view of the aromatic region ¹H NMR of 1-Chloro-2,3,4,5-tetraphenylboracyclopentadiene·Et₂O [15a·Et₂O]



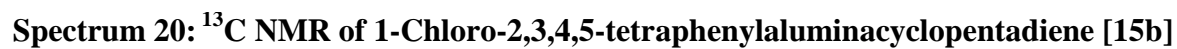
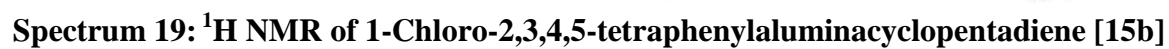
Spectrum 16: ¹H NMR of 1-Chloro-2,3,4,5-tetraphenylboracyclopentadiene·Et₂O [15a·Et₂O]

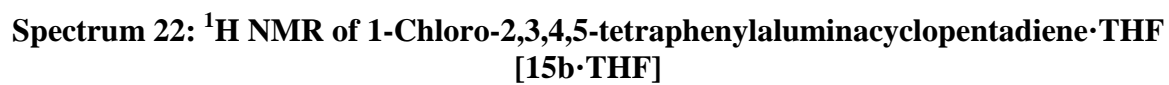


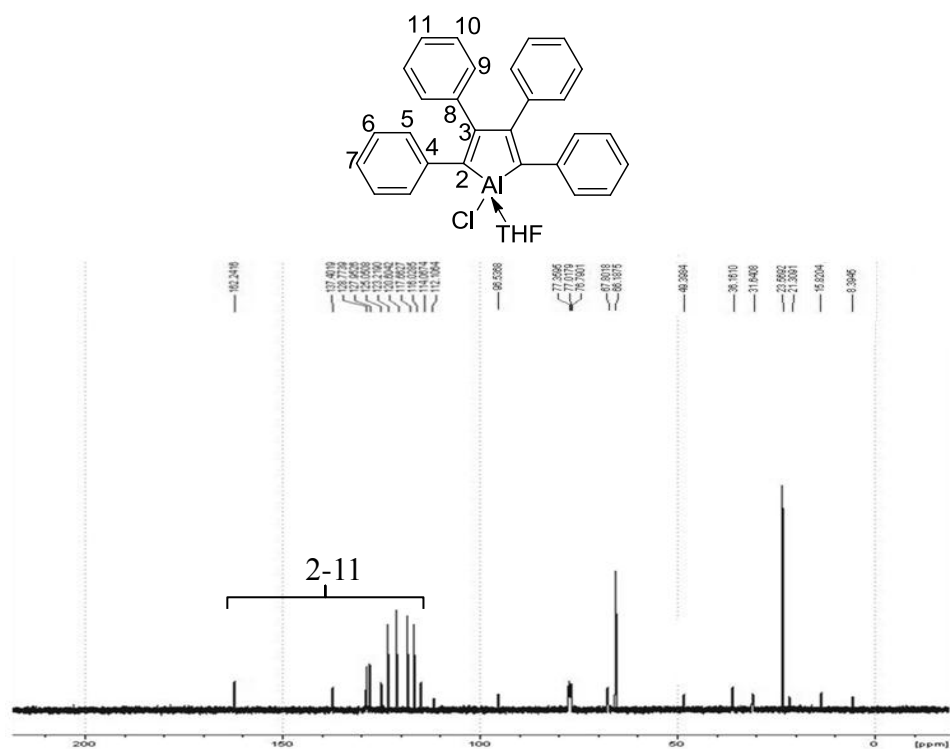
Spectrum 17: ^{13}C NMR of 1-Chloro-2,3,4,5-tetraphenylboracyclopentadiene·Et₂O [15a·Et₂O]



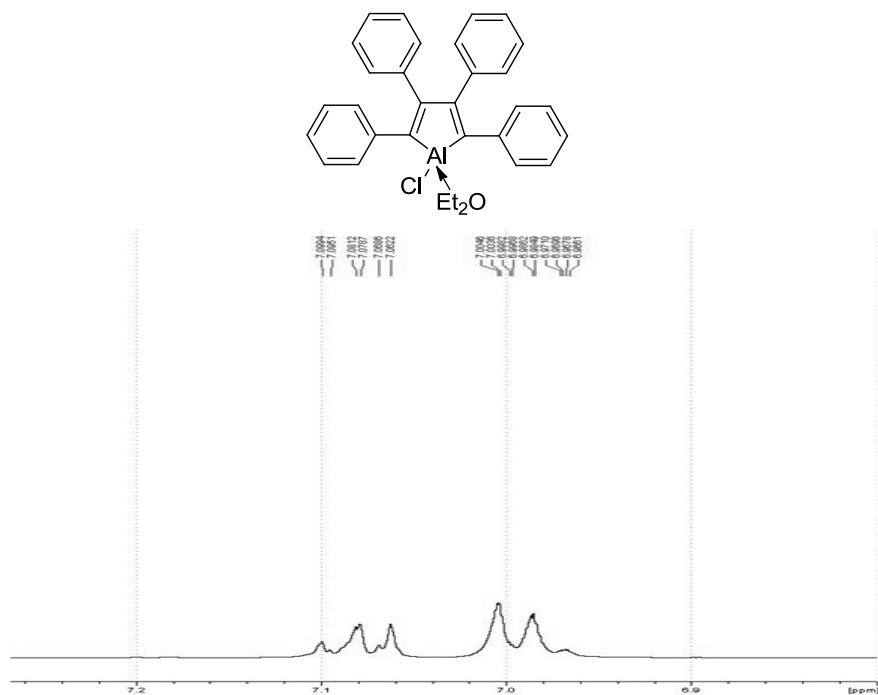
Spectrum 18: Enlarged view of the aromatic region ^1H NMR of 1-Chloro-2,3,4,5-tetraphenylaluminacyclopentadiene [15b]



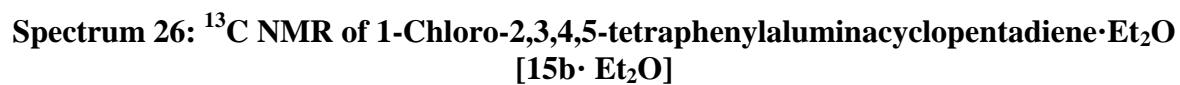
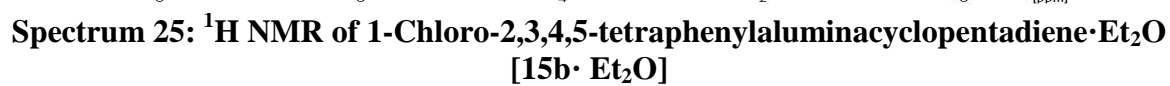


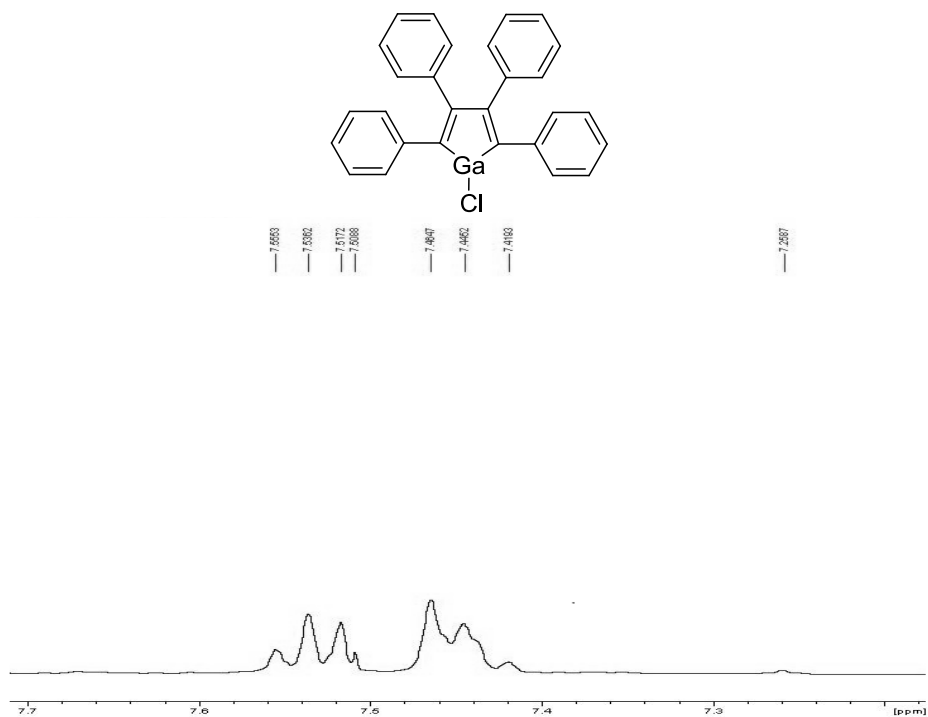


Spectrum 23: ^{13}C NMR of 1-Chloro-2,3,4,5-tetraphenylaluminacyclopentadiene·THF [15b·THF]

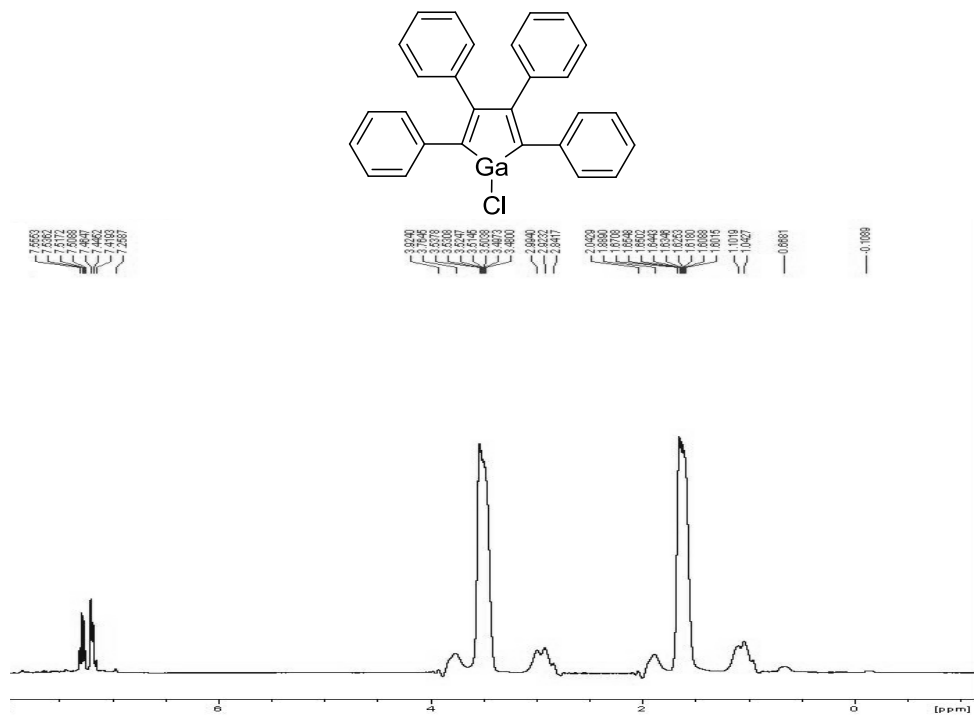


Spectrum 24: Enlarged view of the aromatic region ^1H NMR of 1-Chloro-2,3,4,5-tetraphenylaluminacyclopentadiene·Et₂O [15b·Et₂O]

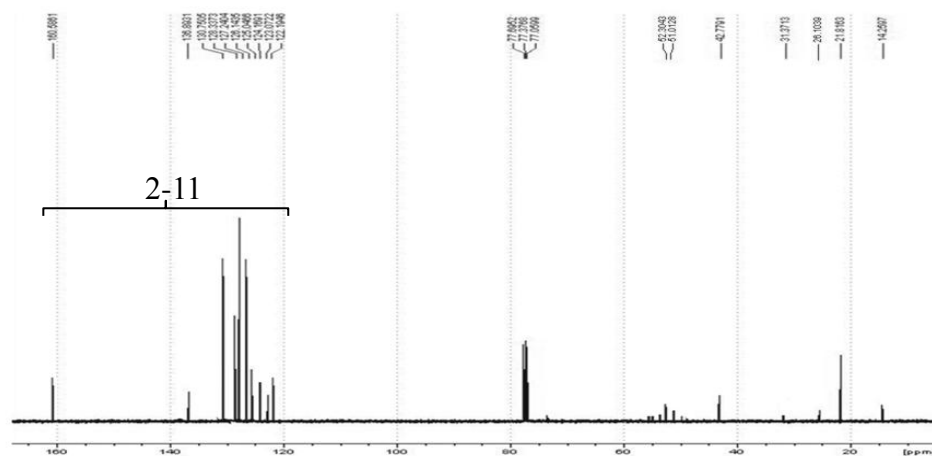
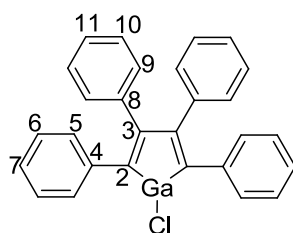




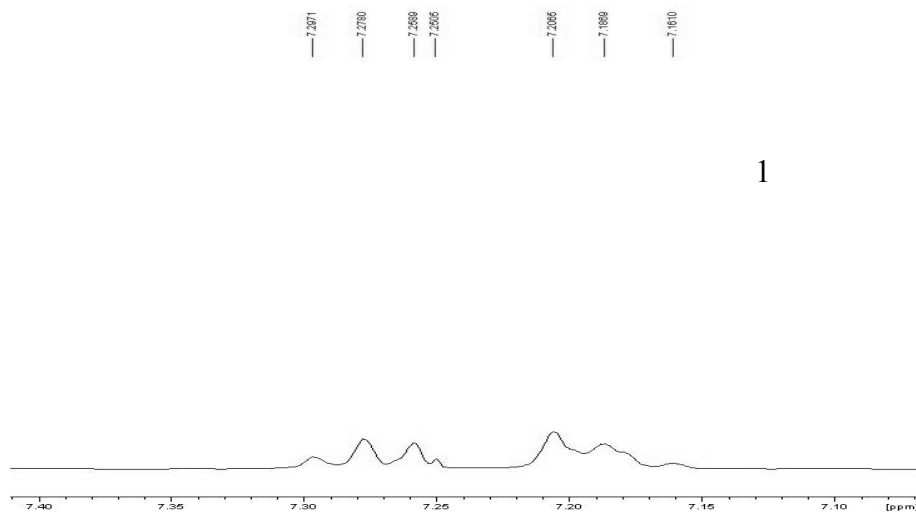
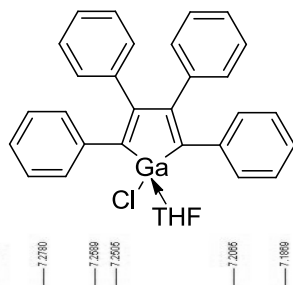
Spectrum 27: Enlarged view of the aromatic region ^1H NMR of 1-Chloro-2,3,4,5-tetraphenylgallacyclopentadiene [15c]



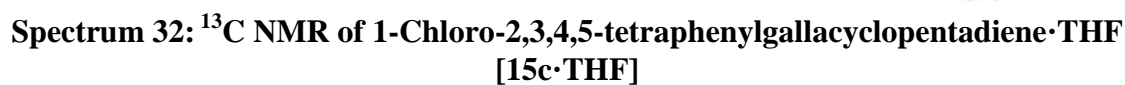
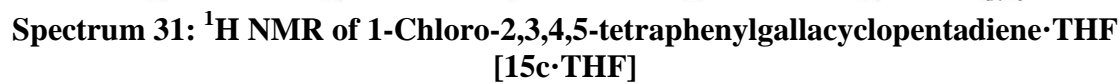
Spectrum 28: ^1H NMR of 1-Chloro-2,3,4,5-tetraphenylgallacyclopentadiene [15c]



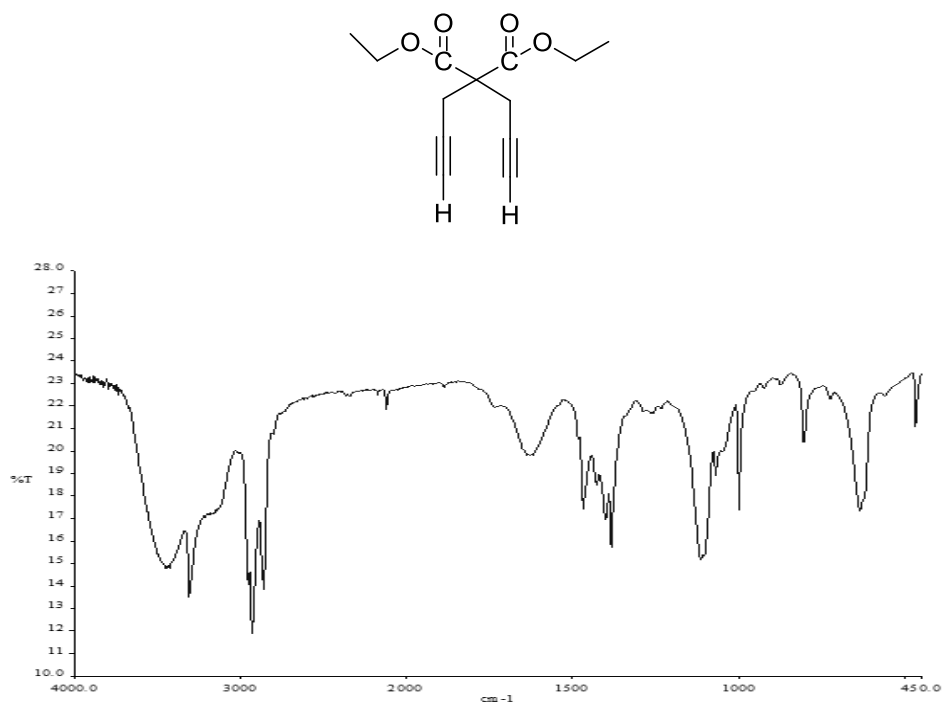
Spectrum 29: ^{13}C NMR of 1-Chloro-2,3,4,5-tetraphenylgallacyclopentadiene [15c]



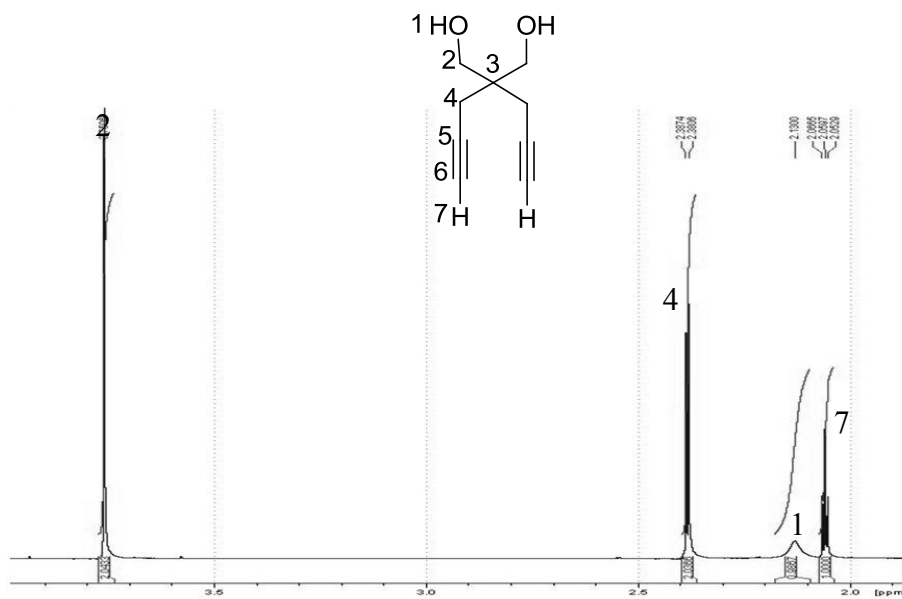
Spectrum 30: Enlarged view of the aromatic region ^1H NMR of 1-Chloro-2,3,4,5-tetraphenylgallacyclopentadiene·THF [15c·THF]



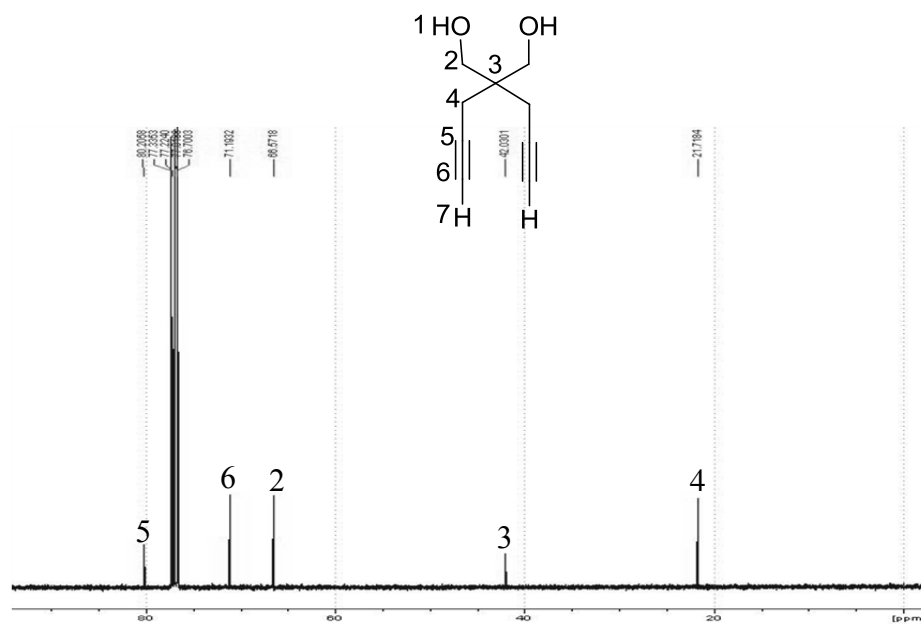




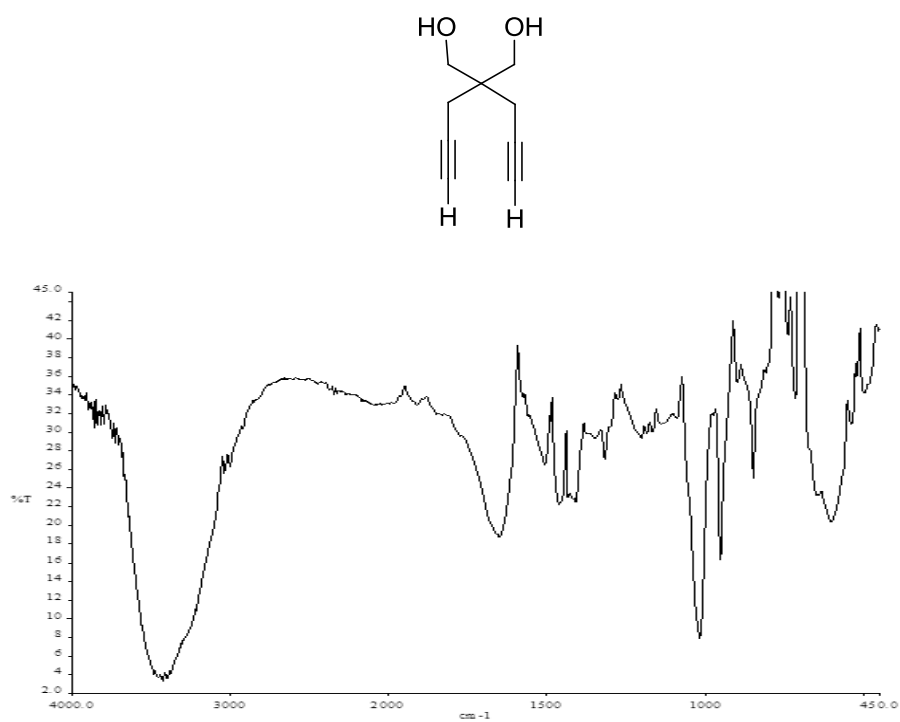
Spectrum 35: IR (neat, KBr, cm⁻¹) of Diethyl dipropargylmalonate [21]



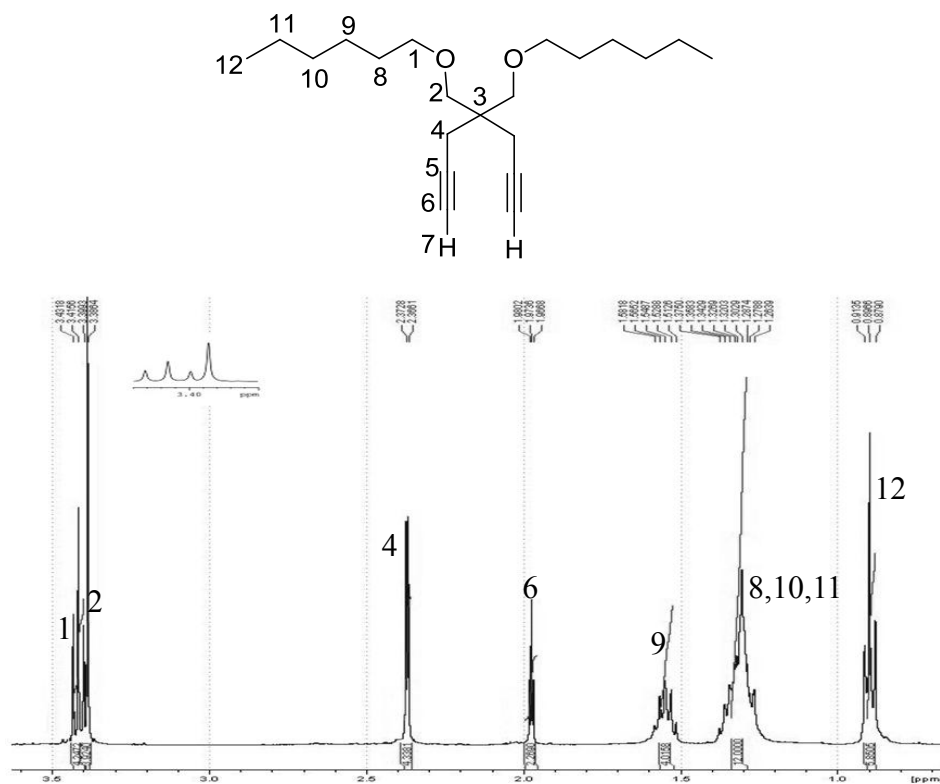
Spectrum 36: ¹H NMR of 4,4-bis(hydroxymethyl)-1,6-heptadiyne [22]



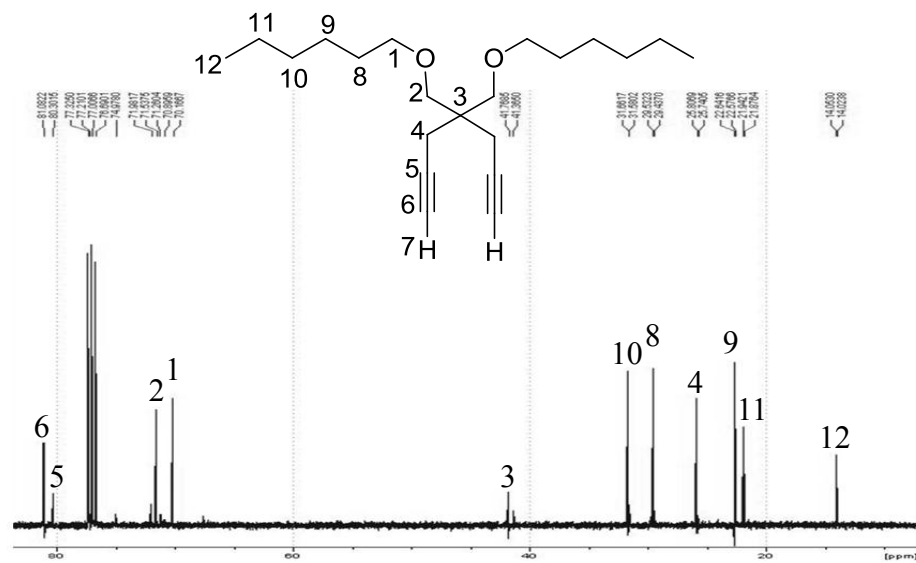
Spectrum 37: ¹³C NMR of 4,4-bis(hydroxymethyl)-1,6-heptadiyne [22]



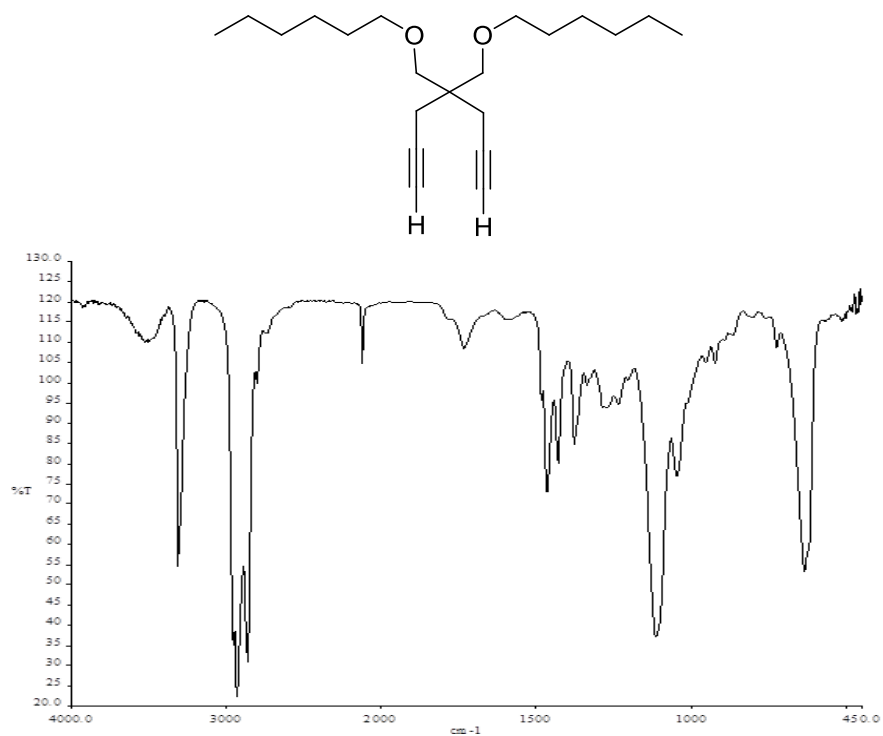
Spectrum 38: IR (neat, KBr, cm⁻¹) of 4,4-bis(hydroxymethyl)-1,6-heptadiyne [22]



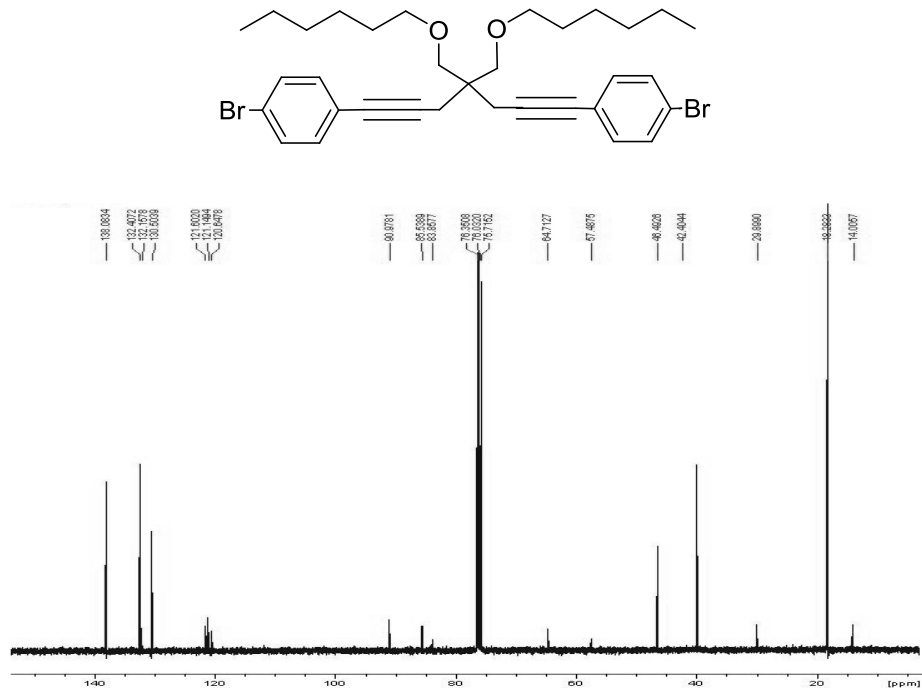
Spectrum 39: ^1H NMR of 4,4-bis(hexyloxymethyl)-1,6-heptadiyne [23]



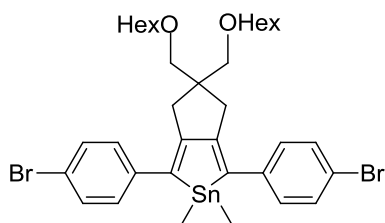
Spectrum 40: ^{13}C NMR of 4,4-bis(hexyloxymethyl)-1,6-heptadiyne [23]



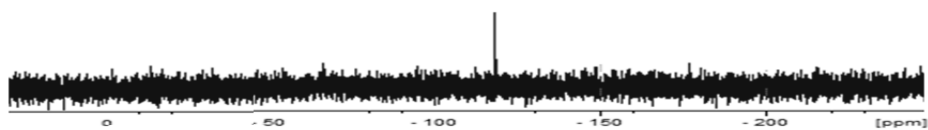
Spectrum 41: IR (neat, KBr, cm⁻¹) of 4,4-bis(hexyloxymethyl)-1,6-heptadiyne [23]



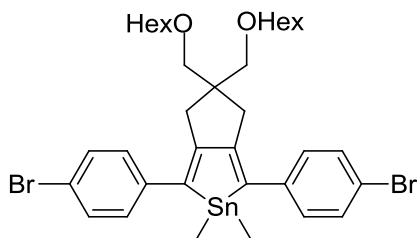
Spectrum 42: ¹H NMR of 4,4-bis(hexyloxymethyl)-1,7-bis-*p*-bromophenyl-1,6-heptadiyne [24]



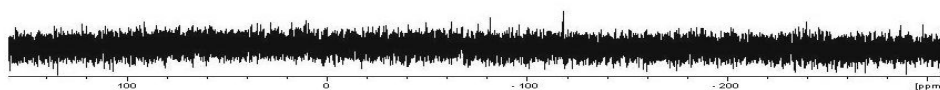
117.638



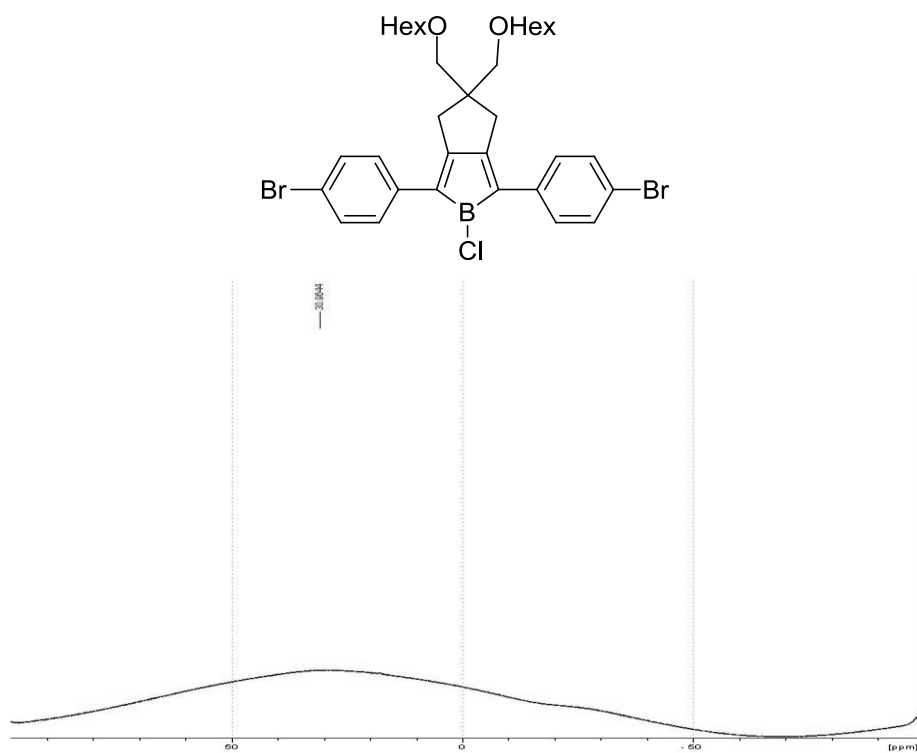
Spectrum 43: ^{119}Sn NMR of 2,5-diphenylstannole [26] *via* method (I)



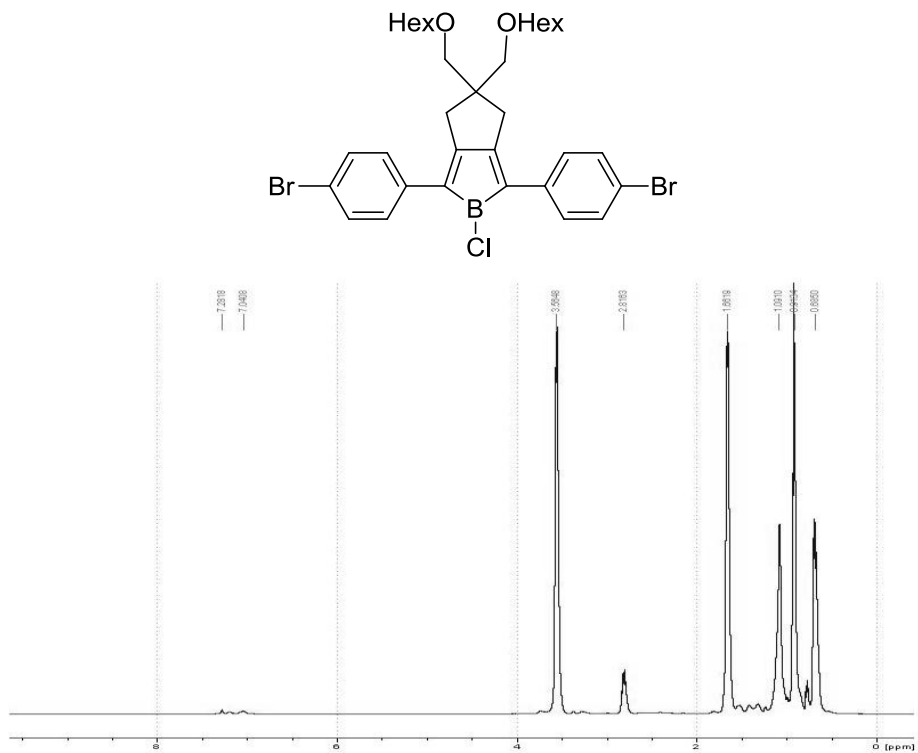
117.481



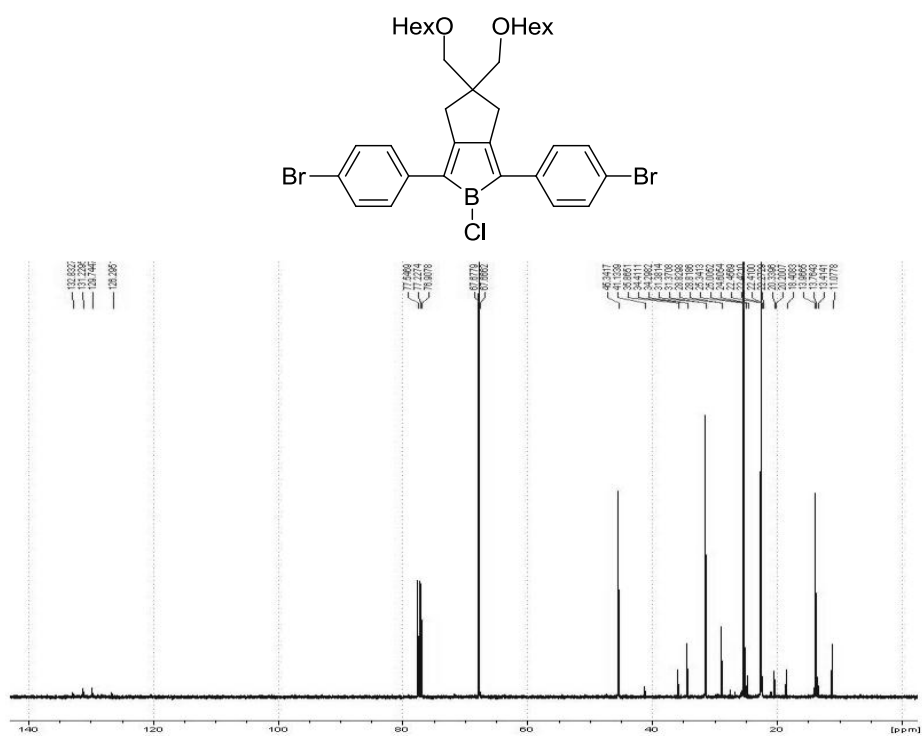
Spectrum 44: ^{119}Sn NMR of 2,5-diphenylstannole [26] *via* method (II)



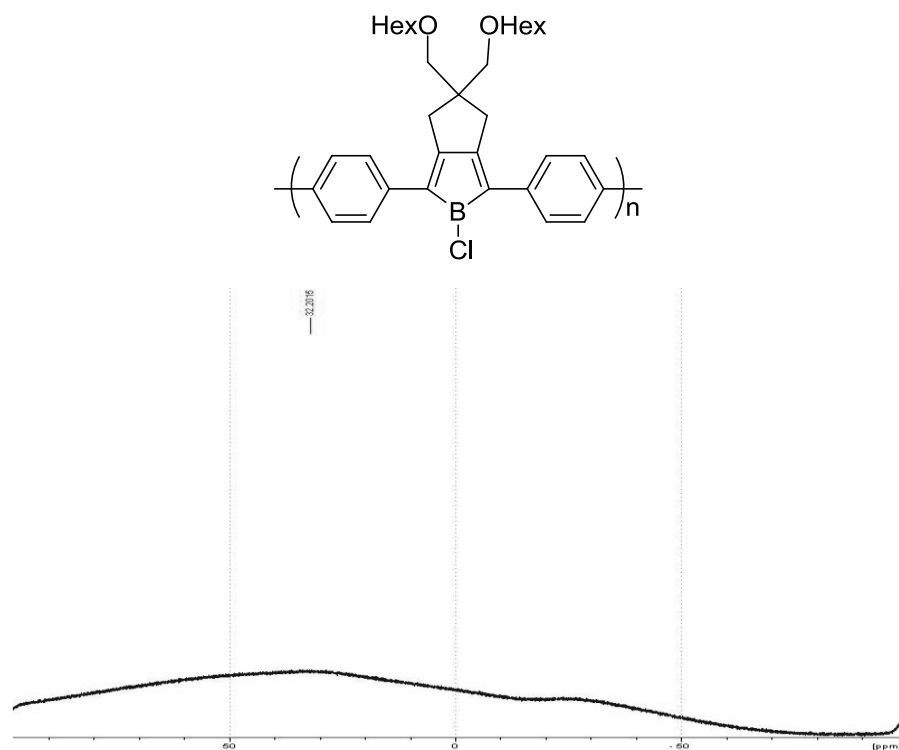
Spectrum 45: ^{11}B NMR of monomer [16a]



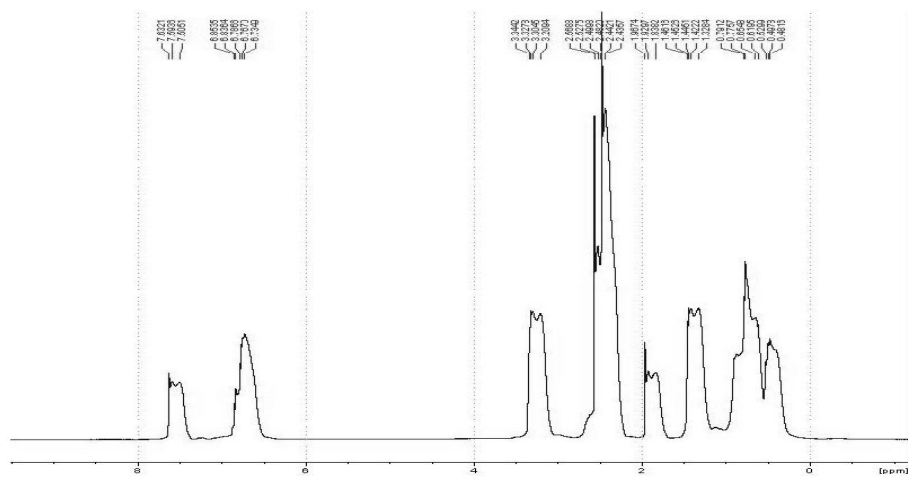
Spectrum 46: ^1H NMR of monomer [16a]



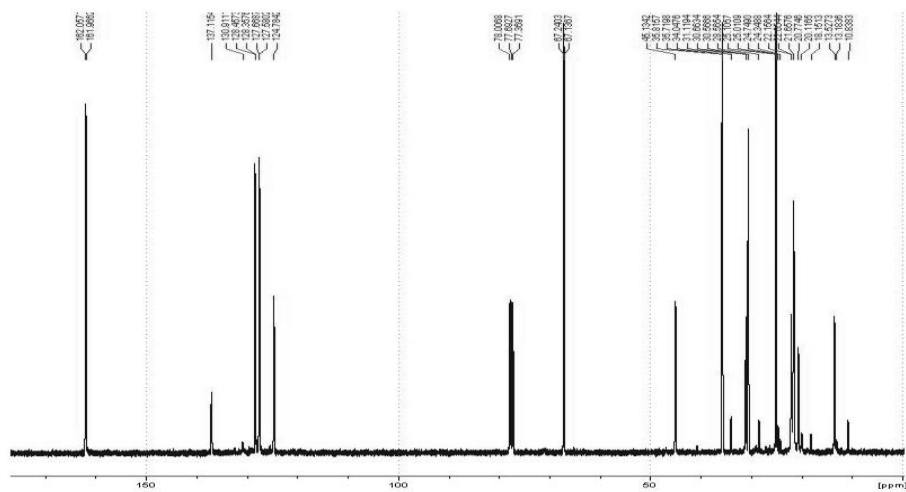
Spectrum 47: ^{13}C NMR of monomer [16a]



Spectrum 48: ^{11}B NMR of polymer [17a·THF]



Chemical structure of a poly(phenylene) derivative. The central boron atom (B) is bonded to a chlorine atom (Cl) and two phenyl rings. The boron atom is also part of a five-membered ring system, which is substituted with two hexyloxy groups (HexO and OHex). The entire structure is enclosed in brackets with a subscript 'n'.



96

REFERENCES

1. J. Hornback. (2006). Organic chemistry. 2nd Edition. Belmont, USA: Brooks/cole.
2. I. Fernandez and G. Frenking. (2006). π -Conjugation in donor-substituted cyanoethynlethenes: an EDA study. *Chem. Commun*, 5030-5032.
3. E. Taylor. Ed. (1993). *The chemistry of Heterocyclic Compounds*. New York: Wiley.
4. C. Wong. (1993). Ed. *Polymers for electronic and photonic applications*. Boston MA: Academic.
5. A. Jahnke, G. Howe, and D. Seferos. (2010). Polytellurophenes with Properties Controlled by Tellurium-Coordination. *Angew. Chem. Int. Ed*, 49, 1-6.
6. a) T. Baumgartner. (2006). Pi-conjugated heterocyclic fused bithiophene materials. *J. Inorg. Organomet. Poly.Mater*, 15, 389-409. b) T. Baumgartner and M Hobbs. (2007). Recent developments in phosphole-containing oligo and polythiophene materials. *Eur. J. Inorg. Chem*, 3611-3628. c) T. Baumgartner and U. Dienes. (2009). Tuning the photophysical properties and solid-state organization of perfluorophenyl-functionalized Dithieno[3,2-*b*:2',3'-*d*]phospholes. *Z. Anorg. Allg. Chem*, 635, 244-328.
7. H. Shirakawa, E. Lewis, A. MacDiarmid, C. Chiang, and A. Heeger. (1977). Synthesis of Electrical Conducting Organic Polymers: Halogen Derivatives of Polyacetylene, (CH)_x. *J. Chem. Soc. Chem. Comm*, 578-580.
8. M. Hissler., P. Dyer and R. Reau. (2003). Linear organic π -conjugated systems featuring the heavy group 14 and 15 elements. *Coordination chemistry Reviews*, 244, 1-44.
9. D. Pavia, G. Lampman, and G. Kriz. (2001). *Introduction to Spectroscopy*. 3rd Edition. Bellingham, Washington: Books/Cole.
10. S. Miao, P. Schleyer, J. Wu. K. Hardcastle and U. Bunz. (2007). *N,N*-Dihydroquinoxaline: Antiaromatic but Isolable. *Org. Lett*, 9(6), 1073-1076.
11. B. Streetman and S. Banerjee. (2000). *Solid state electronic devices*. 6th Edition. Upper Saddle River, NJ: Prentice Hall.

12. J. Roncali. (2007). Molecular engineering of the band gap of π -conjugated systems: Facing Technological Applications. *Macromol. Rapid Commun*, 28, 1761-1775.
13. W. Braye, and I. Caplier. (1961). New Unsaturated Heterocyclic Systems I. *J. Am. Chem. Soc*, 83(22) 4406-4413.
14. A. Wakamiya and S. Yamaguchi. (2008). Design and synthesis of boron-containing functional π -electron materials. *J. Syn. Org. Chem. Jpn*, 66(9), 858-868.
15. S. Yamaguchi, T. Shirasaka, and K. Tamao. (2000). Tridurylboranes extended by three aryethynyl groups as a new family of boron-based π -electron system. *Org. Lett*, 2(26), 4129-4132.
16. H. Braunschweig, C. Chiu, A. Damme, K. Ferkinghoff, K. Kraft, K. Radachi and J. Wahler. (2011). Unwinding Antiaromaticity in 1-bromo-2,3,4,5-tetraphenylborole. *Organometallics*, 30, 3210-216.
17. B. Clive (Ed.). (1996). Comprehensive Heterocyclic Chemistry II. 2, 919-932.
18. a) J. Eisch, J. Gelle and S. Kozima. (1986). The chemical consequences of cyclic conjugation in borocyclopolynes. The antiaromatic character of pentaarylboroles. *J. Am. Chem. Soc*, 108, 379-385. b) J. Eisch, N. Hota and S. Kozima. (1969). Synthesis of pentaphenylborole, a potentially antiaromatic system. *J. Am. Chem. Soc*, 91(16), 4575-4577.
19. A. Cowley, F. Gabbai, A. Decken and R. Schluter. (1994). Novel heterocyclic ring systems containing heavier group 13 elements. Phosphorus, Sulfur and Silicon. 93-94(1-4), 153-158.
20. a) H. Fang, C. Zhao, G. Li and Z. Xi. (2003). Reaction of aluminacyclopentadienes with aldehydes affording cyclopentadiene derivatives. *Tetrahedron*, 59, 3379-3786. b) Z. Xi. (2005). New methods for the preparation of multiply substituted cyclopentadienes and related compounds. *Topics in Catalysis*, 35(1-2), 63-71.

21. a) P. Fagan, W. Nugent, and J. Calabrese. (1994). Metallacycle transfer from zirconium to main group elements: a versatile synthesis of heterocycles. *J. Am. Chem. Soc.*, 116, 1880-1889. b) P. Fagan, and W. Nugent. (1988). Synthesis of main group heterocycles by metallacycle transfer from zirconium. *J. Am. Chem. Soc.*, 110(7), 2310-2312.

22. W. Hehre. (2003). A guide to molecular mechanics and quantum chemical. Chapters 1-5. Irvine, Ca: Wavefunction, Inc.

23. T. Tilley, B. Lucht, and M. Buretea. (2000). Poly(2,5-diphenylgermole): Incorporation of a germole ring into a conjugated polymer. *Organometallics*, 19(18), 3469-3475.

24. J. Ferman, J. Kakareka, W. Klooster, J. Mullin, J. Quattrucci, J. Ricci, W. Vining, S. Wallace and H. Tracy. (1999). Electrochemical and photophysical properties of a series of group 14 metalloles. *Inorganic Chemistry*, 38(10), 2464-2472.

25. S. Bragg. (2011). Developing an important stannole intermediate towards the synthesis of novel Lewis acidic macrocycles and adducts. B.Sc. Thesis. Department of Chemistry and Biology. Toronto, On: Ryerson University.

26. Y. Gal, W. Lee, H. Lee, S. Jang, and S. Choi. (1997). Cyclopolymerization of Diethyl dipropargylmalonate and triethyl dipropargylphosphonoacetate by molybdenum pentachloride. *Journal of Macromolecular Science. Part A*, 34(11), 2251-2267.

27. S. Jin, J. Jin, S. Moon, H. Lee, Y. Gal, H. Kim, S. Kim, and K. Koh. (2002). Synthesis and electrical properties of polyacetylene derivatives. *Journal of Polymer Science: Part A: polymer Chemistry*, 40, 958-964.

28. P. Harrison, S. Ulrich and J. Zuckerman. (1971). ^{119}Sn Chemical Shifts by the Double Resonance of Organotin Compound. *J. Am. Chem. Soc.*, 93(21), 5398-5402.

29. a) T. Kupfer and H. Braunschweig. (2008). Direct functionalization at the boron center of antiaromatic chloroborole. *Chem. Commun.*, 4487-4489. b) I. Fernandez, G. Frenking and H. Braunschweig. (2008). Structural Evidence for antiaromaticity in free boroles. *Angew. Chem. Int. Ed.* 47, 1951-1954.

30. K. Sonogashira, Y. Tohda, N. Hagihara (1975). A convenient synthesis of acetylenes: catalytic substitutions of acetylenic hydrogen with bromoalkenes, iodoarenes and bromopyridines. *Tetrahedron Letters*, 16(50), 4467–4470.
31. K. Ura, Y. Li, Z. Xi, and T. Takashi. (1998). Cu(I) catalyzed or promoted metallacycle transfer of zirconacycles to stannacycles. *Tetrahedron Letters*, 2787-2790.
32. V. Bonifacio, J. Morgado and U. Scherf. (2008). Polyfluorenes with On-chain dibenzoborole units-Synthesis and anion-induced photoluminescence quenching. *J. Polym. Sci. Part A: Polym. Chem*, 46, 2878-2883.